UNCLASSIFIED
SECURITY CLASSIFICATION OF THIS PAGE

AFR FILE COPY

REPORT DOCUMENTATION PAGE

AD-A216 629

DTIC ELECTE JAN 05 1990 S D

REPORT SECURITY CLASSIFICATION: Unclassified	1b. RESTRICTIVE MARKINGS: None
SECURITY CLASSIFICATION AUTHORITY	3. DISTRIBUTION / AVAILABILITY OF REPORT: Approved for public release, distribution unlimited
DECLASSIFICATION / DOWNGRADING SCHEDULE	
PERFORMING ORGANIZATION REPORT NUMBER(S)	5. MONITORING ORGANIZATION REPORT NUMBER(S): AFOSR-TR- 89-1878
NAME OF PERFORMING ORGANIZATION: Department of Aeronautics and Astronautics	6b. OFFICE SYMBOL (If applicable): 31-264
7a. NAME OF MONITORING ORGANIZATION: See #8 AFOSR/ Bolling AFB, DC 20332	
ADDRESS (City, State, and ZIP Code): 77 Massachusetts Avenue, Cambridge, MA 02139	7b ADDRESS (City, State, and ZIP Code): See #8
8a. NAME OF FUNDING / SPONSORING ORGANIZATION: AFOSR	8b. OFFICE SYMBOL (If applicable): NA
9. PROCUREMENT INSTRUMENT IDENTIFICATION NUMBER: Grant #AFOSR-87-0398	
8c. ADDRESS (City, State, and ZIP Code): AFOSR, Building 410, Bolling AFB, DC 20332-6448	10. SOURCE OF FUNDING NUMBERS

PROGRAM ELEMENT NO.	PROJECT NO.	TASK NO.	WORK UNIT ACCESSION NO.
61102F	2307	A4	

11. TITLE (Include Security Classification)

Active Stabilization of Aeromechanical Systems

12. PERSONAL AUTHOR(S)
J. Dugundji, A.H. Epstein, E.M. Greitzer, G.R. Guenette, L. Valavani

13a. TYPE OF REPORT	13b. TIME COVERED	14. DATE OF REPORT (Year, Month, Day)	15. PAGE COUNT
Final	FROM 9/87 TO 10/89	89-12-14	125

16. SUPPLEMENTARY NOTATION

17. COSATI CODES		
FIELD	GROUP	SUB-GROUP

18. SUBJECT TERMS (Continue on reverse if necessary and identify by block number)
Active Control, Compression System Flow Instabilities, Unsteady Flow, Fluid-Structure Interaction.

19. ABSTRACT (Continue on reverse if necessary and identify by block number)

This document is a final report on the program "Active Stabilization of Aeromechanical Systems," Grant No. AFOSR-87-0398, covering the period September 1, 1987 to October 31, 1989. Three separate sections are included. The first is a brief review of the work done on active control of rotating stall under this contract. The second is a paper (to be presented at the 1990 ASME Gas Turbine Conference, and published in the ASME Journal of Turbomachinery) on the existence of precursor travelling waves in compressor annuli and on some of the signal processing techniques used to examine such waves. The third section is a paper describing first-of-a-kind (as far as we are aware) experiments in which tailored system structural properties have been used to suppress compression system aerodynamic instability (surge).

Keywords:

20. DISTRIBUTION / AVAILABILITY OF ABSTRACT	21 ABSTRACT SECURITY CLASSIFICATION
☒ UNCLASSIFIED/UNLIMITED ☐ SAME AS RPT ☐ OTIC USERS	UNCLASSIFIED

22a. NAME OF RESPONSIBLE INDIVIDUAL	22b. TELEPHONE (Include Area Code)	22c. OFFICE SYMBOL
CAPTAIN H. E. HELIN	202 767 0471	AFOSR/NA

DD FORM 1473, 84 MAR — 83 APR edition may be used until exhausted. All other editions are obsolete.

SECURITY CLASSIFICATION OF THIS PAGE

UNCLASSIFIED

Gas Turbine Laboratory
Department of Aeronautics and Astronautics
Massachusetts Institute of Technology
Cambridge, MA 02139

Final Report
on
Grant No. AFOSR-87-0398

entitled

ACTIVE STABILIZATION OF AEROMECHANICAL SYSTEMS

submitted to

Air Force Office of Scientific Research
Building 410
Bolling Air Force Base, DC 20332-6448

Attention: Capt. H. Helin
Dr. James McMichael

INVESTIGATOR: J. Dugundji, Professor of Aeronautics and Astronautics
A.H. Epstein, Associate Professor of Aeronautics and Astronautics, Associate Director, Gas Turbine Laboratory
E.M. Greitzer, H.N. Slater Professor of Aeronautics and Astronautics, Director, Gas Turbine Laboratory
G.R. Guenette, Research Engineer, Department of Aeronautics and Astronautics
L. Valavani, Assistant Professor of Aeronautics and Astronautics

STUDENTS: V. Garnier
D. Gysling
P. Silkowski
J. Paduano

PERIOD OF INVESTIGATION: September 1, 1987 - October 31, 1989

December 1989

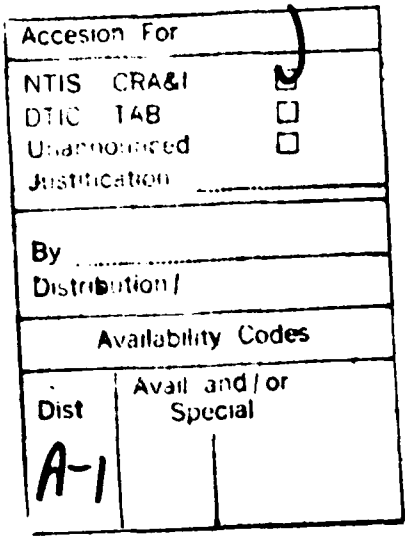

Summary

This document is a final report on the program "Active Stabilization of Aeromechanical Systems," Grant No. AFOSR-87-0398, covering the period September 1, 1987 to October 31, 1989. Three separate sections are included. The first is a brief review of the work done on active control of rotating stall under this contract. The second is a paper (to be presented at the 1990 ASME Gas Turbine Conference, and published in the ASME *Journal of Turbomachinery*) on the existence of precursor travelling waves in compressor annuli and on some of the signal processing techniques used to examine such waves. The third section is a paper describing first-of-a-kind (as far as we are aware) experiments in which tailored system structural properties have been used to suppress compression system aerodynamic instability (surge).

Introduction

This document reports on progress made in controlling instabilities in aeromechanical systems during the past two years. The specific test bed used in this study is the broad class of instability phenomena generic to propulsion and pumping systems. This first part of the report presents, in broad brush, an overview of the research that has been carried out on active control of rotating stall and a description of the approaches used. The interdisciplinary aspects of the work, which we feel are a key part of the program, are also discussed.

This initial part is organized as follows. A brief review of the types of fluid instabilities that occur in high performance propulsion systems is first presented, along with an introduction to the conceptual approach taken for application of active control. Discussion is then given of the different research areas being pursued at MIT in connection with this research: fluid modelling, control theory application, preliminary controller design, sensor considerations, and conceptual and actual design of the wave launching devices. Finally, we pose some of the scientific questions that need to be addressed in this research.

At the outset, we stress that this research effort is truly interdisciplinary, at least in the manner that we have approached it. It has been very clear in the two years that we have been working on this problem that knowledge of control, fluids, structures, and instrumentation are all important to the overall goal. To put it more bluntly, if we did not have personnel with expertise in all these areas, we would be limited in our ability to deal conceptually, let alone on the level of implementation, with the problem of practical concern.

PART I: AN OVERVIEW OF RESEARCH ON ACTIVE CONTROL OF ROTATING STALL

Introduction: Phenomenology of Compressor Instabilities.

Compressors and compression systems exhibit different modes of generic fluid dynamic instabilities. The "zeroth order mode" known as surge, is an oscillation of the overall (annulus averaged) flow in the compressor. The details of the oscillation depend not only on compressor geometry (blading) but on system parameters (plenum volumes, duct lengths) as well. In the fully developed state, surge can be associated with mass flow fluctuations over 100% of the steady state value. A surge cycle of this type is a nonlinear limit cycle in time.

The higher order modes of instability are associated with rotating or propagating stall. In rotating stall, a zone, or zones, of stalled flow propagates round the compressor annulus, at a speed typically from twenty to fifty percent of the rotor speed. The flow in the stalled zone, or "stall cell", is generally reversed, while the flow per unit area in the rest of the annulus can be higher than the design flow rate. In contrast to surge, the annulus average mass flow rate in rotating stall is constant with time, the stall cells serving merely to redistribute the flow round the annulus. Fully developed rotating stall can be looked at as a limit cycle in θ, the angular variable [1].

For an aircraft gas turbine engine, the consequences of these instabilities can be severe. For a compressor with a pressure ratio of ten, say, prior to the onset of instability, the pressure ratio in rotating stall may be between two and three, and the mass flow may be also decreased by over fifty percent. The result is greatly decreased thrust and, occasionally, mechanical distress. Under certain conditions, furthermore, there can be substantial hysteresis associated with the return to unstalled operation, hysteresis so large that the only way to clear the stall is to shut down the engine [2].

The central background points are thus: the instabilities of interest have a strong consequence for practical devices, and they are generic in nature. Although the two modes, surge and rotating stall, are quite different, they can be coupled by nonlinearity, so that general transients in gas turbine engines include some admixture of pure surge and pure rotating stall in a complex

manner. While a theory to describe this interaction has been given by Moore and Greitzer [3], in the present context we will be most interested in the incipient (linear) state of these disturbances in which, to first order, they can be regarded as uncoupled.

Conceptual Basis of the Approach to Control

The conceptual basis of the approach is that both surge and rotating stall, and indeed a wide class of fluid dynamic instabilities, are instabilities which start as small oscillating disturbances. Feedback control can be used to suppress the growth of such disturbances, provided one can sense them and devise suitable disturbance generators.

Our interest is the application of feedback control to this broad class of fluid dynamic instabilities, and stabilization of the instabilities that occur in compressors and compression systems appears to us as a canonical application. Surge, at least in its incipient form, is a disturbance which can be treated in a lumped parameter, or one-dimensional manner. There is an extensive stability modelling that exists in the literature. The frequencies of interest are low, so that the actuator movement requirements are not severe. In addition, only a single sensor and actuator are required. Further, suppression of surge has a large practical benefit for many compression systems. All of these considerations make examination of surge an ideal first step in the application of active control.

Note that we do not restrict the possibilities for control to an active feedback loop. The necessary feedback path can also be through coupling of the system aerodynamics with the structural properties, and this is another concept that has been pursued. It will be described in detail in Part III, but the central idea is to tailor the system structure so that it responds to the aerodynamic disturbances. The structural motion, given an appropriately designed structure, can thus be made such that damping is provided to overcome the negative damping due to the flow through the compressor. As will be seen in Part III, this idea can be applied to achieve a significant increase in stable flow range by suppression of surge.

Suppression of rotating stall brings in many other issues. The basic phenomenon, i.e., the fluid mechanic aspects, are much less known. The system is more complex, in that one may have

to control on the order of ten to one hundred airfoils. The complexity of the real system invokes questions of sparse sampling, optimum ways to launch fluid waves, and modelling for control, questions which are of high interest for many other fluid applications. Finally, suppression of rotating stall is a prime problem for aircraft engines.

Initial work in suppressing surge using active control has been reported elsewhere by Pinsley [4] and Ffowcs Williams and Huang [5]. The conclusion from both of these studies is that the active suppression of surge is definitely possible and feasible and that work should be focussed on doing this in an optimal manner. We will thus not discuss the surge aspect further in this part, but rather concentrate on the suppression of rotating stall, i.e. the stabilization of propagating disturbances in the compressor annulus*. The goals of the research are modelling of stall inception and control methodology, experimental delineation of rotating stall "precursor waves", and optimization of real time stall anticipation.

The first of these topics has also been described at length elsewhere [3], [6], and it will not be discussed except to state that our conclusion is that many of the overall features of the evolution of the initial small disturbances (see below and also Part II) into rotating stall are captured by the model.

The second issue, that of a precursor to stall, is a quite recent finding. Data taken at MIT and at the Whittle Laboratory, Cambridge University [7], seem to show that the onset of rotating stall is linked to the presence of small amplitude travelling waves in the compressor annulus. This is somewhat at odds with the "traditional" view of stall inception, which is based on the idea of one blade stalling and creating a disturbance.

In the experiments carried out here at MIT, the disturbance waves are sensed using a circumferential array of eight hot wires, approximately 0.4 radii upstream of the compressor. Putting the sensors this far upstream means that the higher harmonic components of the disturbances are filtered (the decay rate is like $e^{nx/R}$, where n is the harmonic number). With eight

* Part III, however, will focus on surge, from the point of view of dynamic control using tailored structures.

wires, one can examine the first and second disturbance harmonics and obtain, from the Fourier analysis, their phase and amplitude. A plot of the former quantity is shown in the top part of Fig. 1, which gives data from a three-stage, low speed research compressor. The phase is plotted versus rotor revolutions, this being the natural unit of time. It is clear from the figure that the disturbance can clearly be detected by its constant phase velocity long before it is evident as a velocity disturbance (upper part of the figure). The influence of the number of wires is shown in Fig. 2, where it can be seen that four wires is minimal for the first mode, while eight does a better job, although questions of sensor numbers are still being investigated. It should perhaps be stated here that it is the low order harmonics that are most often seen and that are most dangerous. Further information on the waves is given in Part II.

Control System Design for Compressor Stabilization

Four aspects have to be considered in the control design: modelling, noise estimation, control algorithm, and implementation. The approach used for the first of these, modelling, is generic in nature. It concentrates on the aggregate quantities that best capture the process (i.e. the compressor and associated flow field) behavior. A control loop schematic of the system is shown in Fig. 3.

The models used for control purposes are different from those one uses for the "best" fluid mechanic description of the phenomenon, so that the original partial differential equation models must be adapted for control. To do this, we start with the rotating stall description of Moore and Greitzer [3]:

$$\frac{\Delta p}{\rho U^2} = \frac{\partial \psi}{\partial \phi}\Delta\phi + \frac{\partial \psi}{\partial \gamma}\Delta\gamma - \lambda\frac{\partial(\Delta\phi)}{\partial\theta} - \frac{r\mu}{U}\frac{\partial\Delta\phi}{\partial t}$$

where $\Delta p/\rho U^2$ = non-dimensional pressure perturbation
$\Delta\phi$ = flow perturbation
$\partial\psi/\partial\gamma$ = "control effectiveness coefficient"
λ,μ = compressor blading parameters
γ = stagger angle

The variables are then expressed in terms of spatial modes with the state variables being the complex coefficients of each mode.

The above equation describes an idealized system. To obtain a description useful from the control point of view, we must augment this with additional dynamics to reflect the behavior of sensors, anti-aliasing filters, sampling processes, the servo-motors used for the actuation, and the unsteady response of the fluid to the actuation. One can then use the model for wave detection, noise estimation, and control implementation.

For the wave detection, two observations are required: wave angular position and growth rate. There are multiple techniques available to obtain this information, such as low pass filtering, model based observers (Luenberger-type), optimized observers (Kalman filters), and system identification. We have used an optimized observer and made use of the noise information to optimize the gains. We assumed that fluid noise in the compressor, turbulence at the sensor, and electrical noise were all white. Optimizing the observer yields the noise from each source, and allows a Kalman filter design without *a priori* noise information. We thus have the "best" linear filter for wave phase detection. Using this observer, a comparison of phase prediction in a region of very low signal to noise is shown in Fig. 4. It can be seen that the phase estimate, based on the observer, is close to what we expect the disturbance phase speed to be.

We have also examined the validity of the rotating stall model by fitting it to the existing data [8], [9]. The experimental measurements were used for the model parameters such as disturbance growth rate (damping ratio), disturbance frequency, and noise amplitudes. Part II shows these results for both first and second modes (see Figs. 23 and 24 of Part II), and it can be seen that the model fits the data well. This gives confidence that the model can be used to predict the IGV angular motion required to cancel the disturbance wave.

The next problem to be addressed is controller design. There are several issues to be faced. First, control design methodology is not well established for systems with parametric uncertainty. Second, the control of unstable systems has inherent limitations. For these reasons, we initially examined alternative approaches based on the system representation. A multivariable control

framework was applied in the stationary frame, and multiple, uncoupled systems were used in the rotating frame.

The philosophy adopted was to design the controller in frame where the analysis is easiest. In the present situation, this is the rotating frame. Using this approach, we can convert the multiple input multiple output into single input single output systems, in particular into two (unstable) decoupled first order systems. Doing this avoids the "underdamped" character of coupled multiple input multiple output. A key facet is the recognition that the initial waves have a stable rotation rate, which implies that time lags can be converted into spatial lags. This reduces controller bandwidth requirements somewhat.

The central point is that the moving reference frame design is very useful for a fluid dynamic stability setup. In the matrix representation of moving frame control, the rotating frame representation eliminates the off-diagonal elements and decouples the system.

A preliminary controller design has been carried out for a single stage, low speed compressor. The hardware descriptions assumed were: controller effectiveness, $\partial\psi/\partial\gamma$ (this is not well known, so one must design for parametric uncertainty), and an actuator bandwidth of 600 rad/sec. The sensors and signal conditioners were modelled as Bessel filters, and the computer time delay and zero order hold were modelled using Pade approximiations. The design method employed was continuous LQG/LTR [10]. A plot of the compensator response is shown in Fig. 5.

The next facet of the problem to be considered is the wave sensing. We examined a limited class of sensor types: hot wires (axial velocity) and hot films (boundary layer shear) for low speed compressors, and wall static pressure for high speed compressors. In picking the sensor geometry, there are also placement considerations. Putting the sensors upstream of the compressor filters blade perturbations. For high speed compressors, local static pressure taps may be preferred. The sensor number required is dependent on mode order. Eight sensors are sufficient for the first and second modes but, as stated, the quantitative signal-to-noise tradeoffs have not yet been done.

For wave launching and actuation, the schemes examined at the outset included: oscillating

vanes, vanes with flaps, jet flaps, jets, tip bleed, and rotor whirl. In the end, oscillating inlet guide vanes were chosen on the basis of minimum technical risk, i.e. we believed we could calculate what sort of wave would be achieved, as well as construct the vanes that were needed.

The design questions to be answered are: How many IGV's in the blade row and how many should oscillate? What are the bandwidth and amplitude requirements? What are the airfoil parameters: shape, chord, pitch? What type of actuators should be used: electric or hydraulic, continuous or discrete? How do we sense the position of the vanes: continuous or discrete? Should the blade position servo loop design be separate or integrated into the main control loop?

As with many aerospace devices, the design of the oscillating airfoils introduces tradeoffs. The wave amplitude increases for a given vane motion as the airfoil count increases, but cost and complexity scales with airfoil count. Hydraulics have much greater torque to inertia ratio, but DC servo motors are much cheaper. A longer airfoil chord requires fewer airfoils, but at the expense of airfoil inertia and the motors are constrained by torque to inertia ratio. Thicker airfoils give better off-angle performance, but this increases the airfoil inertia. Integrating servo math into the basic loop saves hardware, but increases the computer CPU speed requirements.

To estimate the effectiveness of the array of oscillating airfoils as wave launchers, we initially calculated the flowfield using a (quasi-steady) singularity method. This gave us a rough tool for trading the cascade design variables: solidity (airfoil count), fraction of cascade actuated, and blade chord. We also evaluated the detailed high angle of attack performance with a viscid-inviscid design code [11]. Figures 6 and 7 show the results of these two steps. Since the first mode-reduced frequency is roughly 0.3, we also checked the quasi-steady assumption using an unsteady singularity method, and found that unsteady effects had little influence on the original design trades.

The wave launcher design adopted uses moving inlet guide vanes, consisting of 12 oscillating airfoils, of aspect ratio 0.9 and solidity 0.6. The section is NACA 65-0009 with zero stagger and zero camber. The oscillating blades are low density plastic to minimize inertia. The blade motion design point was chosen at $\pm 10°$ at 100 Hz (8 times stall frequency) and the actuators

selected were high torque to inertia ratio DC servo motors. There are individual hardware digital position servo loops on each blade, with optical encoders used for blade position sensing. We have constructed and tested the prototype and plan to, in the very near future, verify the overall system performance using hot wires to verify the relation between computer command and aerodynamic waves.

We can scope the software requirements in terms of a strawman controller, which must be able to accept and process the input of compressor measurements (8 hot wires, RPM, mass flow). It must filter to get the perturbation velocities and carry out a discrete spatial Fourier transform to compute the disturbance phase and phase speed. The control algorithm is a table lookup for gains, an 8th order difference equation, and limiter logic. It must estimate the phase of wave to be launched, carry out an inverse discrete Fourier transfer, output to the individual blade position servo loops, and conduct various housekeeping functions (data storage for analysis, debugging, etc.).

The controller hardware selection is set by CPU speed requirements (main rotating stall control loop and individual blade position control loops), I/O bandwidth (sensors in, blade positions out, storage for post-test analysis), operating system overhead, and cost. Our final selection was a commercial 20 MHz 80386 PC (400 Hz loop bandwidth). This yields the schematic representation of the active stabilization system shown in Figs. 8 and 9.

The status as of the end of the contract period is that the rig construction and preliminary shakedown testing have been completed. The casing ring, with the twelve inlet guide vanes mounted in it, has ben installed in the MIT single-stage compressor facility. Hardware and software for moving the blades has also been checked out. We are now starting the measurements to determine the aerodynamic transfer function of the moveable guide vanes, which is a prerequisite to implementation of the active control.

Research Issues

We see several main scientific issues which, again, cut across disciplinary boundaries. The first of these concerns the limitations to the modelling approach that has been adopted. While it is

certainly correct to analyze the flow in the compressor in terms of its eigenmodes, the basic question is: To what level does one have to go with such a description? Does the structure that is included have to be of a length scale associated with the blade passage or smaller, or is the approach taken here sufficient? Initial data taken at MIT and at Cambridge seem to show that the answer to the latter basic question is yes, at least in some circumstances, but considerably more investigation is needed to put the topic on a firm foundation. The unsteady fluid mechanics must also grapple with the presence of self-generated versus convected disturbances, the influence of compressibility, and nonlinearity and multimode coupling. A very important item is the reconciliation of these modal approaches and the models that are at the core of the turbomachine design process.

Methods for wave launching are also not well understood. We have utilized moving blades as an example of a reasonably (?) well understood approach. A topic of considerable interest is what are other methods for creating the necessary disturbances by (for example) manipulating the boundary layer and the shear layers that form the blade wakes. Are there means for altering the flow about the blade to do this which do not involve gross motion of the blades?

In addition to the above, there are also unanswered questions concerning the control theories. In many of the systems of practical interest, there is insufficient information about the key fluid parameters. Designing with parametric uncertainty is thus an important issue. In addition, guaranteeing performance with system degradation is also of great interest.

To answer these questions, one can call out a program of research on both low and high speed compressors. For the former, the initial item is the demonstration of the feasibility of the approach presented here. This could be carried out in a single stage or, with a bit more uncertainty, in a multistage compressor. Even for the single stage, however, there are the questions mentioned above of modal structure, distortion, self-generated distortion, and alternate implementations. The questions apply to the multistage environment as well. Finally, controlling just rotating stall is only part of the picture since in the actual environment one must deal with coupled surge and rotating stall instabilities. For high speed machines, we forsee a program of

research to first examine the stall initiation behavior. The stability modelling must also be carried out to include effects of compressibility. Following this, one should be well placed to address an initial rig demonstration of rotating stall control, perhaps on a single stage rig but then a multistage, as well as to focus on the combined (surge and rotating stall) problem at high speed.

Summary and Conclusions

An interdisciplinary research program is being carried out on the active suppression of flow field instabilities (surge and rotating stall) in propulsion systems.

These instabilities are generic and furnish an excellent test bed for the fluids, control and structural research tools that are necessary to develop this field.

Experiments carried out clearly demonstate the feasibility of both active and passive control of surge, and the degree to which one can model surge dynamics.

Analysis and design has been carried out on the controller and the wave launcher for the control of rotating stall in an axial compressor, and a prototype controller/blade/actuator system has been built and installed in a single-stage compressor, and is now ready for testing.

The use of feedback control to alter the dynamic behavior of aeropropulsion systems appears to offer considerable potential for improving performance and reducing design constraints.

References

1. Moore, F.K., "A Theory of Rotating Stall in Multistage Compressors, Parts I, II, and III," *ASME J. Eng. Power*, Vol. 106, April 1984, pp. 313-336.

2. Stetson, H.D., "Designing for Stability in Advanced Turbine Engines," in AGARD CP 324, Engine Handling, October 1982.

3. Moore, F.K., Greitzer, E.M., "A Theory of Post-Stall Transients in Axial Compression Systems, Parts I and II," *ASME J. Eng. for Gas Turbines and Power*, Vol. 108, January 1986, pp. 68-76, and April 1986, pp. 231-239.

4. Pinsley, J.E. et al., "Active Stabilization Of Centrifugal Compressor Surge," to be presented at the 1990 ASME Gas Turbine Conference and to appear in *ASME J. of Turbomachinery*.

5. Ffowcs Williams, F.E., Huang, X., "Active Stabilization of Compressor Surge," *J. of Fluid Mechanics*, Vol. 204, 1989, pp. 245-262.

6. McCaughan, F., "Application of Bifurcation Theory to Axial Flow Compressor Instability," ASME Paper 88-GT-231, 1988.

7. MacDougall, N.M., Cumpsty, N.A., Hynes, T.P., "Stall Inception in Axial Compressors," ASME Paper 89-GT-63, 1989.

8. Ljung, L., System Identification: Theory for the User, Prentice Hall, 1987.

9. Maybeck, P.S., Stochastic Models, Estimation and Control, Academic Press: New York, 1979.

10. Stein, G., Athans, M., "The LQG/LTR Procedure for Multivariable Feedback Control Design," IEEE *Transactions on Automatic Control*, Vol. AC-32, No. 2, February 1987, pp. 105-114.

11. Drela, M., Private communication, 1988.

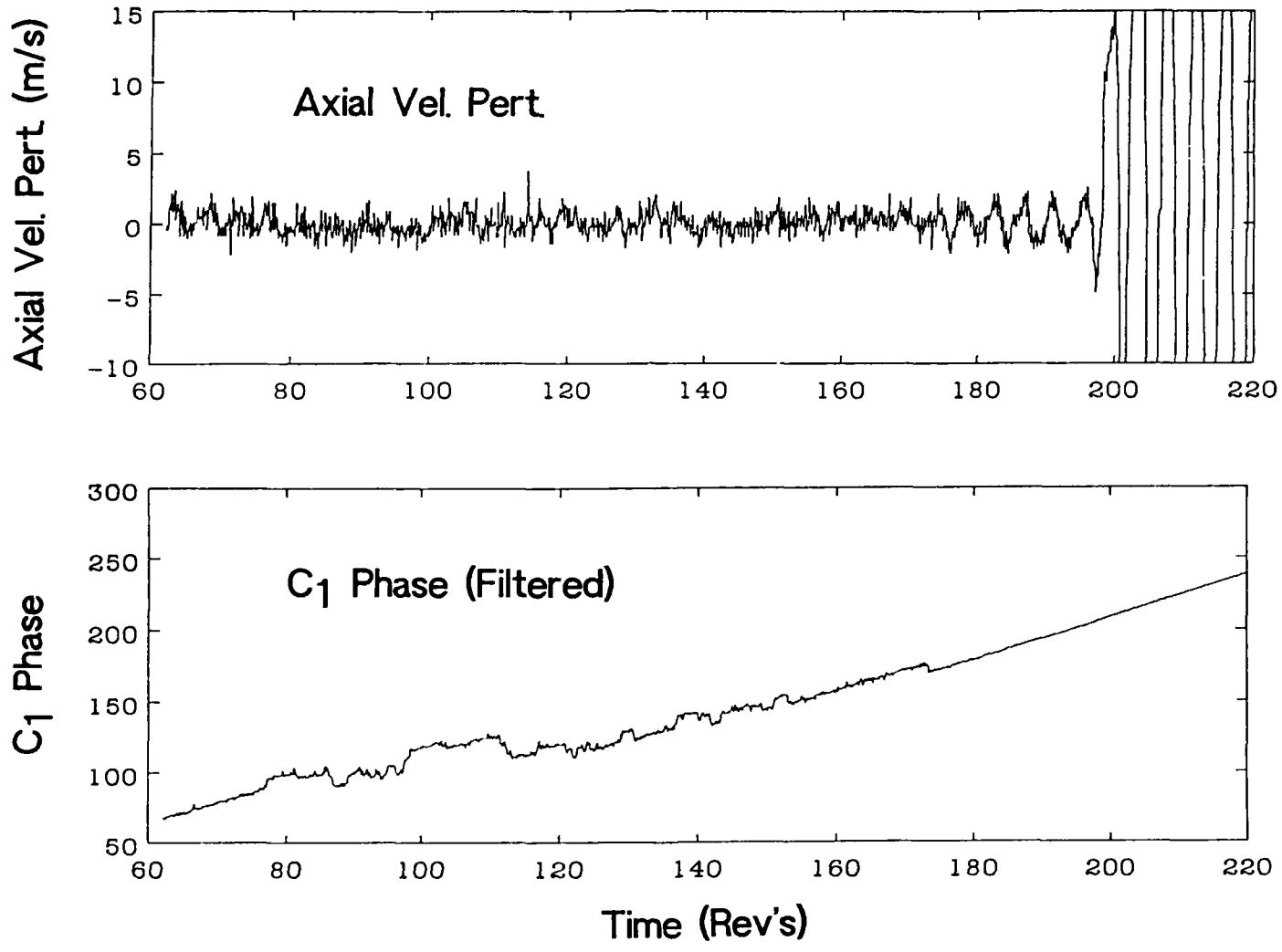

Fig. 1: The axial velocity perturbation as detected by a single sensor and the corresponding phase speed of the first mode of the rotating wave estimated from 8 sensors about the circumference.

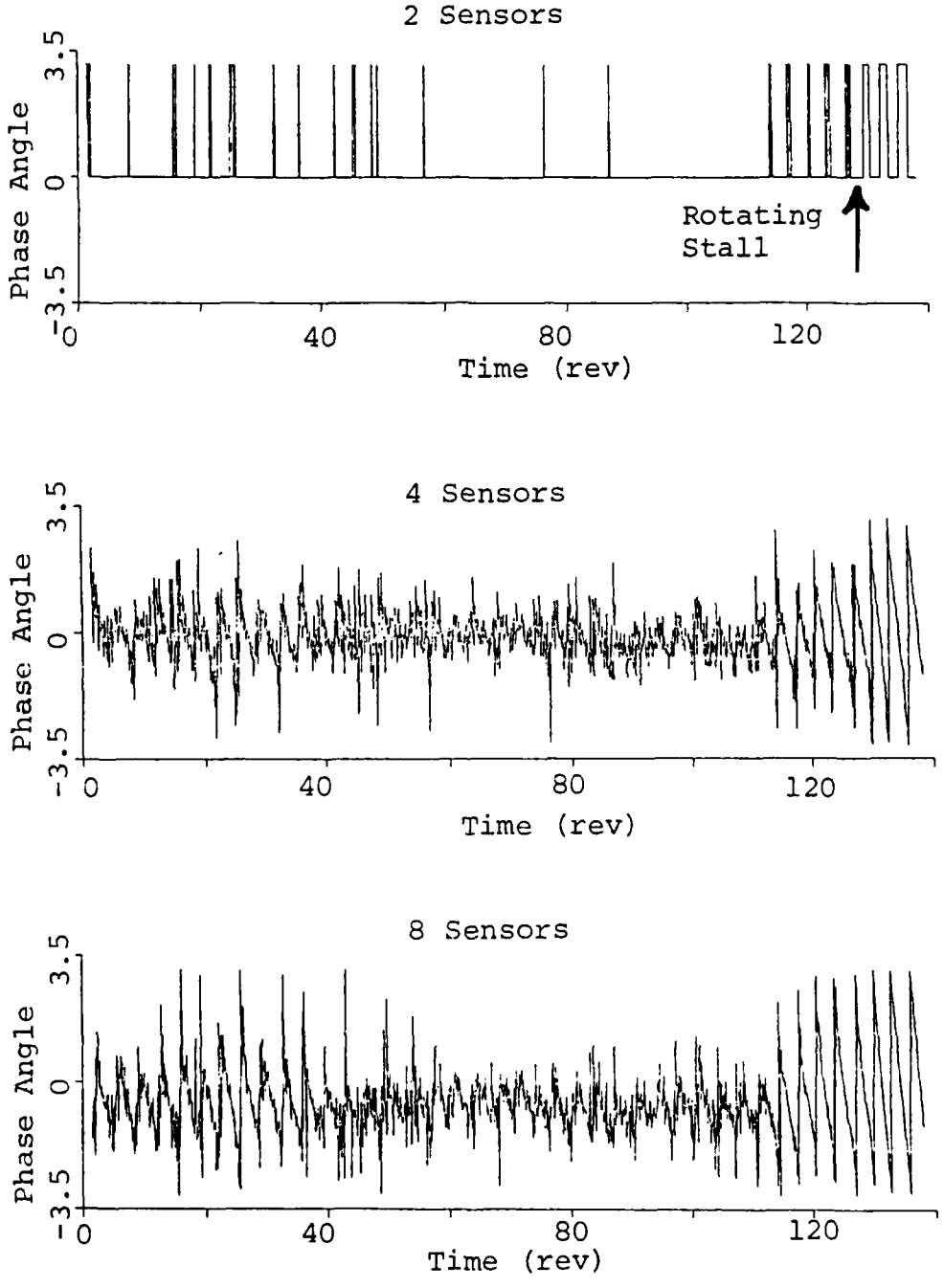

Fig. 2: The influence of sensor number on the estimation of first mode rotating wave phase speed.

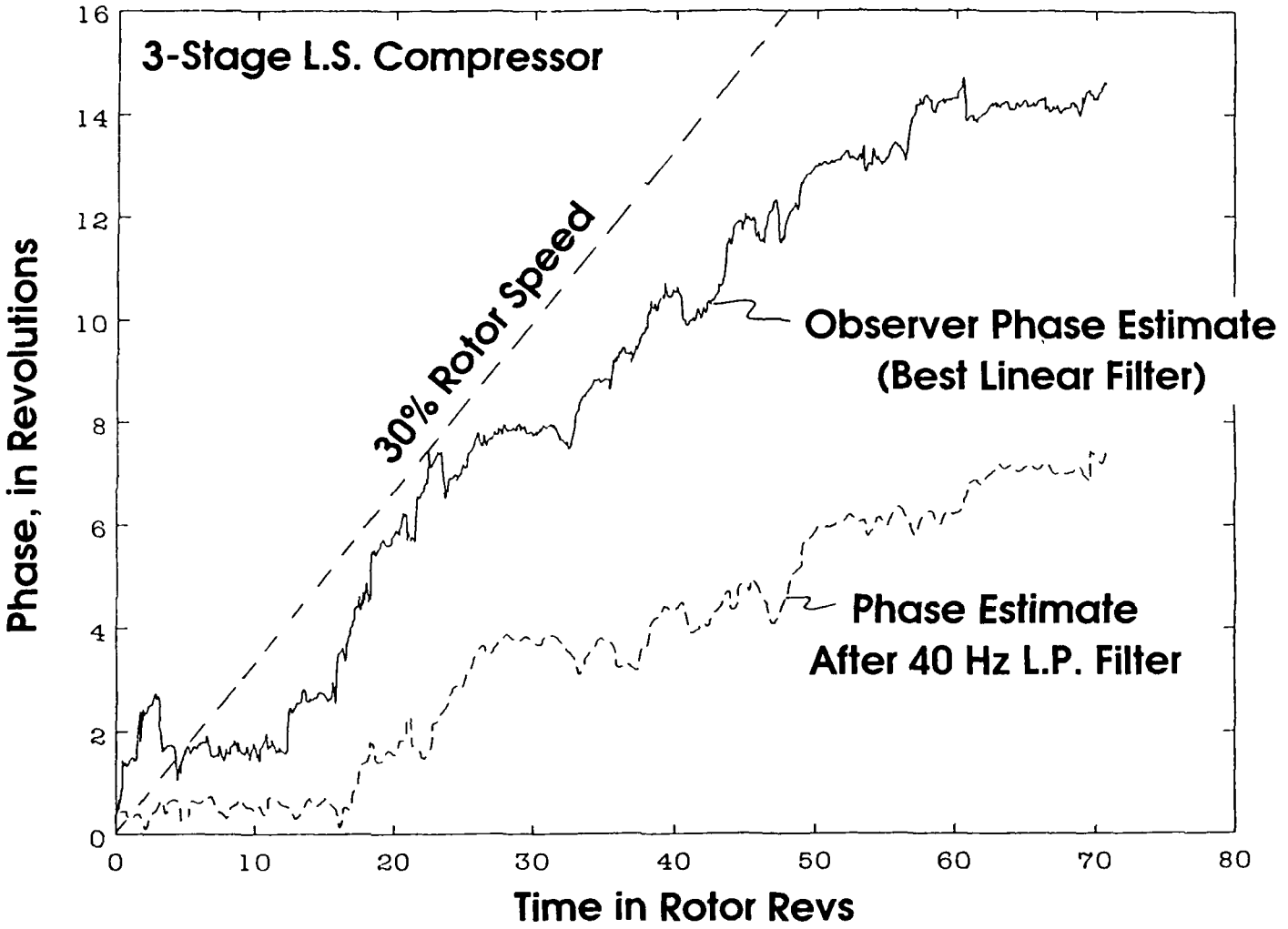

Fig. 4: Comparison of rotating wave phase estimation techniques.

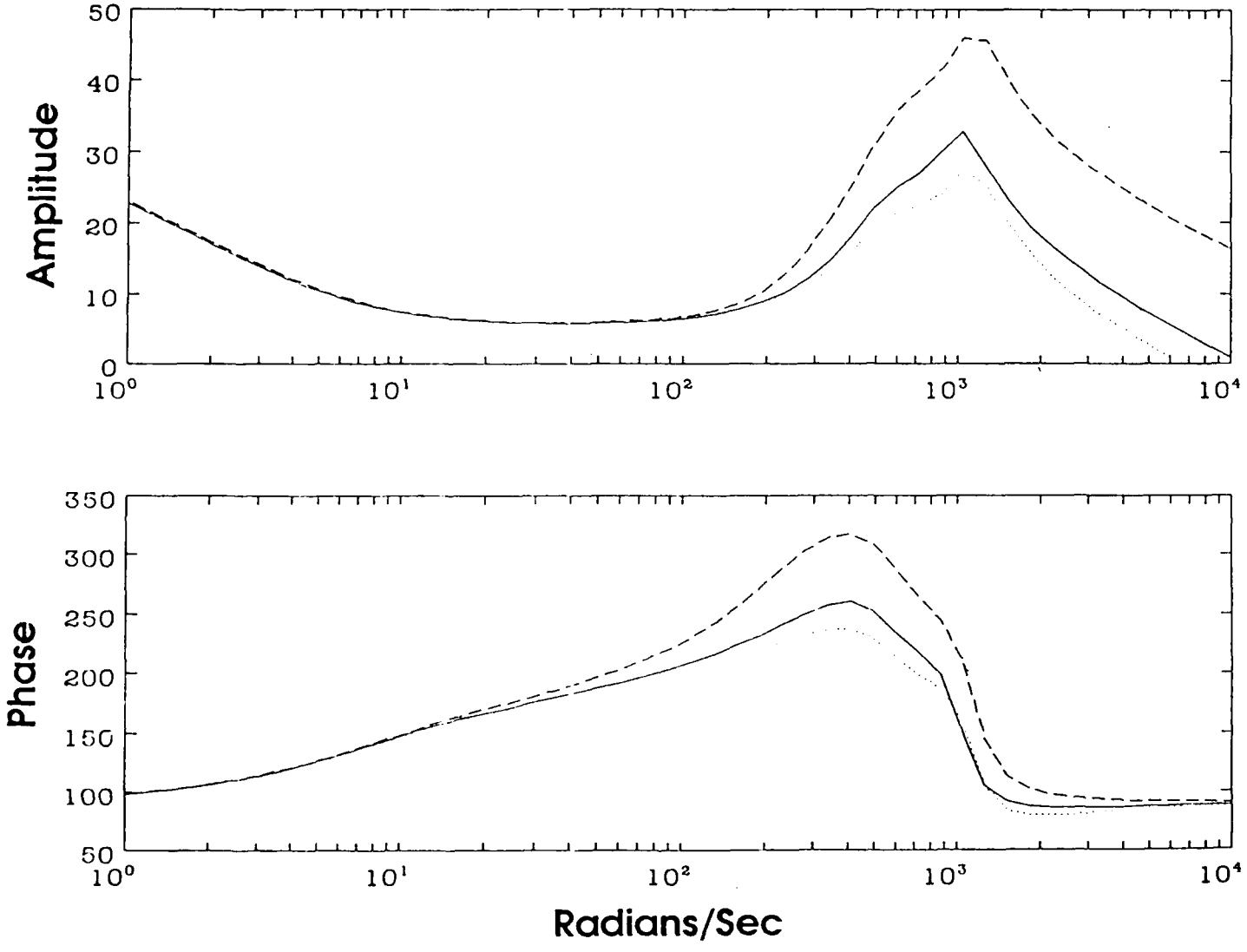

Fig. 5: Response of a model-based compensator designed for rotating stall controller

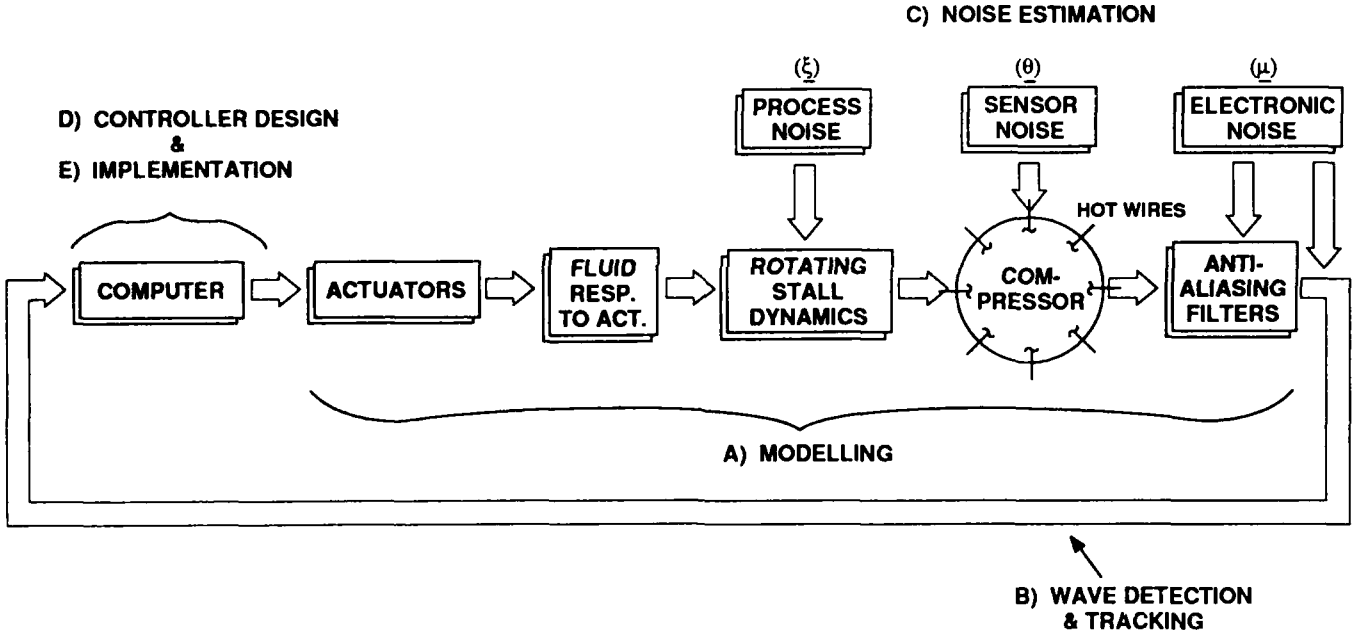

Fig. 3: Control loop schematic of actively stabilized axial compressor

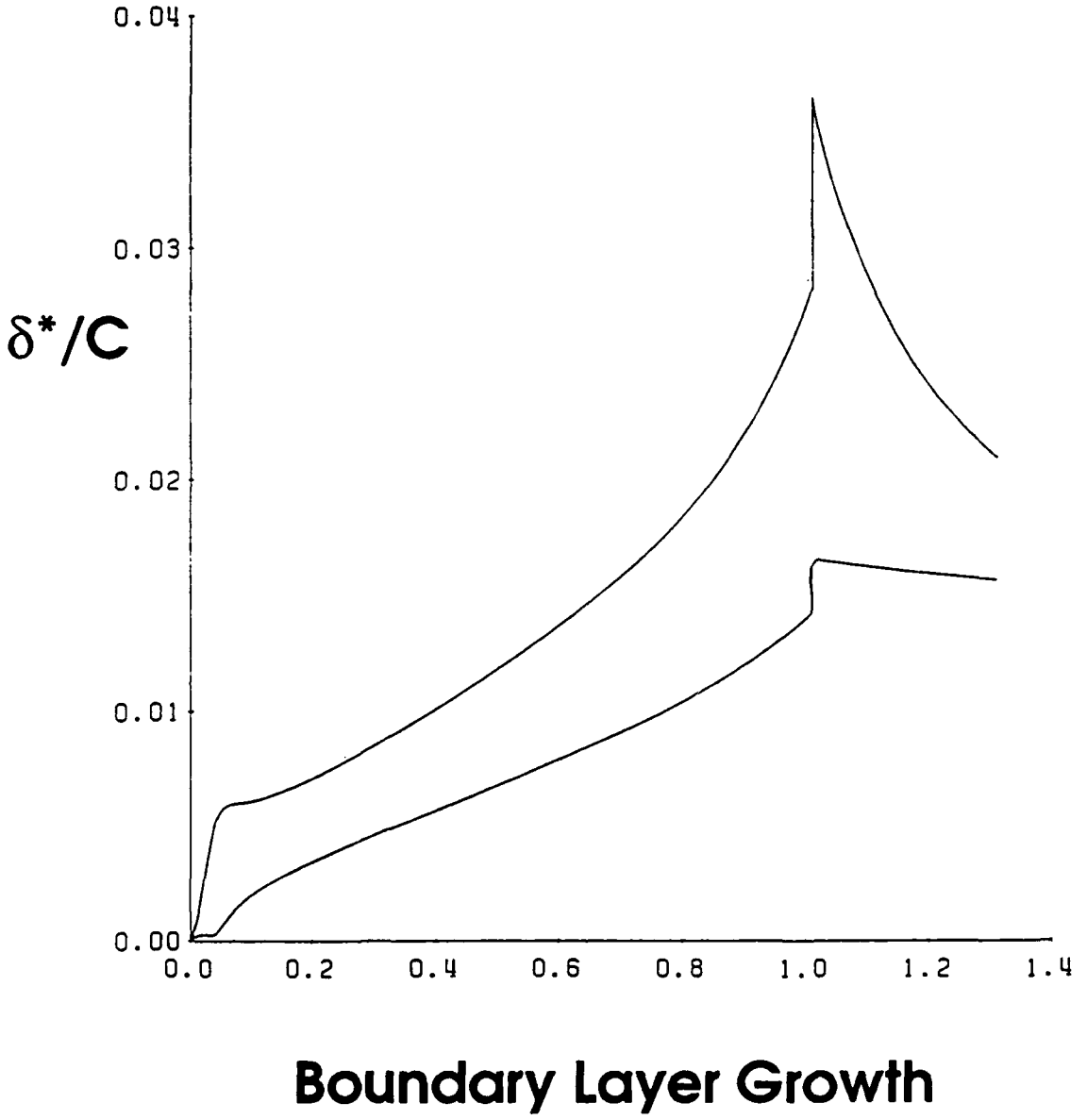

Fig. 6: Boundary layer growth on IGV airfoil at 15° angle of attack

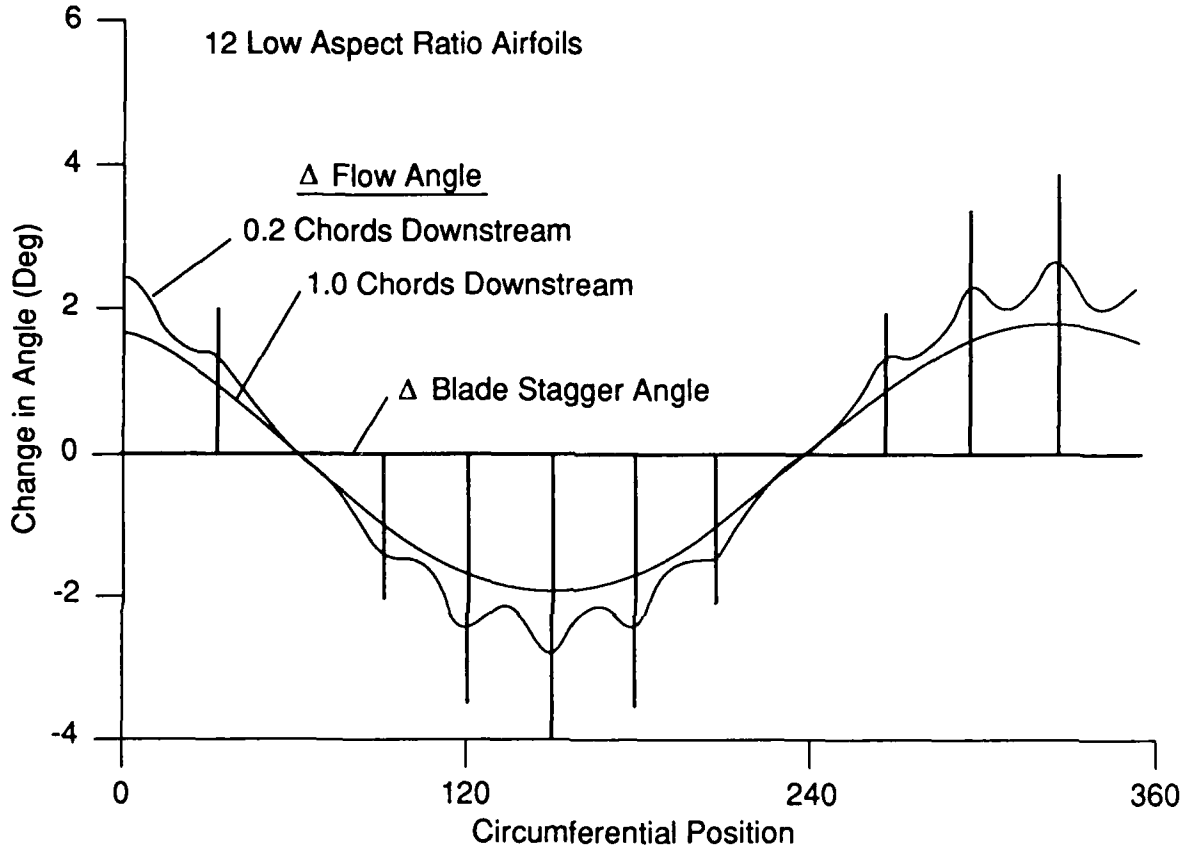

Fig. 7: Axial flow wave from 12 variably staggered inlet guide vanes

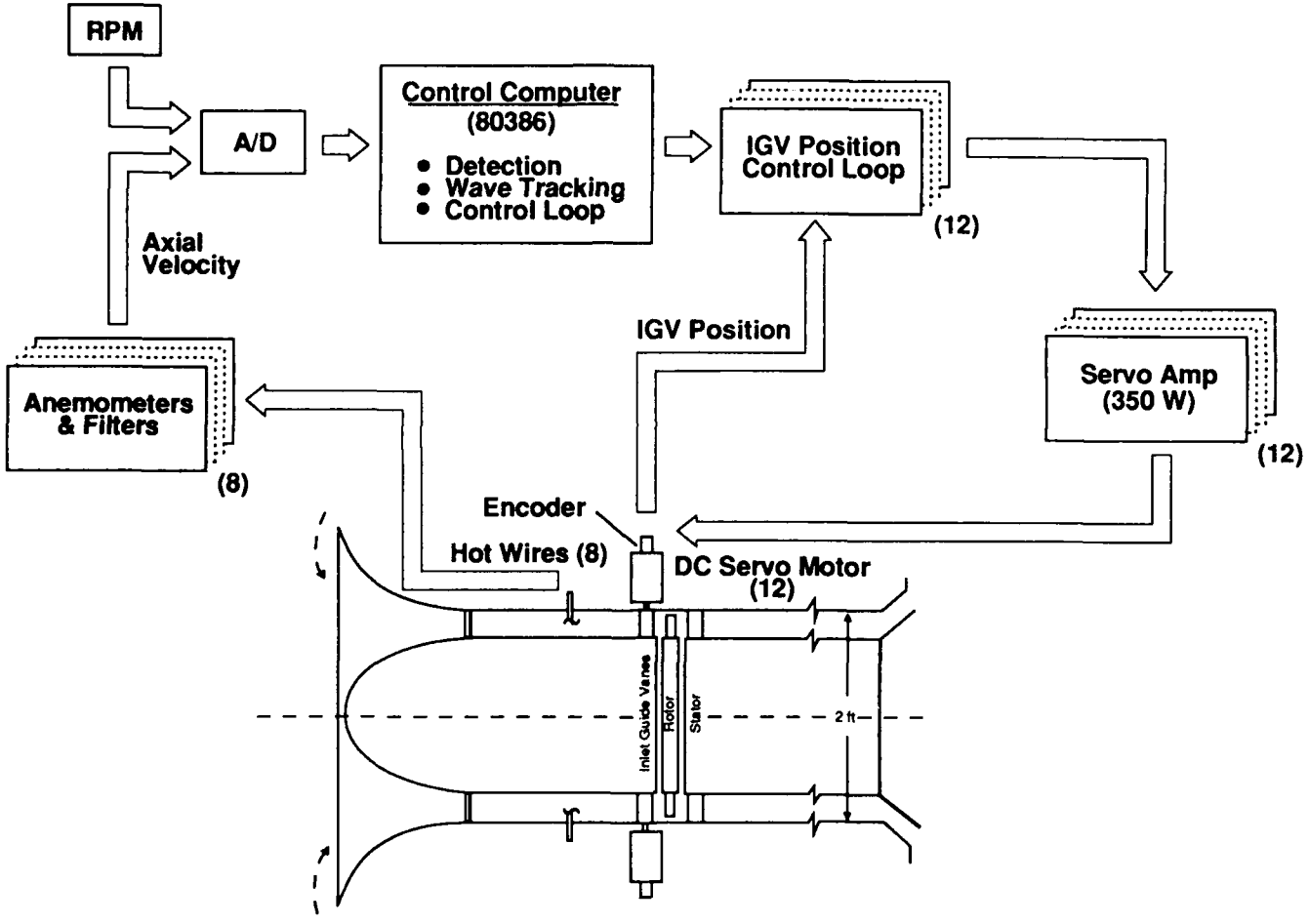

Fig. 8: Schematic of the hardware implementation of the actively stabilized axial compressor

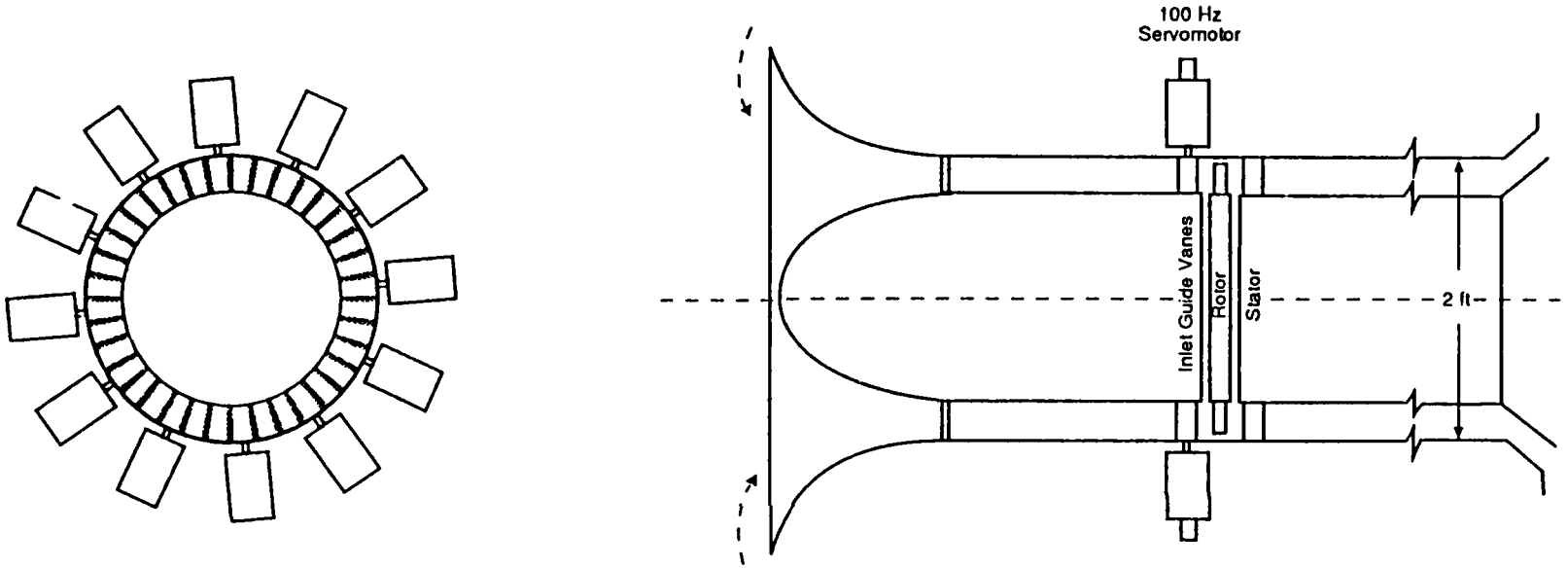

Fig. 9: Single-stage low speed research compressor with "wiggly" inlet guide vanes

PART II: ROTATING WAVES AS A STALL INCEPTION INDICATION IN AXIAL COMPRESSORS

Abstract

Stall inception has been studied in two low speed compressors (a single-stage and a three-stage) and in a high speed three-stage compressor using temporally and spatially resolved measurements. In all three machines, rotating stall was preceded by a period in which small amplitude waves were observed travelling around the circumference of the machine at a speed slightly smaller than the fully developed rotating stall cell speed. The waves evolved smoothly into a stall without abrupt changes in phase or amplitude, implying that, in the machines tested, the prestall waves and the fully developed rotating stall are two stages of the same phenomenon. The growth rate of these disturbances was in accord with that predicted by current analytical models. The prestall waves were observed both with uniform and with distorted inflow, but were most readily discerned with uniform inflow. Engineering uses and limitations of these waves are discussed.

Introduction

Axial compressors are subject to two distinct aerodynamic instabilities which can severely limit compressor performance. These are rotating stall and surge. Rotating stall is characterized by a wave travelling about the circumference of the machine, surge by a basically one-dimensional fluctuation in mass flow through the machine. Whether these phenomena are viewed as distinct (rotating stall is local to the blade rows and dependent only on the compressor characteristics, while surge involves the entire pumping system -- compressor, piping, plenums, and throttle) or as related (both are eigenmodes of the compression system with surge being the zeroth order mode), they cannot be tolerated during compressor operation. Both rotating stall and surge reduce the pressure rise in the machine, causing rapid heating of the blades, and can induce severe mechanical distress.

The instabilities are commonly avoided by operating the compressor at a reduced pressure rise so as to leave a safety margin (the so-called stall margin) between the operating point of the compressor and the point at which the machine surges. The requirement for a surge margin reduces the available operating pressure rise from a given machine and often reduces the operating efficiency as well. Reduction of surge margin can then translate directly into compressor weight and efficiency improvement so that there is great practical incentive to reducing the surge margin required. In the high speed compressors common to aircraft engines, rotating stall and surge are closely coupled. As the machine moves along a constant speed operating line toward lower mass flow (Fig. 1), it first goes into rotating stall, which then "triggers" the surge, often after only one or two rotor revolutions. Thus, surge and stall must both be considered; the compressor surge line could really be considered the rotating stall line, and the surge margin the stall margin.

We are aware of several alternate approaches under investigation to reduce the stall margin required. They can be considered to fall into one of two categories -- those based on moving the operating point close to the stall line in situations when surge and stall do not threaten, and those based on moving the surge line itself and thus increasing the stable range of the compressor.

Efforts in the former category include: (a) a real-time assessment of the stall margin by correlation of the instantaneous aircraft flight parameters with the test stand compressor stall behavior; and (b) stall avoidance in which the control system detects rotating stall and then quickly moves the compressor operating point to higher mass flows, away from stall. Dynamic compressor stabilization is in the second category. Here, the stall point is moved to lower mass flows by active feedback control. This and stall avoidance rely on the use of real-time measurements within the compressor to assess the machine stability. Clearly, the earlier a control system can detect a stall or even an incipient stall, the more effective (and less demanding) the control becomes.

This paper describes an experimental study of the rotating stall inception and growth process in three axial compressors. Its goals were both to illuminate the manner in which stall cells are born and developed, and also to establish, as suggested by theory, whether real-time information can be extracted from the compressor which would warn of an impending stall before the stall actually developed. This stall warning or "precursor" could have significant practical benefit if the warning is sufficiently in advance of the stall as to permit time for control system response. The longer the warning, the greater the potential utility.

In the following sections, we review the relevant theoretical background on rotating stall development, describe the experimental arrangement, present data for three compressors and under a variety of operating conditions, and finally comment on the generality of these findings and their usefulness.

Background

A large amount of experimental data taken over the last twenty years shows that, if measured at a single point in the compressor, rotating stall is seen as a sudden event with a growth period on the order of the stall cell period. Stall detection schemes based on this sort of measurement have thus not been successful in providing appreciable warning time. During the same period, however, a theoretical basis for the description of rotating stall has arisen based on the understanding of rotating stall as one class of the natural instabilities of the compression

system. At its current state of development (Moore and Greitzer, 1986), the model describes the time evolution of surge and rotating stall in a compressor treated mathematically as a two-dimensional incompressible device (i.e. large hub-to-tip ratio) with three-dimensional phenomena represented only through empirical inputs. The results of a prediction by this model (Fig. 2) show an instability evolving as a small amplitude wave in axial velocity which grows as it travels around the circumference of the compressor until it triggers the large nonlinear disturbance (a surge). It is in the context provided by this model that we initiated this work.

As shown in the appendix, we can describe the stability of a compressor in terms of the time evolution of an asymmetric perturbation of the velocity potential, $\tilde{\phi}$, namely

$$\tilde{\phi} = \sum_{|k|\neq 0} b_k \, e^{|k|\eta - \sigma_k \xi} \, e^{i(k\theta - \omega_k \xi)} \tag{1}$$

Each Fourier mode (k) is the product of two exponentials. $\mathrm{Exp}(i[k\theta-\omega_k\xi])$ represents a travelling wave function of circumferential position (θ) and time (ξ); ω_k is the wave frequency. $\mathrm{Exp}(|k|\eta-\sigma_k\xi)$ gives the dependence of the wave on axial position (η) and time; σ_k is the damping of the wave. (By analogy, Eq. (1) describes the behavior of an oscillator rotating about the circumference of the compressor.) The growth of the wave (i.e. the stability of the compressor) is determined by the instantaneous damping σ. When the damping is negative, the oscillations grow and the flow in the compressor is unstable. Active control schemes aim to increase this damping. Here we make use of Eq. (1) to design an experiment to detect the rotating waves and measure the instantaneous stability of the compressor.

McDougall (1988, 1989) was the first person known to the authors to have made measurements of these rotating waves. Examining a single-stage, low speed compressor, he found small disturbances rotating about the machine just prior to the onset of stall, in qualitative accord with the above theory. He included a good summary of previous experimental work.

To explore the use of the travelling waves as a stall precursor or warning, we pose the following questions:

- Do prestall waves exist in most (many, all) compressors?

- At what rate do these waves grow? How long do they persist?
- At what rate do they travel?
- How can they be observed?
- How is this behavior affected by inlet distortion and mass flow transients?
- Do high speed (compressible) machines behave similarly?

In sum, these questions address both the basic assumptions inherent in the Moore/Greitzer model and its utility in providing real-time warning of an impending compressor stall. In the following, we experimentally examine these issues.

Experimental Apparatus

Prestall behavior of three compressors was examined -- two low speed and one high speed machine. The low speed, single-stage compressor consisted of IGV's, rotor, and stator. It is described in more detail by Johnson (1987) and Lee (1988). The low speed, three-stage compressor is described by Gamache (1985) and Lavrich (1988). Speedlines are shown in Fig. 3. Both low speed compressors were operated at tip speeds below 100 m/s, so that compressibility effects were negligible. The high speed, three-stage compressor is a modern experimental design at Pratt & Whitney Div., United Technologies Corp. This machine was equipped with fast-acting bleed valves which quickly moved the operating point away from stall when it occurred to prevent mechanical damage. Experiments on that machine were conducted by Pratt & Whitney personnel and the raw data provided to the authors.

Instrumentation

All the compressors were outfitted with standard pitot-type instrumentation to provide the steady state operating characteristics of the machines. Time-resolved instrumentation consisted of hot wire anemometers in the low speed compressors (oriented so as to measure axial velocity), and wall-mounted, high frequency response, static pressure transducers in the high speed compressor. The high speed machine had eight transducers mounted about the circumference at each of four axial stations. The low speed machines had either eight transducers at a time at one axial station or

three rows of four mounted at various stations. The low speed data was digitized in real time (with suitable low pass anti-aliasing filters), while the high speed data was first recorded on analog magnetic tape. All data was d.c. coupled.

The hot wires were calibrated in place prior to each test to a velocity accuracy of ±3%. The net resolution of the anemometers was 0.8% of the average prestall axial velocity. The pressure transducers in the high speed experiment were calibrated by Pratt & Whitney personnel. One pressure transducer had significantly less amplitude than all its neighbors so that its gain was raised in post-test processing to yield the same level of RMS fluctuations.

Signal Processing and Probe Placement Considerations

Experiments were conducted to look for small amplitude travelling waves whose spatial and temporal structure was important. Probe placement and signal processing were therefore carefully considered. Also, since the measurements in both time and space were discrete, aliasing was of concern in both dimensions.

Probe number was determined by the number of spatial harmonics (N) to be examined. 2N+1 measurement points are required about the circumference at each axial station. Eight were used in most cases, providing definition of the first three spatial harmonics. We expected most of the energy in the lowest order modes but were still concerned about aliasing of the higher order modes and blade passing phenomena. Since the small upstream disturbances due to the compressor are irrotational, they decay exponentially with upstream distance. Thus, the first measurements were made one-half compressor radius upstream so that the fluid mechanics would act to filter out the high order (shorter length) scale disturbances. These disturbances appeared not to be a problem and measurements were subsequently made throughout the compressors.

We expect the waves to travel about the circumference at close to the rotating stall frequency, 20-50% of rotor shaft speed. Thus, the data was digitally band-pass filtered in the computer. The pass band was 0.1 to 1.2 times rotor shaft frequency. These frequencies were determined mainly by trial and error by comparison to the unfiltered data. Due care was taken to

preserve phase information.

The filtered time histories of the individual sensors could now be used to calculate the modal information by taking a discrete Fourier transform in space about the circumference of the compressor at each point in time. Given N measurements about the machine, the complex Fourier coefficients for each mode k are given by

$$C_k = \frac{1}{N} \sum_{n=0}^{N-1} V_n \exp\left[-\frac{2ikn\pi}{N}\right] \tag{2}$$

where V_n is the axial velocity at angular position n. For most measurements described herein, eight sensors were used so that N = 8, $-3 \leq k \leq 4$, and, since V_n is real, C_k and C_{-k} are complex conjugates. The Fourier coefficients contain all the information on the wave position and amplitude as a function of time.

Low Speed Compressor Experiments

The low speed single-stage and three-stage compressors were used to explore the nature of the stall initiation process and the prestall travelling wave behavior, examine alternate sensor placements, establish the travelling statistical behavior, and determine the influence of inlet distortion and throttle (mass flow) transients.

Quasi-Steady Stalling Behavior

During these experiments, the compressor operation was first stabilized very close to stall (within 0.005 in flow coefficient of the stall point in Fig. 3) and then the throttle closed very slowly so that machine would stall within 10 to 20 seconds. Data was taken during this entire period from the eight hot wires about the compressor annulus. Unless otherwise specified, the hot wires were positioned 0.5 compressor radii upstream of the IGV's.

Figure 4 shows the time history of the axial velocity as measured by a single sensor during the stalling transient. Here, time equal to zero has been defined, somewhat arbitrarily, as the time at which the velocity has grown to 50% of the fully stalled maximum excursion. As can be seen,

the prestall fluctuations have a very small amplitude compared to the rotating stall itself, during which the velocity fluctuations are greater than 100% of the prestall mean velocity. The time history of all eight sensors about the circumference is shown in Fig. 5 on a magnified scale, and regular disturbances can be observed here for a considerable time before the stall. The amplitude of the first Fourier component (the modulus of C_1), calculated from this data with Eq. (2), is shown in Fig. 6. This is a measure of the strength of the first mode of the rotating wave. Although it is very small compared to the amplitude during fully developed rotating stall ($t > 0$), it is non-zero for a considerable period (90 revs) before the stall. The argument of C_1 is the phase angle of the travelling wave, and this is shown in Fig. 7 along with the phase of the second harmonic (arg C_2). The slopes of these lines are the speeds at which the harmonics of the waves travel around the compressor annulus (the annulus has been unwrapped in the figure so that 2π radians is one trip around). The key point from this figure is that the phase speed of the first harmonic of the travelling waves is essentially constant and readily discernible for almost 90 rotor revolutions before the stall. There is a small shift in wave speed at the stall point, from 0.35 rotor speed before the stall to 0.38 rotor speed with fully developed stall. For this experiment, the second harmonic signal is too weak (i.e. the signal-to-noise ratio is too small with the instrumentation used) to give useful information.

A three-dimensional representation of the C_1 component during the last 20 revs before stall is shown in Fig. 8 in a format similar to that of the calculation shown in Fig. 2. The wave nature of the disturbance in this machine is quite evident.

The behavior of a system described by Eq. (1) is such that, near the neutral stability point (damping, σ, close to zero), the growth or damping of the oscillations (in this case the travelling waves about the circumference) should be sensitive to the level of disturbances in the system (the forcing). Re-examining Fig. 7 we see that there is a stretch of constant phase speed between -140 and -125 revs, followed by a period of ill-defined speed to -95 revs, and then finally constant phase speed until stall at 0. In the context of the model, we interpret this to imply that the damping of the compressors (σ) is very close to zero, so that the travelling waves are very lightly damped.

They can grow and then decay, depending upon the level of external disturbances forcing the system. Thus, we might expect to see some test-to-test variation in the time during which the prestall waves propagate strongly enough to be evident. This was examined by carrying out nine tests on the three-stage compressor under nominally identical conditions. The mean prestall period of constant wave propagation was approximately 60 rotor revolutions with a high of 250 and a low of 30. (In all cases, the wave speed was 35% of rotor speed before stall and 38% during stall.) Thus, there is considerable statistical variation in the time during which the prestall waves were tracked. We have not characterized the source of these variations but hypothesize that they may be related to low amplitude disturbances (noise) convected into the compressor inlet. Overall, these data establish that rotating stall starts as a small amplitude travelling wave in the two low speed compressors studied.

Throttle Transient and Inlet Distortion Effects

The influence of throttle (mass flow) transients and inlet distortion (spatially non-uniform inlet total pressure) is of interest since we know from engine experience that rotating stall is often associated with these phenomena. Experiments were conducted on both the one- and three-stage compressors with qualitatively similar findings.

The throttle transient experiments were conducted at three different throttle rates which varied by a factor of 150 to 1, the fastest corresponding to a flow coefficient range of 0.1 (Fig. 3) per 100 rotor revolutions. Distortion was generated by blocking off 180° of the annulus approximately one compressor diameter upstream of the IGV's. This generated a roughly square wave total pressure distortion with an amplitude of 0.5 dynamic heads based on the mean velocity. The time-resolved mass flow for these experiments was estimated using the average of the hot wire measurements. The time derivative of the mass flow at stall was obtained by a least-squares fit to the last second of data preceding stall. The absolute uncertainty of these measurements was estimated at 5%.

The prestall behavior of the three-stage compressor with a uniform (Fig. 9) and distorted

(Fig. 10) inlet flow was measured at three throttle rates. In both cases, the stall is always preceded by readily discernible low amplitude waves travelling at constant speed. The prestall duration of these waves is inversely proportional to the throttle rate. This is consistent with the stability model in that the higher the throttle rate, the less time the machine spends at the low flow (ϕ) region of the speedline which has low damping (σ) and, thus, the shorter the period during which the prestall waves can propagate and grow. The flow coefficient (ϕ) at which the prestall waves are first discerned is shown in Fig. 11 for the single-stage compressor as a function of throttle rate ($d\phi/dt$), which shows that the waves appear at close to the same value of ϕ independent of the throttle rate (over the rates examined, the waves appear slightly later as $d\phi/dt$ increases). The prestall period of constant travelling wave speed (the straight line segments in Figs. 9 and 10) is plotted in Fig. 12 as a function of the throttle rate and exhibits roughly a $1/\phi$ dependence.

The effects of inlet distortion are evident in Figs. 9-11. The prestall period at near-zero throttle rate is at least an order of magnitude smaller with the inlet distortion than without. This behavior is also consistent with a model such as that described by Eq. (1) if we consider that wave propagation velocity and amplitude are functions of the local flow conditions and thus will vary about the annulus in the case of distorted inflow. We infer that the signal processing technique used here (Eq. (2)), which looks only for sinusoidal waves, is not optimal with inlet distortion. Instead, a method based on the true eigenmodes of the system -- and is thus independent of wave shape -- should be used. (These could be calculated using the procedure outlined by Hynes and Greitzer (1987).)

Sensor Placement Influence

Data was taken with the circumferential array of sensors at five different axial stations upstream, downstream, and between the blade rows of the single-stage compressor to evaluate the influence of sensor placement on travelling wave detection. The waves were clearly discernible at all axial stations. The amplitude increased as the sensors were moved downstream but so did the noise, so that the signal-to-noise ratio varied considerably. This is reflected in Fig. 13, which

shows the standard deviation divided by the mean of the amplitude of the first harmonic ($|C_1|$) of the wave. The signal is cleanest upstream of the IGV's.

Disturbance Growth Rate

The model summarized by the Eq. (2) describes the evolution of the travelling wave system in the compressor and so should be capable of quantitatively predicting the growth of the waves. The only inputs required for the calculation are the compressor geometry (lengths, blade stagger angles, etc.) and the steady state compressor characteristic. A comparison of a model prediction with experimental measurement for the single-stage low speed compressor (Fig. 14) shows good agreement. (Note that, since the initial conditions for the model are not known, the zero time reference for the data and calculation are arbitrary.) In our view, this agreement helps establish the validity of the model.

High Speed Compressor Experiments

*The wall static pressure history measured just upstream of the first stage stator in a three-*stage high speed compressor with uniform inlet flow during a slow throttle transient is shown in Fig. 15. The phase speed of the first two spatial harmonics of this data as calculated using Eq. (2) shows that the second harmonic is most readily discerned, Fig. 16. (The prestall amplitude [$|C_N|$] is considerably higher for the second harmonic as well.) The wave speed is constant for more than 100 rotor revolutions, behavior quite similar to that of the low speed compressors. Comparison of the phase speed of the second harmonic as measured at the leading edge of each of the three stator rows (Fig. 17) shows the signal to be the clearest at the first stage. Other measurements and calculations indicate that the first stage stalls first under these flow conditions.

Time history of the wall static pressure on the high speed compressor with a 180° inlet distortion during a very slow throttle transient is shown in Fig. 18. Here we see that the prestall disturbance level is not uniform about the circumference. The phase speeds of the first two spatial harmonics of this data are not readily discerned (Fig. 19) except for a short stretch of the second harmonic. The reason for this may be inferred from the time histories in Fig. 18 which show

prestall disturbances of relatively high amplitude originating on sensor 7 (low flow region) being strongly attenuated as they move by sensors 6 and 5 (high flow region). Cross-correlations of adjoining sensors were taken which indicated a maximum at a time delay corresponding to 13% of rotor speed. A time history of the maximum value of the cross-correlation between sensors 0 and 1 shows (Fig. 20) strong correlation for the period (-100 to -140 revs) during which constant phase speed of the second harmonic can be discerned. The correlation increases again as stall is approached.

These high speed data support the view that the distorted compressor acts (crudely) as parallel compressors with wave speed and damping varying about the circumference as the local flow field varies. The cross-correlations of both high and low speed compressor data show that there is local real-time information available on the instantaneous compressor stability, which may require more sophisticated data processing than represented by Eq. (2).

Application of Signal Processing to Compressor Stability Estimation

We believe that the experimental data presented has verified the applicability of the compressor stability model represented by Eq. (1), at least to the three machines studied. In this view, the compressor stability is directly linked to the growth or decay of the travelling waves and rotating stall is simply the mature form of this wave evolution. The question of stall warning thus becomes one of the identifications of the waves and the estimation of their growth rate. The practical implementation of this approach is complicated by two factors. The first is that, during transients, the growth of the disturbance can be quite fast compared to its fundamental period, and this reduces the effectiveness of the more simple time spectra techniques such as fast Fourier transforms (FFT). The second is that the circumferentially nonuniform flowfield of a compressor with inlet distortion means that wave growth and propagation rates are nonuniform about the circumference, greatly reducing the effectiveness of the simple spatial analysis approach of Eq. (2). To extract the maximum information available from the compression system, more sophisticated signal processing is thus required to accommodate the wide ranging temporal and spatial variations

of the compressor stability process. In the following sections, we address only the problem of temporal variability, leaving the spatial variation problem to a later time.

As sketched in the Appendix, the wave behavior of Eq. (1) is associated with the behavior of the Fourier modes (a_k) of the velocity potential of the form

$$\frac{da_k}{d\xi}(\xi) = C_k a_k(\xi) \tag{3}$$

which is the description of a first order system in which C is a constant that depends on geometry. Two interrelated approaches can be brought to bear on this system: spectral analysis and system identification techniques.

Spectral Analysis

In its simplest form, spectral analysis can be used to estimate the power spectral density (PSD) of each important spatial harmonic of the flowfield. A peak should be present at the frequency of the travelling waves (20-40% of rotor rotation) with its height being proportional to the power in the wave. Monitoring the time evolution of this peak yields information on the wave growth and thus the compressor stability. This should be a more discerning technique than the simple phase speed plots (as in Figs. 7, 9, 10, and 15), since the phase is driven by the strongest frequency component present in the signal which is not necessarily that of the travelling waves of interest, while the PSD will not be so affected.

The fast Fourier transform (FFT) is often used to calculate PSD's but has two limitations that are important in this application. The first is that the frequency resolution is proportional to the time interval available for analysis. The second is that the absence of information outside this interval distorts the spectral response. These problems can be particularly troublesome with very short data records and data with time varying spectral content, both of which are present here. Other techniques have been developed, however, which largely overcome these problems. The one adopted here is based on the fitting of a linear model to the data (Kay and Marple) which has the advantage of resolving very sharp spectral features from short data records.

A typical PSD of the first spatial harmonic of the axial velocity in the single-stage low speed compressor before stall clearly shows the prestall travelling wave power (at 0.38 rotor rev's in this case) (Fig. 21). The amplitude of the peak at this frequency increases as the flow coefficient is decreased (Fig. 22), implying that the power in the waves is related to the compressor stability. Note that the power in this first spatial harmonic is considerably reduced when inlet distortion is present, implying that a more sophisticated technique may be required. The direct spectral approach lets us identify flow features but does not directly yield information on compressor stability, since the height of the peak is a function both of the damping of the system and the amplitude of the excitation. System identification techniques can help us in this.

System Identification

We have a model (Eq. (1)) which we believe to be a good description of the physical system, compressor stability. System identification is a technique which allows us to estimate the values of the physical parameters describing the compressor stability by fitting data to the model in real time. A discrete time series y_n can be modelled as the solution of a difference equation

$$y_n = b_1 y_{n-1} + \ldots + b_p y_{n-p} + v_n \qquad (4)$$

where v_n is a noise term (turbulence, electrical noise, convected disturbances, etc.). The p coefficients of b_i in Eq. (4) can be estimated by fitting a p^{th} order linear model to the data. The advantage in this application is that only the parameters need be estimated since the form of the model has been established. Filtering can be used to enhance the results by removing any unmodelled dynamics and correlated noise.

The model can be fit to the data in either the time or frequency domain. The time domain was used here since it is well suited to real-time implementation. Least squares techniques can be used recursively by updating the model parameter estimates for each new data point (Goodwin; Friedlander) and "forgetting" old data to track time varying parameters. We refer the reader to Garnier (1989) for further details.

We rewrite the wave model of Eq. (3) for each spatial harmonic in the form of Eq. (4) as an

ordinary differential equation

$$\frac{dC_{-k}(\xi)}{d\xi} = (\sigma_k - i\omega_k)\, C_{-k}(\xi) + V(\xi) \qquad (5)$$

where C_{-k} is the harmonic of Eq. (2), σ_k the travelling wave damping, ω_k the wave frequency, and $V(\xi)$ the driving noise. In fitting this model to the data at any instant in time, we have estimated the wave damping and frequency for each spatial harmonic. To the degree to which the model of Eq. (2) is valid, wave damping and compressor stability are equivalent. Thus, a real-time estimate of σ is an instantaneous measure of the compressor stability.

The fit of Eq. (5) to the power spectral density of the first spatial harmonic of the single-stage low speed compressor is shown in Fig. 23 for undistorted flow and Fig. 24 for distorted inflow. In both cases, the model fits the general shape of the data well. The distorted data shows a peak frequency of -0.3 which is too close to travelling wave frequency to simply filter, so a second order model was employed to account for this peak. All of the distorted inlet data subsequently used a second order model.

The damping coefficient (σ_1) of the first spatial harmonic estimated with this technique from the data is shown as a function of flow coefficient in Fig. 25, with and without inlet distortion. With undistorted inflow, the compressor is stable until the damping approaches zero. With inlet distortion, the damping is much greater than for the undistorted case away from stall, but drops much faster with flow coefficient until the machine stalls at a somewhat higher value of σ. The frequency of the first spatial harmonic (ω_1) is the same with and without inlet distortion and independent of flow coefficient. The influence of throttle transients is apparently to steepen the drop in damping with flow coefficient as well as delay the stall to a somewhat lower flow coefficient (Fig. 26). How much of the delay is due to unmodelled inertia effects within the compressor and how much is due to time lags in the algorithm has not been determined.

Discussion -- Engineering Uses of Prestall Waves

As we have demonstrated, the compressor damping can be directly estimated on-line, given

sufficient experimental data. The damping is a direct measure of the compressor stability over the period represented by the data and is thus an indication of the likelihood of stall. Whether or not a machine stalls at a given time is determined not just by the system damping, however, but also by the nature and level of the system forcing, which we have not addressed here. The damping by itself, though, is an indication of the susceptibility to the excitation and thus to stall.

One use of this information would be to establish the surge line of a new compressor on the test stand without the necessity of actually stalling the machine. This avoids the requirement to automatically "dump" the compressor to a higher mass flow each time surge is encountered (required to prevent mechanical damage), and may save expensive test time. A second possible use is the location within a multistage compressor of the blade row in which the stall starts. The data from the three-stage low and high speed compressors indicate that the waves are most clearly discerned at this axial station.

One of the most intriguing and challenging uses would be as a real-time prestall indicator in an operational engine. The limited data presented herein suggest that sufficient warning time may be available (tens to hundreds of rotor revolutions) for a more or less conventional engine control system to take corrective action (changing fuel flow, nozzle area, vane settings, etc.) -- thus reducing the surge margin required and the associated penalties. There are many questions which must be examined before the practicality of such a scheme could be established -- not just ones of compressor dynamics as addressed here but also more applied ones such as sensor reliability, computational requirements, system complexity, overall dependability, and cost.

An even more challenging use of these prestall waves is as a control signal for an actively stabilized compressor, one in which external feedback control is used to increase the compressor stability by increasing the wave damping (σ). Epstein, Ffowcs Williams, and Greitzer (1989) first suggested this approach and an ongoing effort was described by Dugundji et al. (1989), who are "wiggling" the inlet guide vanes of a single-stage low speed compressor to cancel the travelling waves.

In order for any of these applications to become practical, considerably more work than

presented here must be done on the sensing and identification of these circumferentially travelling waves. In particular, the sinusoidal nature of the signal processing inherent in Eq. (2) must be relaxed in order to account for more complex systems, such as those with inlet distortion. Algorithm selection and adaptation to minimize the length of time data must be taken to identify the waves is another area where work is needed. We believe these extensions of the present work are straightforward, although not necessarily simple. Somewhat more complicated (or at least tedious) is the analytical inclusion of compressibility to accurately model high speed machines (although the high speed data examined to date is quite similar to that from low speed machines).

An extremely fundamental question is how general are the results presented herein -- do some, most, or all compressors exhibit this prestall wave behavior? We make no claims beyond the results for the compressors we have examined. All exhibit similar behavior, behavior in accord with the theoretical models of compression system stability.

We know of no reason why such waves should not exist in all compressors, although we would not be at all surprised if their strength and duration varied to such a degree as to render them very difficult to discern in some machines. Only more data can answer this question.

Conclusions and Summary

We have examined the flow in two low speed and one high speed compressor. The experiments in these machines show that:

1. Small amplitude (less than 5% of the stall amplitude) waves can be discerned travelling about the compressor annulus at close to the rotating stall speed for 10-200 rotor revolutions prior to the onset of rotating stall.
2. These waves grow into a fully developed rotating stall without apparent discontinuity in phase or amplitude.
3. The prestall period during which these waves were discerned varied by a factor of 5 at a single flow condition, apparently stochastically.
4. The behavior was similar in both the high and low speed compressors, except that the first

spatial harmonic was the strongest in the low speed machines and the second in the high speed.

5. In multistage compressors, the prestall waves are clearest in the stage which stalls first.
6. Inlet distortion reduces the period during which the prestall waves were discerned, using techniques based on the assumption of sinusoidal waves about the circumference.
7. The data fit the model of Moore and Greitzer quite well, including both the qualitative behavior of the prestall waves and the quantitative prediction of the growth rates.

Overall, we believe that this wave behavior can be a useful tool in the study of compressor stability. Future work should encompass more sophisticated signal processing to account for distorted inflow, include the effects of compressibility, and extend the experimental work to a larger number of compressors.

Acknowledgements

The authors would like to acknowledge the assistance of Mr. James Paduano, Dr. G.R. Guenette, and Professor L. Valavani. We thank our colleagues Dr.'s I.P. Day and J.P. Longley for their stimulating discussions and thoughtful comments. The authors are grateful to Pratt & Whitney Government Engines Business for providing the high speed compressor data and permission to publish it. This work was supported by the Office of Naval Research, Dr. R.J. Hansen technical monitor, and by the Air Force Office of Scientific Research, Captain H. Helin and Dr. J. McMichael technical monitors. We thank these gentlemen both for their support and active encouragement.

References

Dugundji, J., Epstein, A.H., Garnier, V., Greitzer, E.M., Guenette, G.R., Paduano, J., Silkowski, P., Simon, J., Valavani, L., "A Progress Report on Active Control of Flow Instabilities: Rotating Stall Stabilization in Axial Compressors," AIAA Paper 89-1008, March 1989.

Epstein, A.H., Ffowcs Williams, J.E., Greitzer, E.M., "Active Suppression of Aerodynamic Instabilities in Turbomachines," J. of Propulsion and Power, Vol. 5, No. 2, March-April 1989, pp. 204-211.

Friedlander, B., "The Overdetermined Recursive Instrumental Variable Method", IEEE Transactions on Automatic Control, Vol. AC-29, No. 4, April 1984, pp 353-356.

Gamache, R.N. "Axial Compressor Reversed Flow Performance", Ph.D. Thesis, MIT Dept. of Aeronautics and Astronautics, May 1985.

Garnier, V., "Experimental Investigation of Rotating Waves as a Rotating Stall Inception Indication in Compressors," M.S. Thesis, Dept. of Aeronautics and Astronautics, MIT, June 1989.

Goodwin, G.C., Sin, K.S., Adaptive Filtering, Prediction and Control, Prentice Hall, 1984.

Graupe, D., Time Series Analysis, Identification and Adaptive Filtering, Robert E. Krieger Publishing Company, Malabar, Florida, 1984.

Greitzer, E.M., "Surge and Rotating Stall in Axial Compressors, Part I: Theoretical Compression System Model", and "Part II: Experimental Results and Comparison with Theory", ASME J. of Eng. for Power, April 1976.

Greitzer, E.M., Moore, F.K., "A Theory of Post-Stall Transients in Axial Compressors: Part II - Applications," ASME J. of Eng. for Gas Turbines and Power, Vol. 108, January 1986, pp. 231-239.

Hynes, T.P., Greitzer, E.M., "A Method for Assessing Effects of Circumferential Flow Distortion on Compressor Stability," ASME J. of Turbomachinery, July 1987.

Johnson, M.C., "The Effect of Hub Treatment on Compressor Endwall Flowfield", M.S. Thesis, MIT Dept. of Aeronautics and Astronautics, January 1985.

Kay, S.M., Marple, L.S,, "Spectrum Analysis - A Modern Perspective", IEEE Proceedings, Vol. 69, No. 11, November 1981, pp1380-1419.

Lavrich, P.L., "Time Resolved Measurements of Rotating Stall in Axial Flow Compressors", PhD Thesis, MIT Dept. of Aeronautics and Astronautics, January 1988.

Lee, N.K.W., "Effects of Compressor Endwall Suction and Blowing on Stability Enhancement", M.S. Thesis, MIT Dept. of Aeronautics and Astronautics, September 1987.

Ljung, L., Morf, M., Falconer, D., "Fast Calculations of Gain Matrices for Recursive Estimation Schemes", International Journal of Control, Vol. 27, No. 19, 1978, pp 1-19.

Marple, L.S., "A New Autoregressive Spectrum Analysis Algorithm", IEEE Transactions on Acoustics, Speech, and Signal Processing, Vol. ASSP-28, No. 4, August 1980, pp 441-454.

McDougall, N.M., "Stall Inception in Axial Compressors", PhD Thesis, Cambridge University, 1988.

McDougall, N.M., Cumpsty, N.A., Hynes, T.P., "Stall Inception in Axial Compressors", submitted to 1989 ASME Gas Turbine Conference.

Moore, F., K., "A Theory of Rotating Stall of Multistage Axial Compressors: Part I - Small Disturbances", ASME Journal of Engineering for Power, March 1983.

Moore, F.K., Greitzer, E.M., "A Theory of Post-Stall Transients in Axial Compressors: Part I - Development of the Equations," ASME J. of Eng. for Gas Turbines and Power, Vol. 108, January 1986, pp. 68-76.

APPENDIX A
BRIEF DESCRIPTION OF THE BASIC STALL INCEPTION MODEL

The underlying ideas of stall inception and the approach to the sensing are connected by a simple model which provides a framework to view the phenomenon. Two points concerning rotating stall onset should be stressed at the outset. First, when one considers the actual flow, there are several disparate length scales involved. What is needed is a description of the interaction between flow on the blade element scale (length scales on the order of blade pitch or smaller) and the wave structure in the annulus (flow phenomena with length scale of the radius of the machine). Second, there is strong evidence that the "region" of the blade passage that is responsible for rotating stall is the endwall. Put another way, the mechanism of stall is generally not two-dimensional, and treatments that view it as such miss the essential fluid mechanics of the situation.

The model that we use was developed by Moore (1984) for rotating stall and later extended by Moore and Greitzer (1986) to encompass generalized disturbances, i.e. combined rotating stall and surge in multistage machines. Here we examine just onset of the former. In the model, the disturbances upstream and downstream of the compressor are viewed as two-dimensional; this would be expected to be the case in compressors of high hub-tip radius ratio. The blade row description, however, makes use of the measured steady-state compressor pressure rise characteristic, with correction to account for unsteadiness. In a very real sense, then, three-dimensional effects are accounted for because the behavior at the endwalls which can be a strong contributor to the "turn over" in the pressure rise versus flow curve, has been included. Although both the blade row modelling and the coupling between large scale disturbance field and blade element dynamics are crude, the model does appear to contain the necessary elements for a description of the stall process. It is this point, with the simplicity as a secondary issue, that suggests use of such a description in the sensing and control problem.

The derivation of the relevant equations have been given several times elsewhere so that we will only sketch out the steps leading to the equations that we need. The flow fields considered are two-dimensional, inviscid, and incompressible upstream and downstream of the compressor. The

flow in these two regions is coupled by three matching conditions across the compressor, two kinematic and one dynamic. With these conditions, representing the modelling of the unsteady and non-axisymmetric compressor performance, we describe the flow in each region as follows.

Upstream Flow Region

Upstream of the compressor the flow is irrotational, and a velocity potential can be used. We express the velocity as a uniform steady flow plus a small asymmetric perturbation which is the gradient of a potential, ϕ, satisfying the two-dimensional Laplace equation, with periodic boundary conditions and vanishing far upstream. ϕ can thus be expressed in terms of its spatial Fourier coefficients as

$$\tilde{\phi}(\eta,\theta,\zeta) = \sum_{|k|\neq 0} a_k(\zeta)\, e^{|k|\eta}\, e^{ik\theta} \qquad (A.1)$$

Across the Compressor

As stated, there are three matching conditions that are applied across the compressor. The first is that the local axial velocity distribution is the same at all axial stations through the compressor. This approximation is made on the basis of the small opportunity for circumferential redistribution within typical compressors. Order of magnitude arguments imply that it is most correct for disturbances with low order harmonic content, and these are precisely the ones of interest here. Discussion of the assumption can be found in the papers by Dunham (1965) or Stenning (1980).

Explicitly, the matching condition is

$$u_u\,(0,\theta,\zeta) = u_d\,(0,\theta,\zeta)$$

where subscript "u" refers to upstream and "d" to downstream.

The second matching condition is constant leaving angle at compressor exit. This is also an approximation, but it should be adequate for the solidities that are of practical concern.

The last matching condition can be expressed in terms of a relation between the pressure

difference across the compressor and the local axial velocity and its derivative. As developed by Moore (1984) (see also Moore and Greitzer, 1986) the matching condition can be written in a linearized form as

$$\left[\frac{\delta P_2 - \delta P_{t_1}}{\rho U^2} = \left(\frac{d\psi}{d\phi}\right)\delta\phi - \lambda\frac{\partial\delta\phi}{\partial\theta} - \mu\frac{\partial\delta\phi}{\partial\xi}\right]_{(0,\theta,\xi)} \tag{A.2}$$

The quantity $(d\psi/d\phi)$ is the slope of the steady-state compressor characteristic and λ and μ are non-dimensional parameters associated with the inertia of the fluid in the compressor blade passages. Their precise values are not critical here since what is of most interest is the general form of the solution, but for reference μ is roughly twice λ and is of order unity.

Downstream Flow Region

The linearized flow field in the downstream region is periodic and obeys the equation

$$\nabla^2 P_d = 0 \tag{A.3}$$

with the boundary condition far downstream of constant static pressure. The downstream pressure field is thus of the form

$$\delta P = \Sigma\, P_n(\xi)\, e^{-|k|\eta + ik\theta} \tag{A.4}$$

Using the linearized forms of the equations of motion in the upstream and downstream region equations, (A.1), (A.2), and (A.4) may be combined into a single equation for $a_k(\xi)$, the Fourier component of the upstream velocity disturbance potential. This is

$$\frac{da_k(\xi)}{d\xi} = \frac{|k|\left|\frac{d\psi_c}{d\phi} - ik\lambda\right|}{(2 + |k|\mu)}\, a_k(\xi) \tag{A.5}$$

If we define

$$\sigma_k = -\frac{d\bar{\psi}_c}{d\bar{\phi}}\,\frac{|k|}{2 + |k|\mu} \tag{A.6}$$

$$\omega_k = k\lambda\,\frac{|k|}{2 + |k|\mu} \tag{A.7}$$

The solution of Eq. (A.5) can be written

$$a_k(\xi) = b_k e^{(-\sigma_k - i\omega_k)\xi} \tag{A.8}$$

and thus

$$\tilde{\phi} = \sum_{|k|\neq 0} b_k e^{|k|\eta - \sigma_k \xi} e^{i(k\theta - \omega_k \xi)} \tag{A.9}$$

Each Fourier mode is the product of two exponentials. The term $e^{i(k\theta-\omega_k\xi)}$ represents a travelling wave, with ω_k the wave frequency. The other exponential, $e^{|k|\eta-\sigma_k\xi}$, gives the dependence of the wave amplitude on axial position (η) and time; σ_k is the damping of the wave.

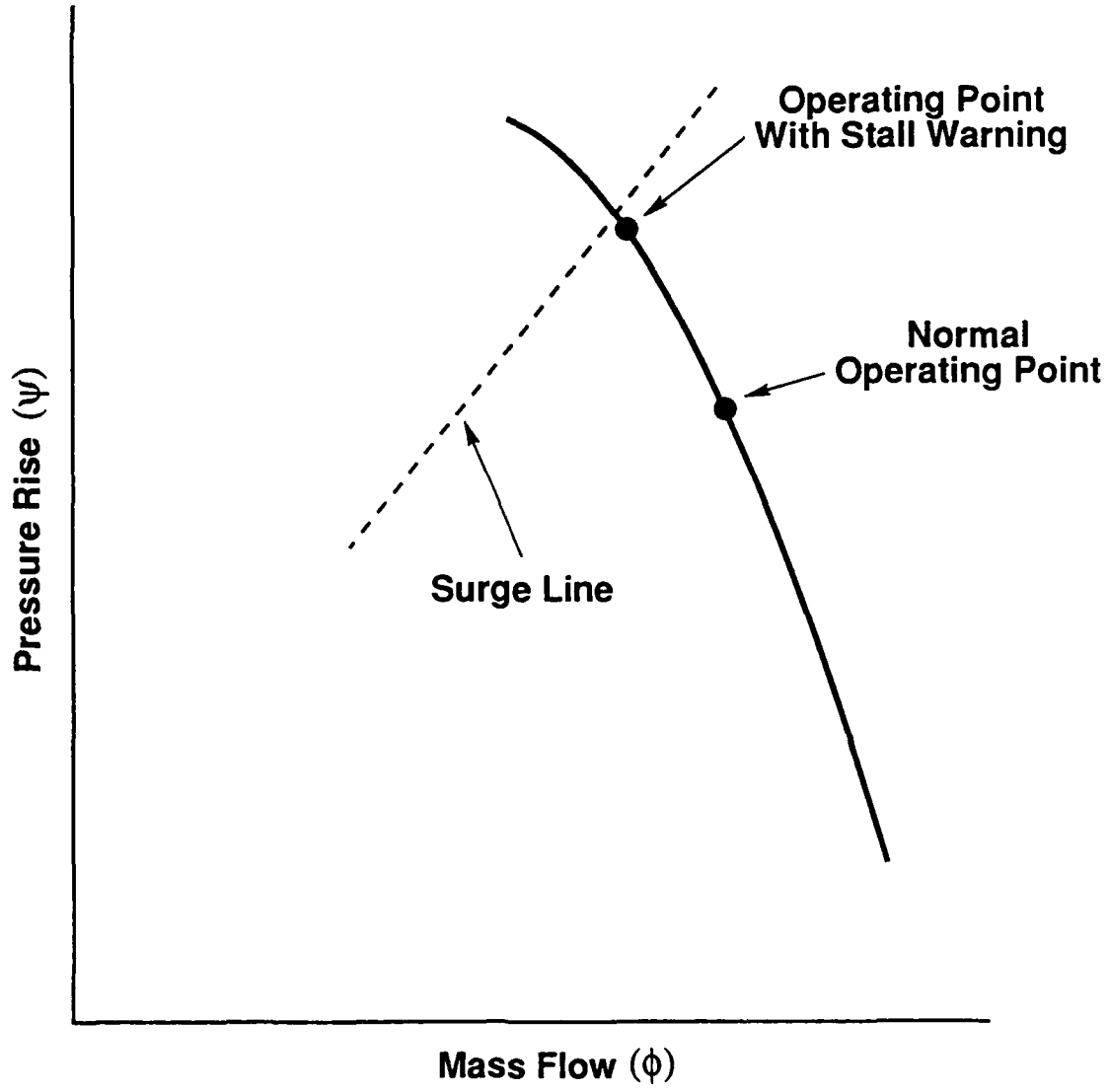

Fig. 1: Compressor performance is characterized by the constant speed line shown (solid line). The compressor cannot be safely operated to the left of the surge line.

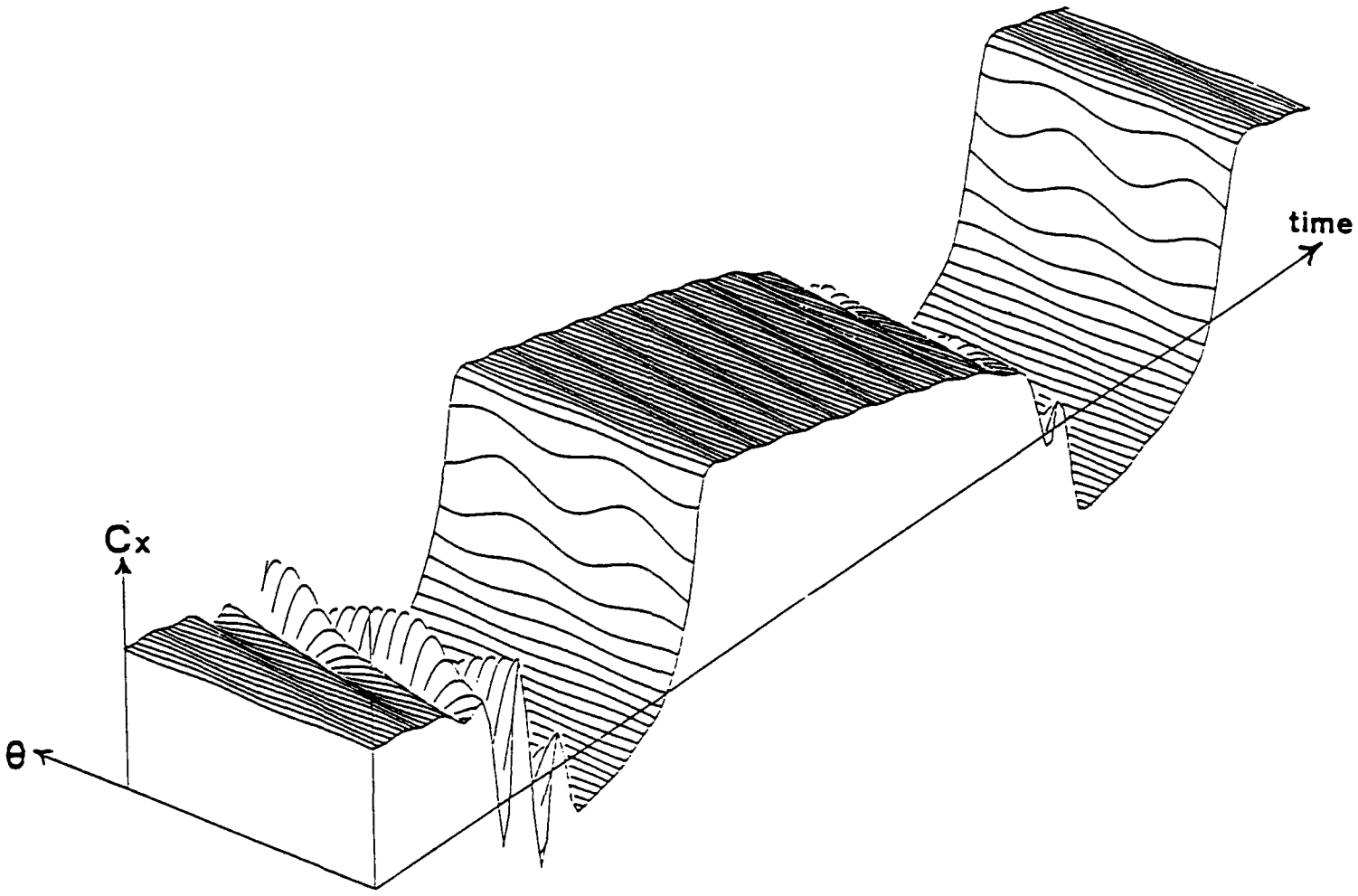

Fig. 2: The time evolution of the axial velocity (C_x) distribution about the compressor circumference ($0 \leq \theta \leq 2\pi$) during compression system instability.

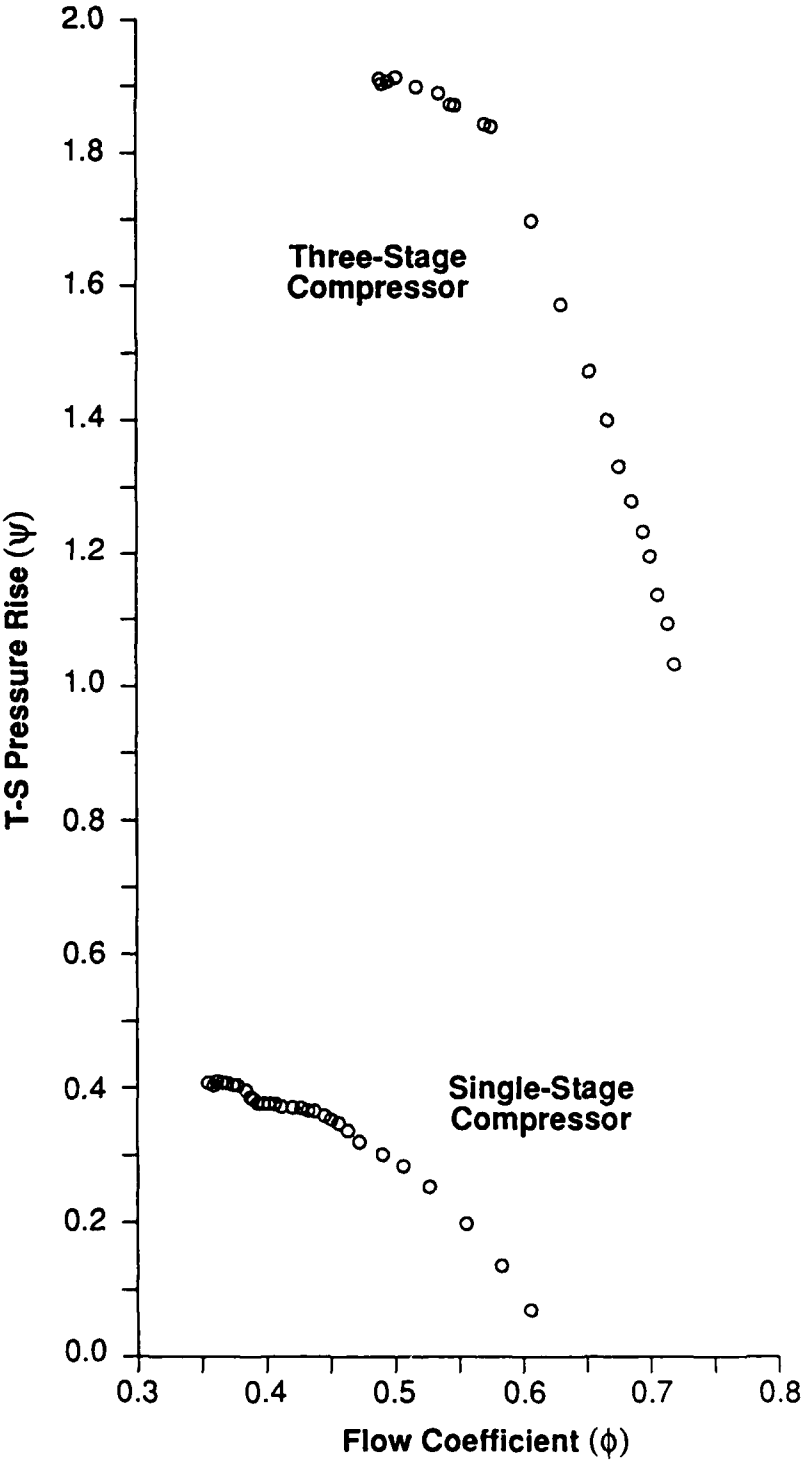

Fig. 3: Compressor characteristics of the two low speed compressors examined in this study.

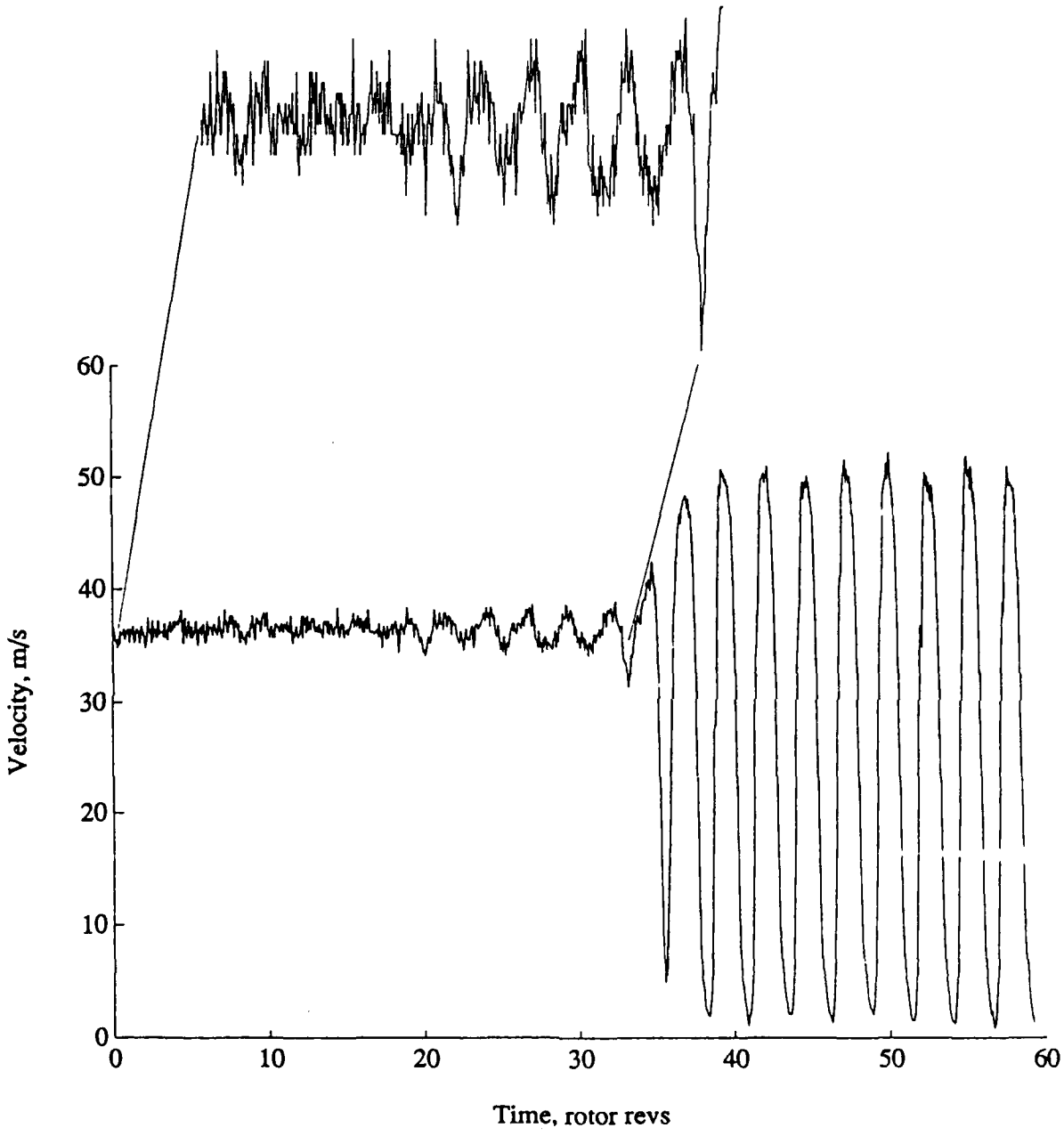

Fig. 4: Time history of axial velocity from a single hot wire positioned upstream of the single-stage compressor. The machine is in rotating stall after a time of 35 rotor revolutions.

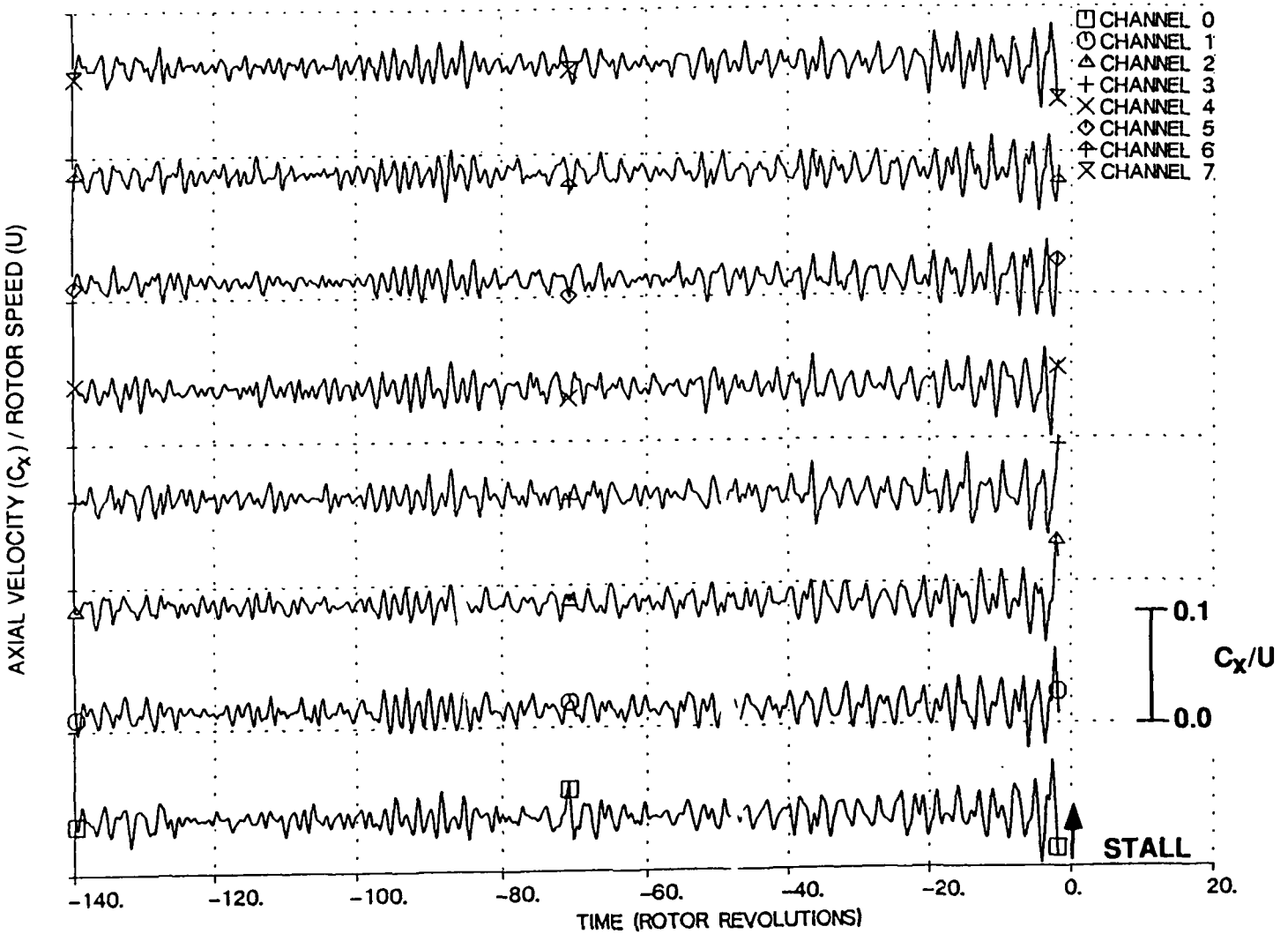

Fig. 5: Time history of axial velocity before stall as measured by 8 hot wires equally spaced 0.4 compressor radii upstream of the IGV's.

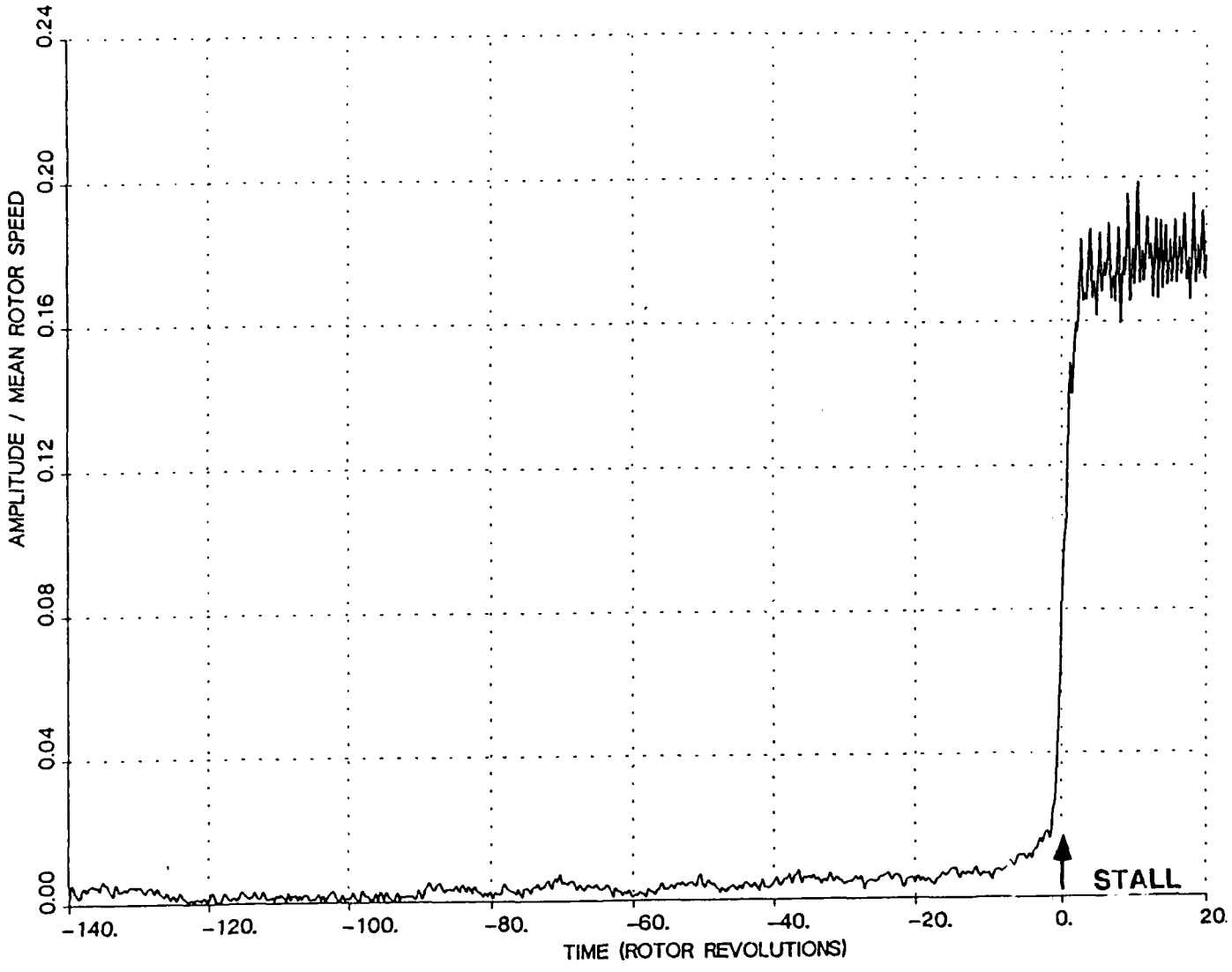

Fig. 6: Amplitude of the first Fourier harmonic ($|C_1|$).

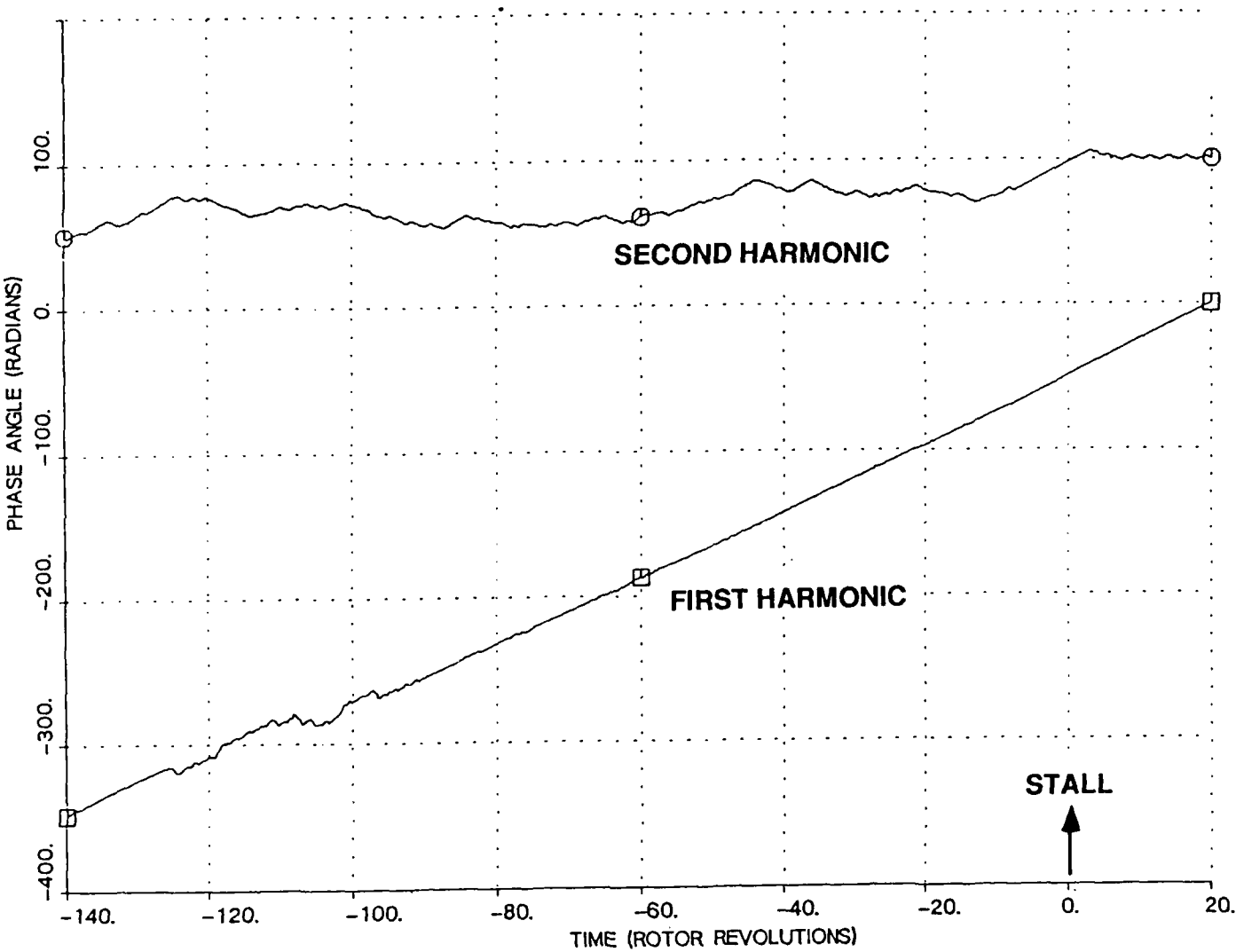

Fig. 7: The time history of the phase of the first and second Fourier coefficients measured upstream of the low speed, three-stage compressor.

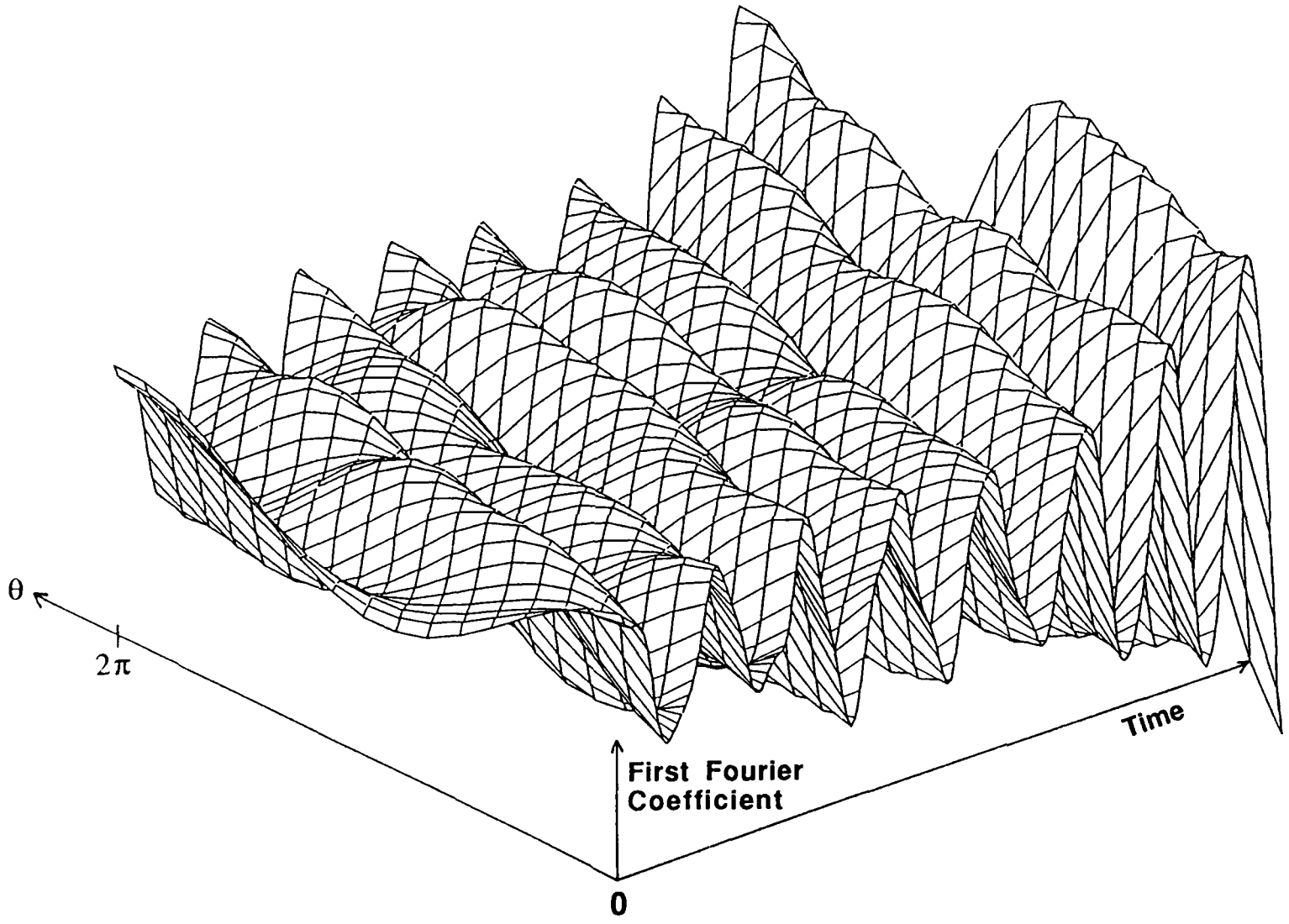

Fig. 8: Measured first harmonic behavior in a format comparable to that of Fig. 2.

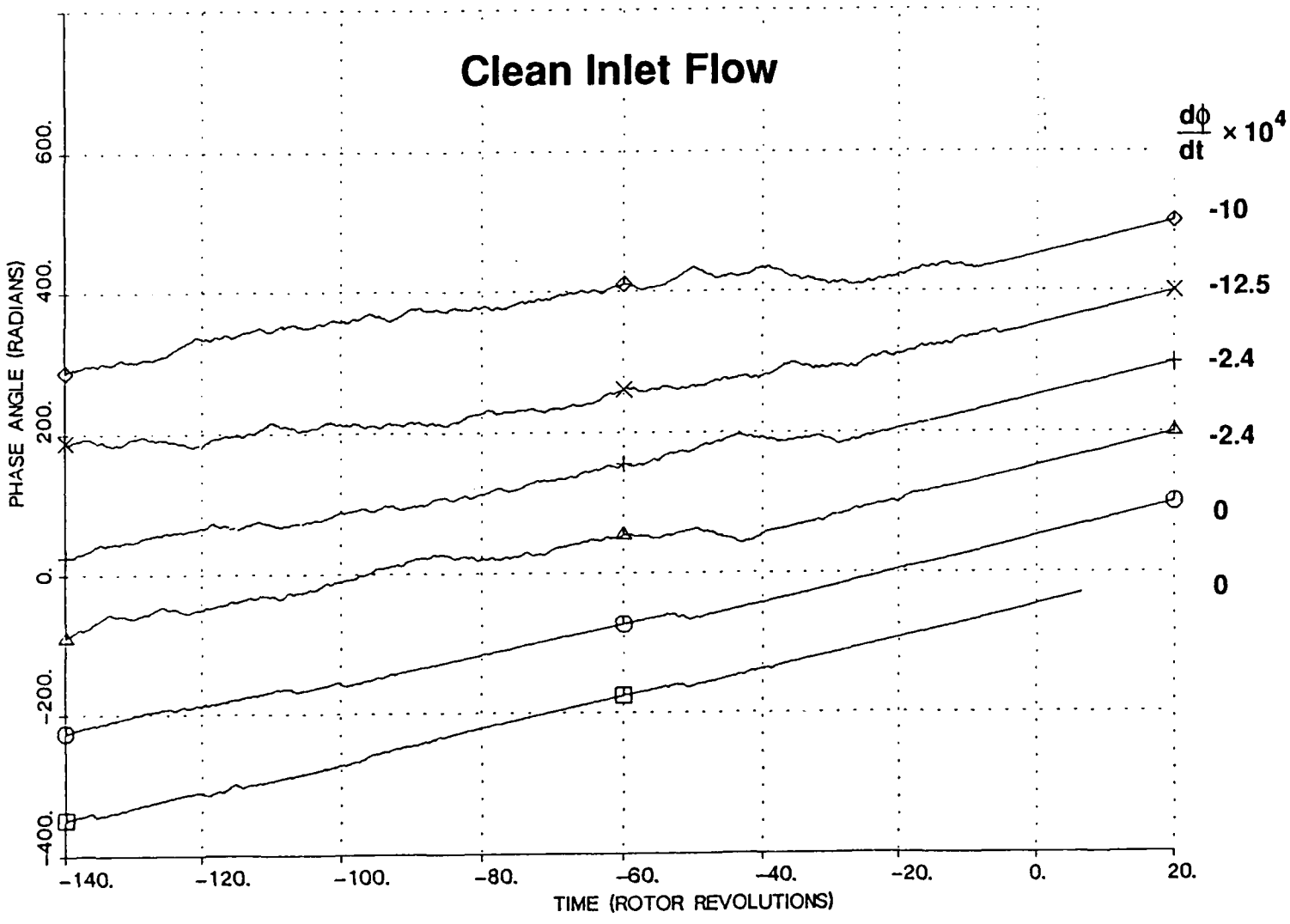

Fig. 9: Phase angle of first harmonic measured on the low speed, three-stage compressor at different throttle rates.

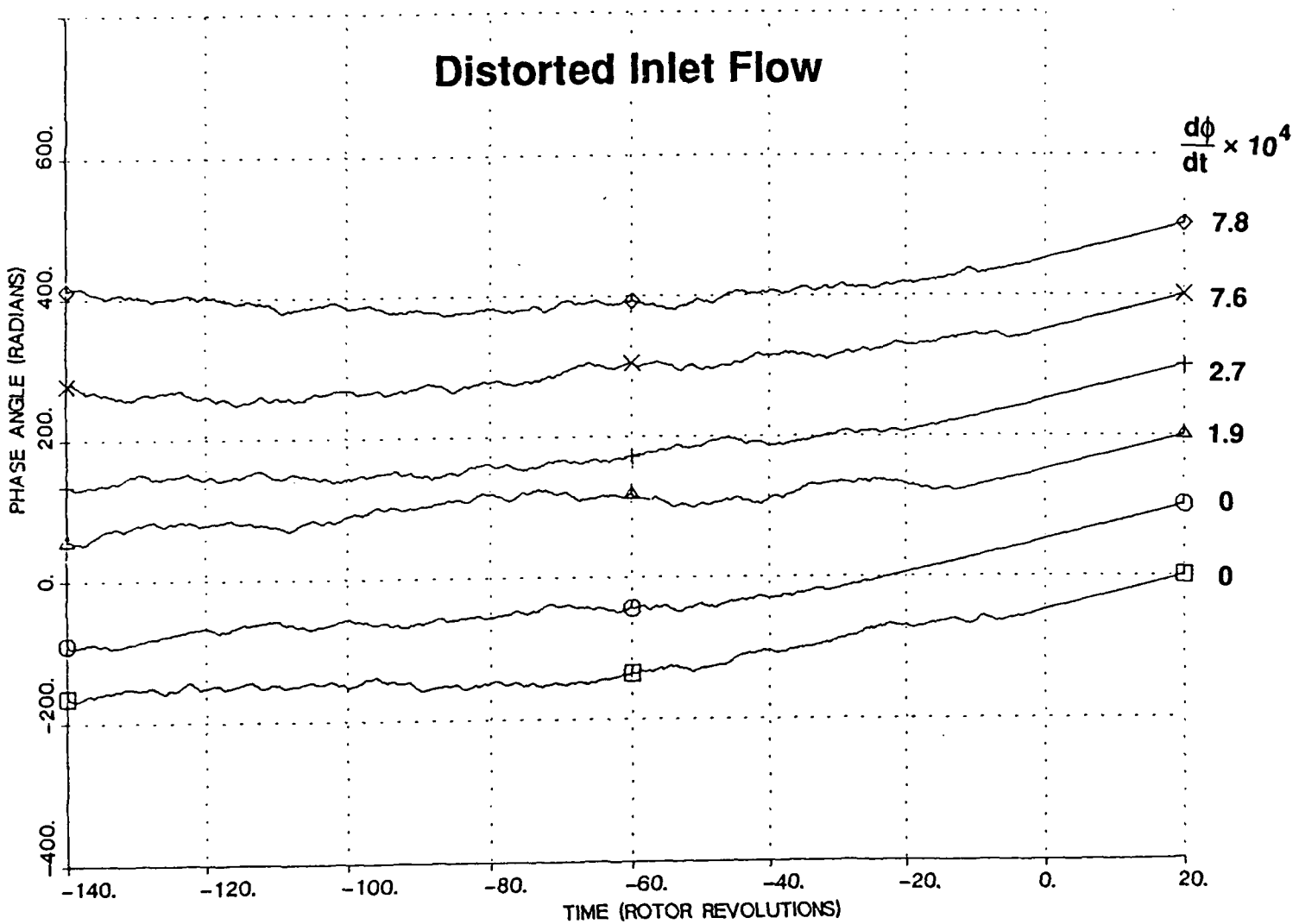

Fig. 10: As Fig. 9, but with inlet distortion.

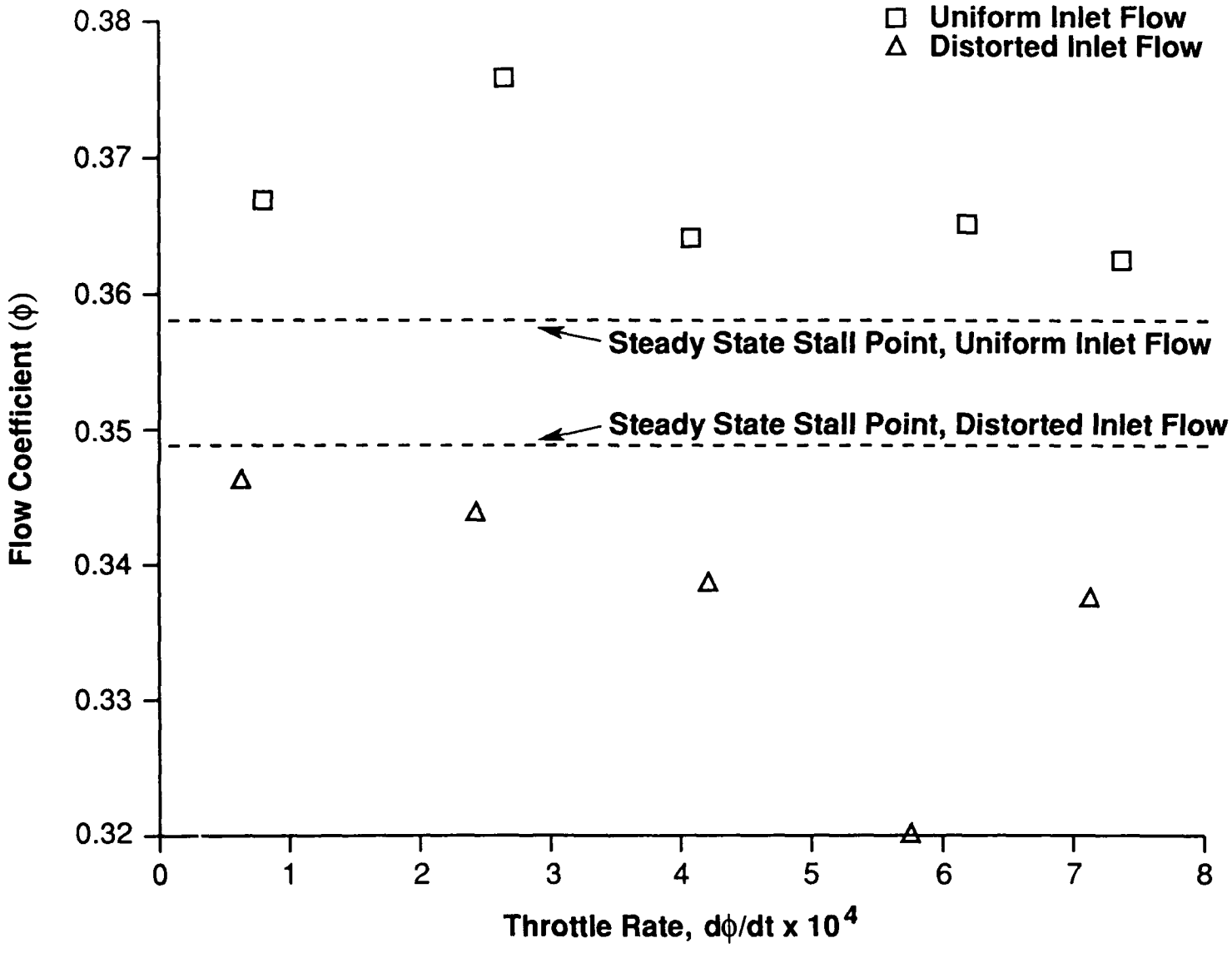

Fig. 11: Flow coefficient (ϕ) at which prestall waves are first discerned in the low speed, single-stage compressor as a function of throttle rate.

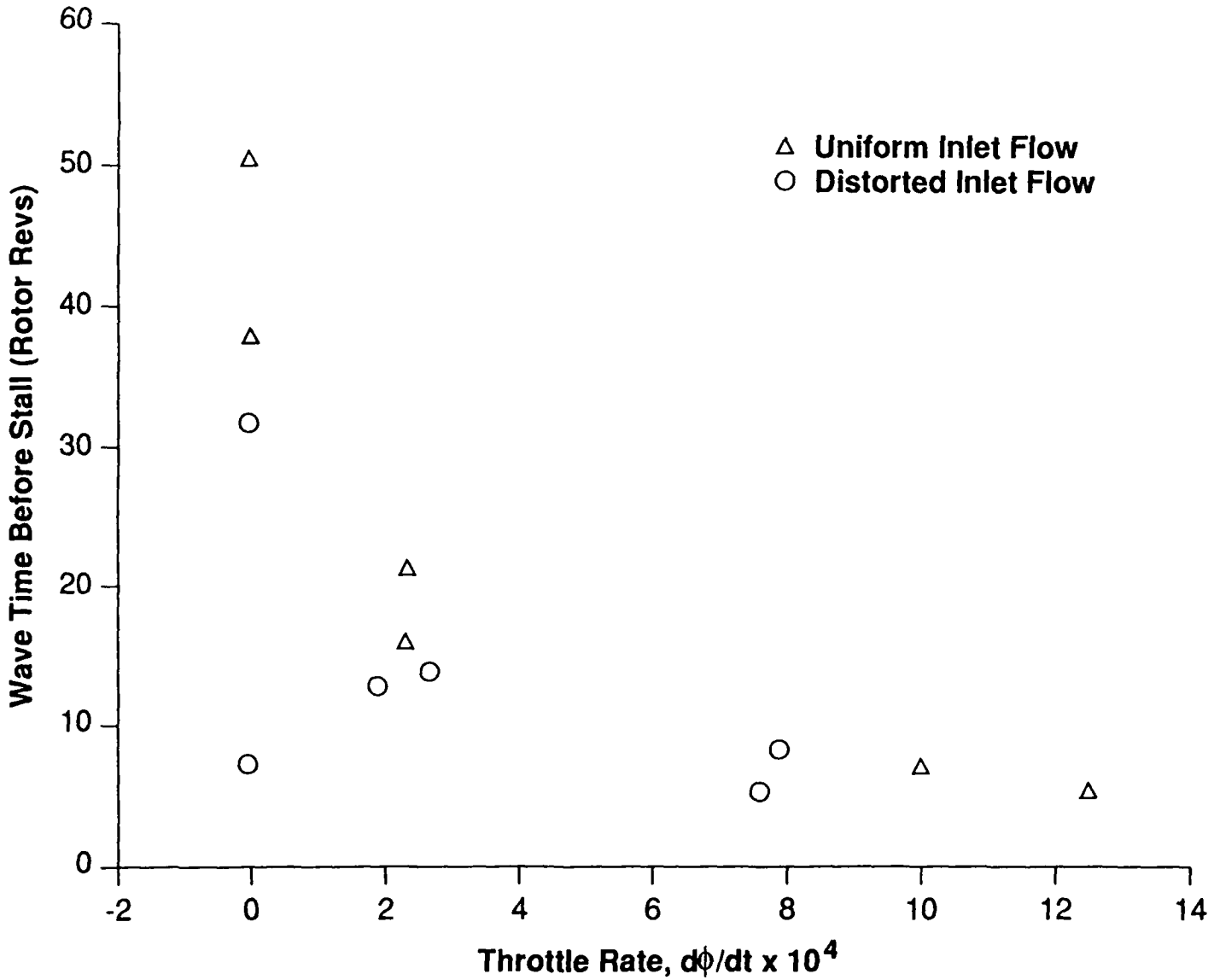

Fig. 12: Period during which the prestall wave is discerned as a function of throttle rate.

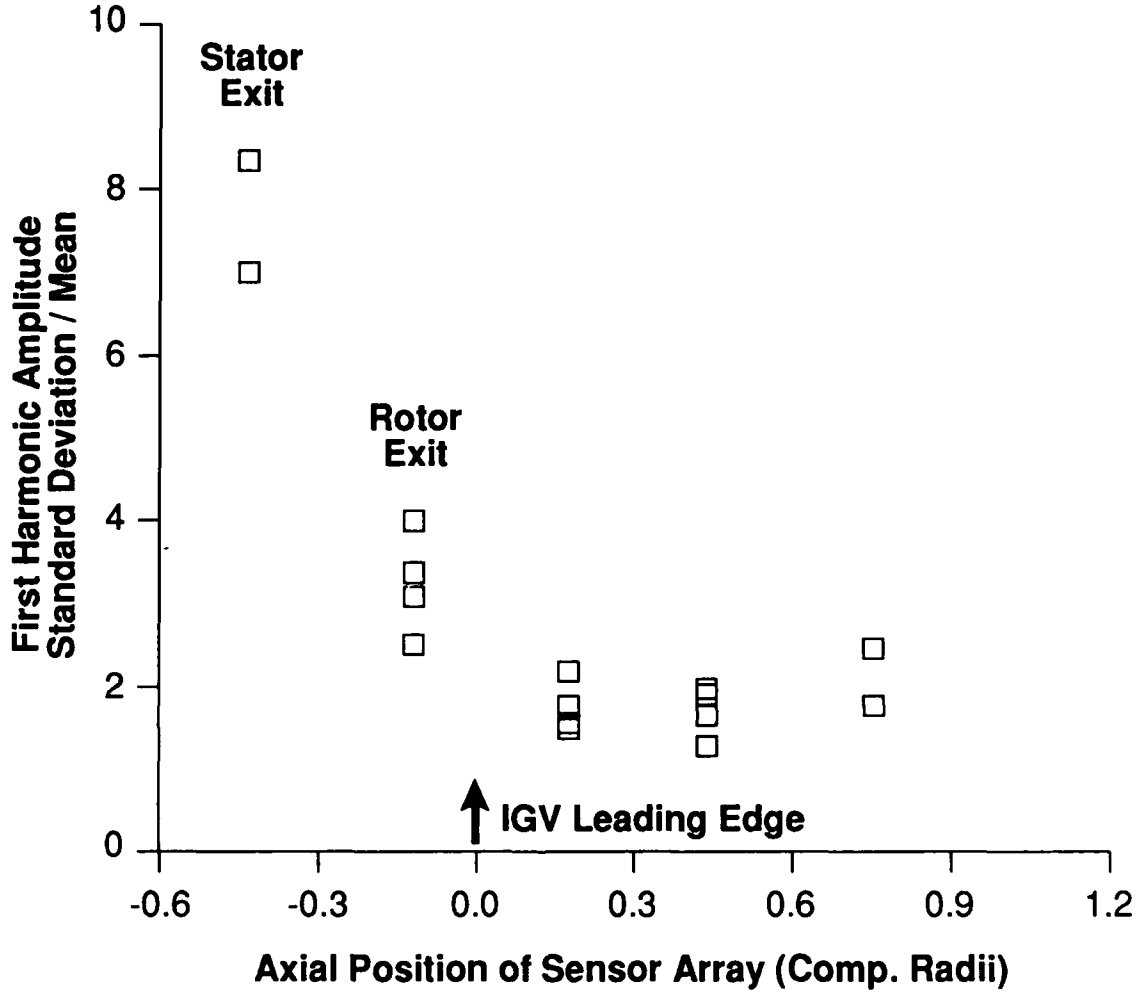

Fig. 13: Signal to noise of first Fourier coefficient amplitude measured at various axial stations in the single-stage compressor.

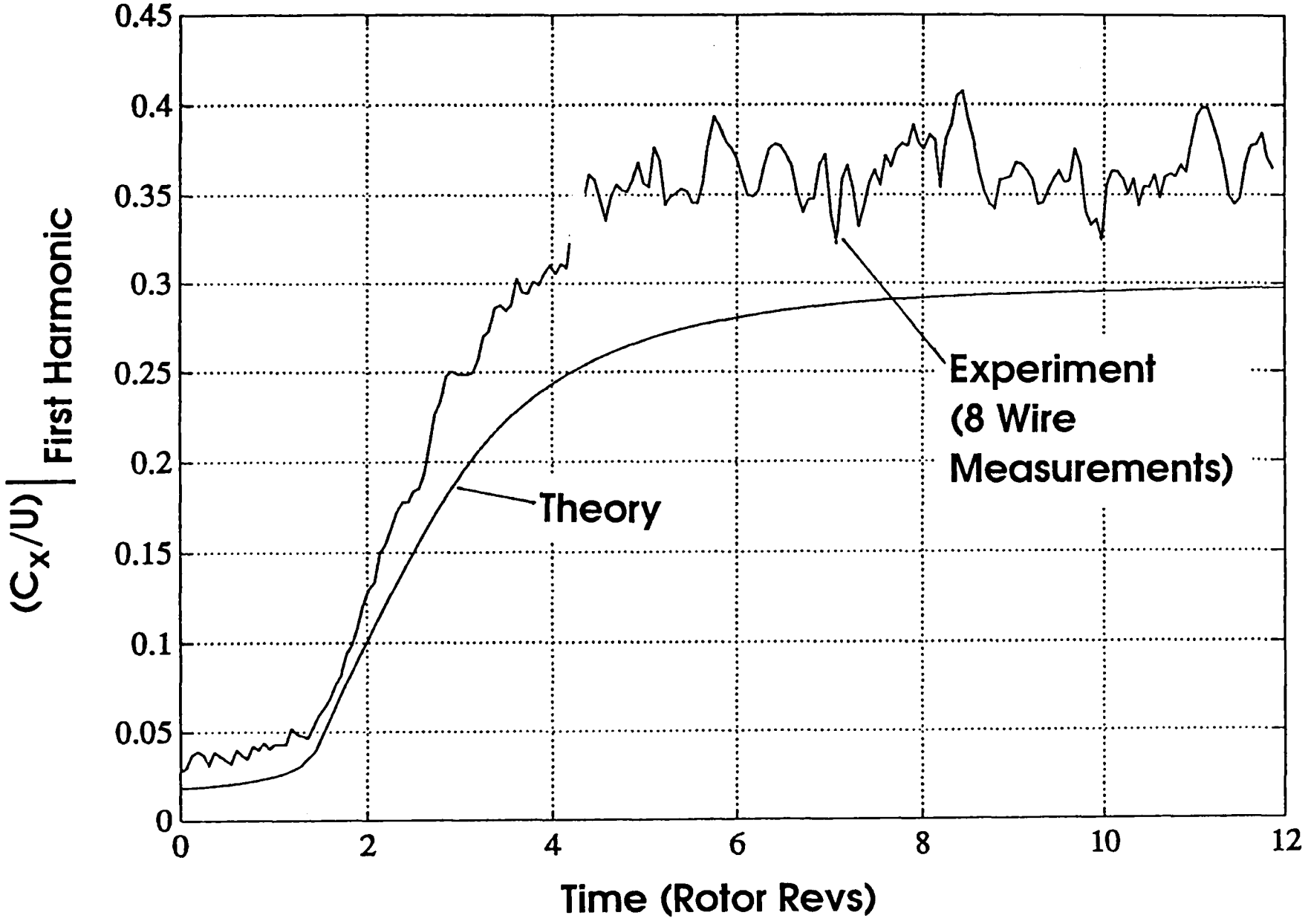

Fig. 14: Time evolution of the first harmonic of the axial velocity in the single-stage compressor during the inception of rotating stall.

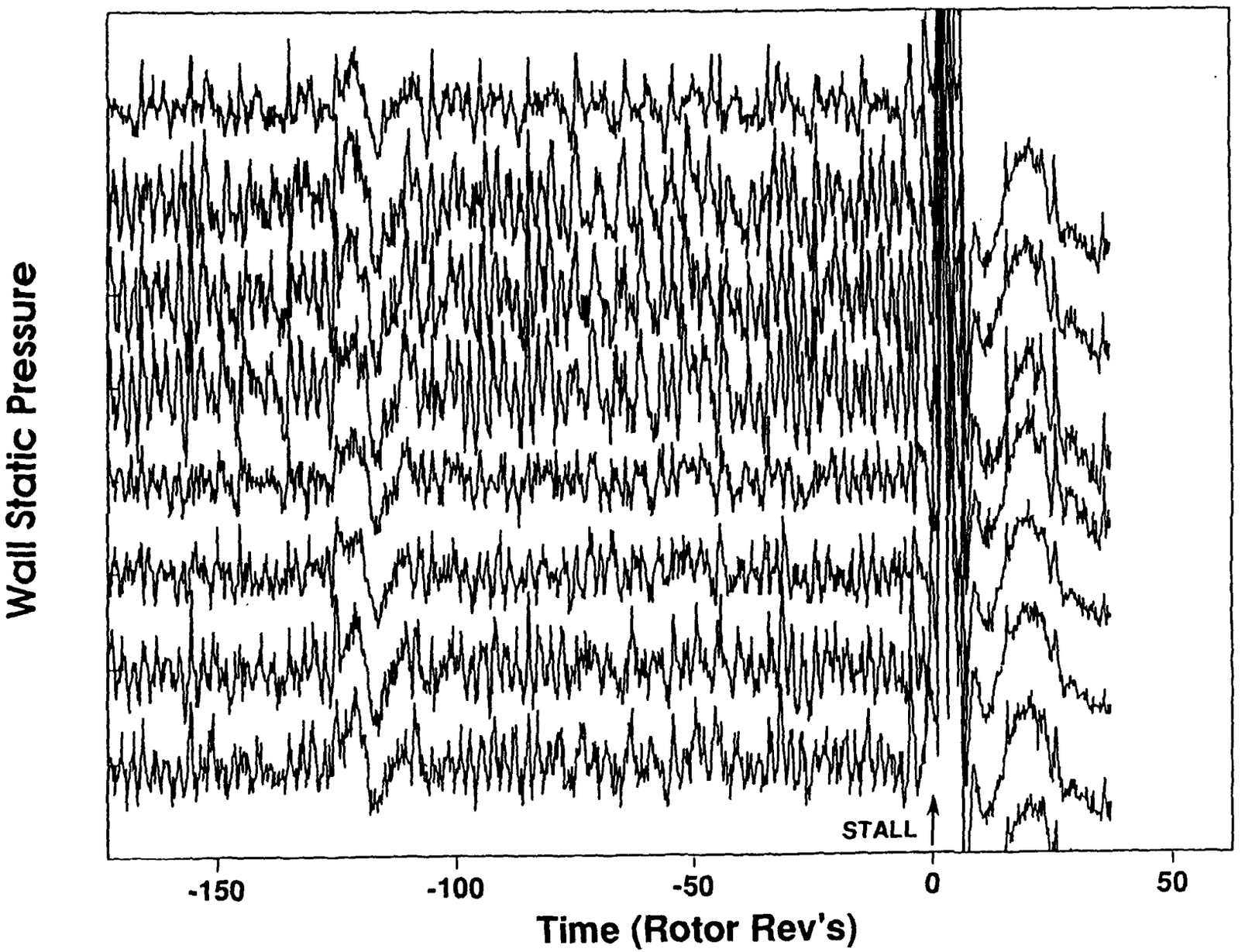

Fig. 15: Time history of 8 wall static pressure transducers located about the circumference ahead of the first stator row in a high speed, three-stage compressor.

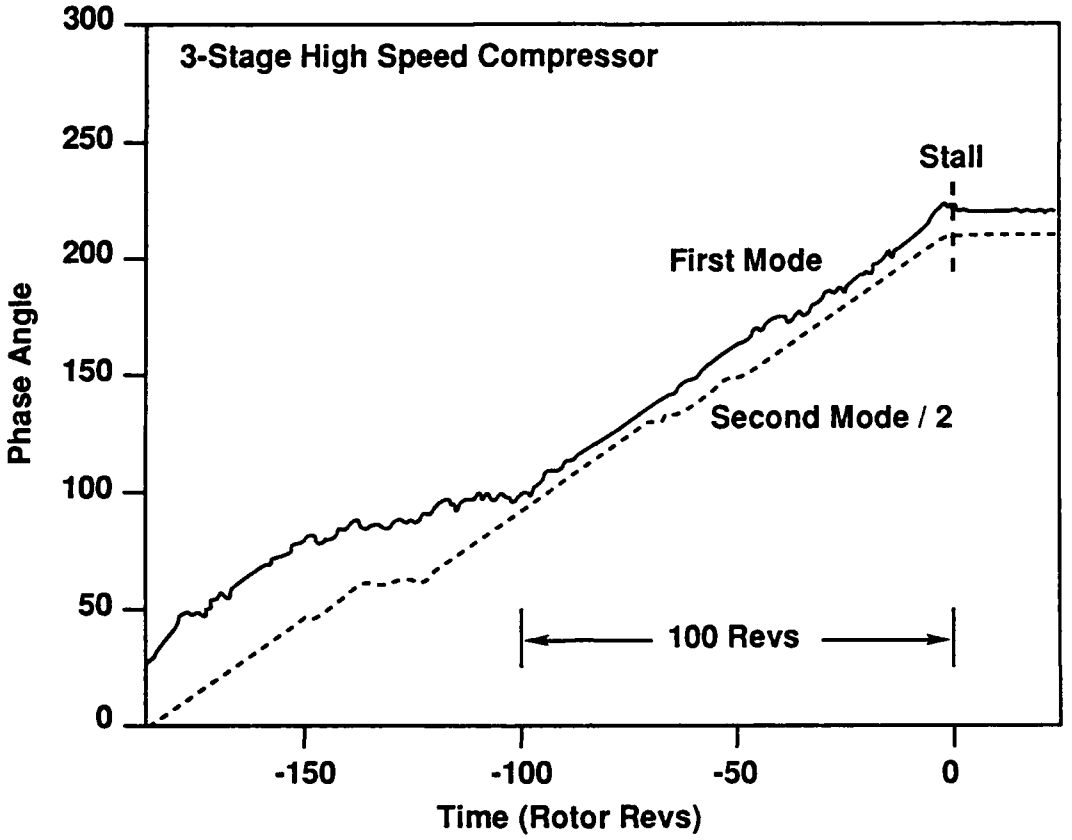

Fig. 16: The phase history of the first two spatial harmonics calculated from the high speed compressor data of Fig. 15.

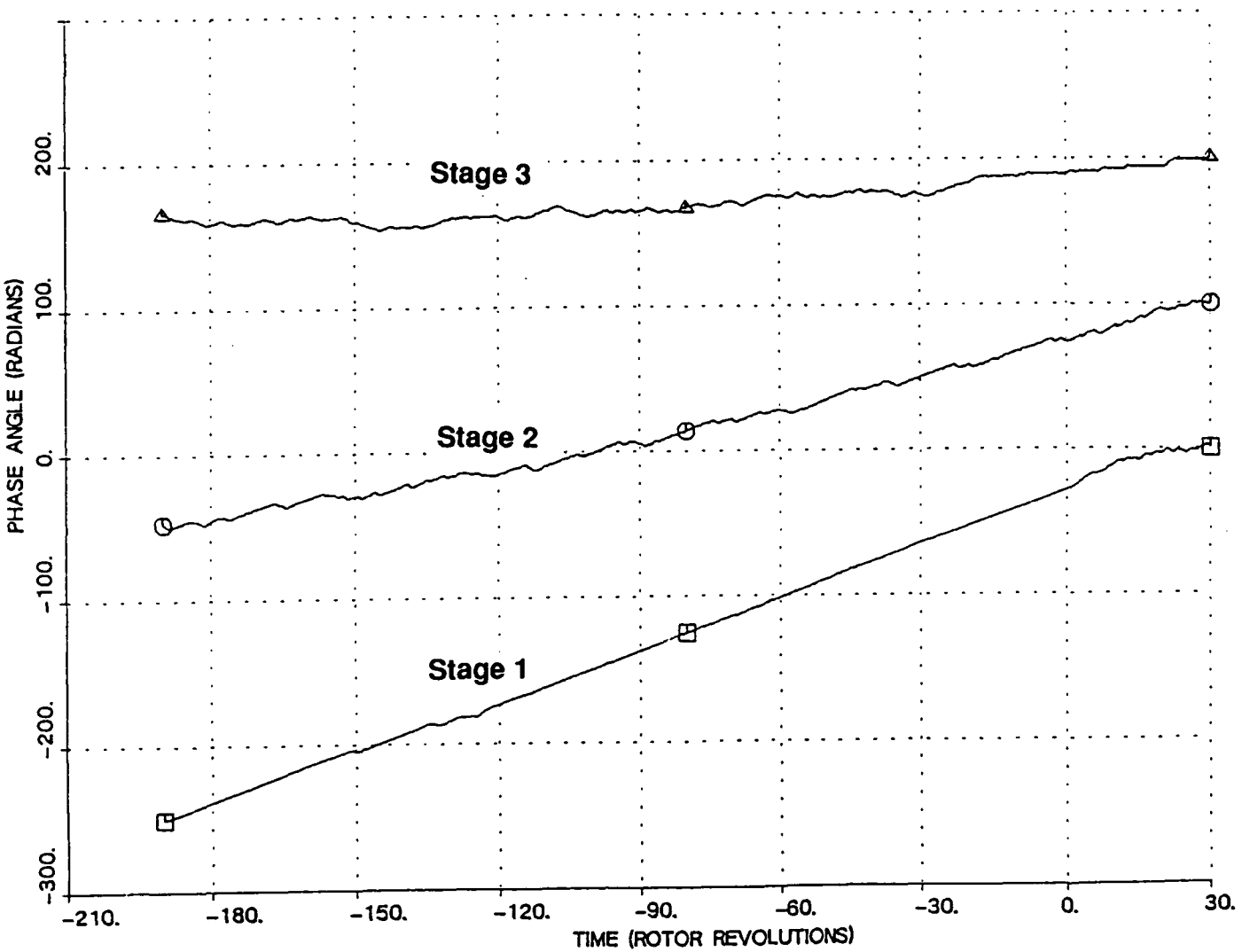

Fig. 17: Phase history of first spatial harmonic from measurements taken at the stator leading edges in a high speed, three-stage compressor.

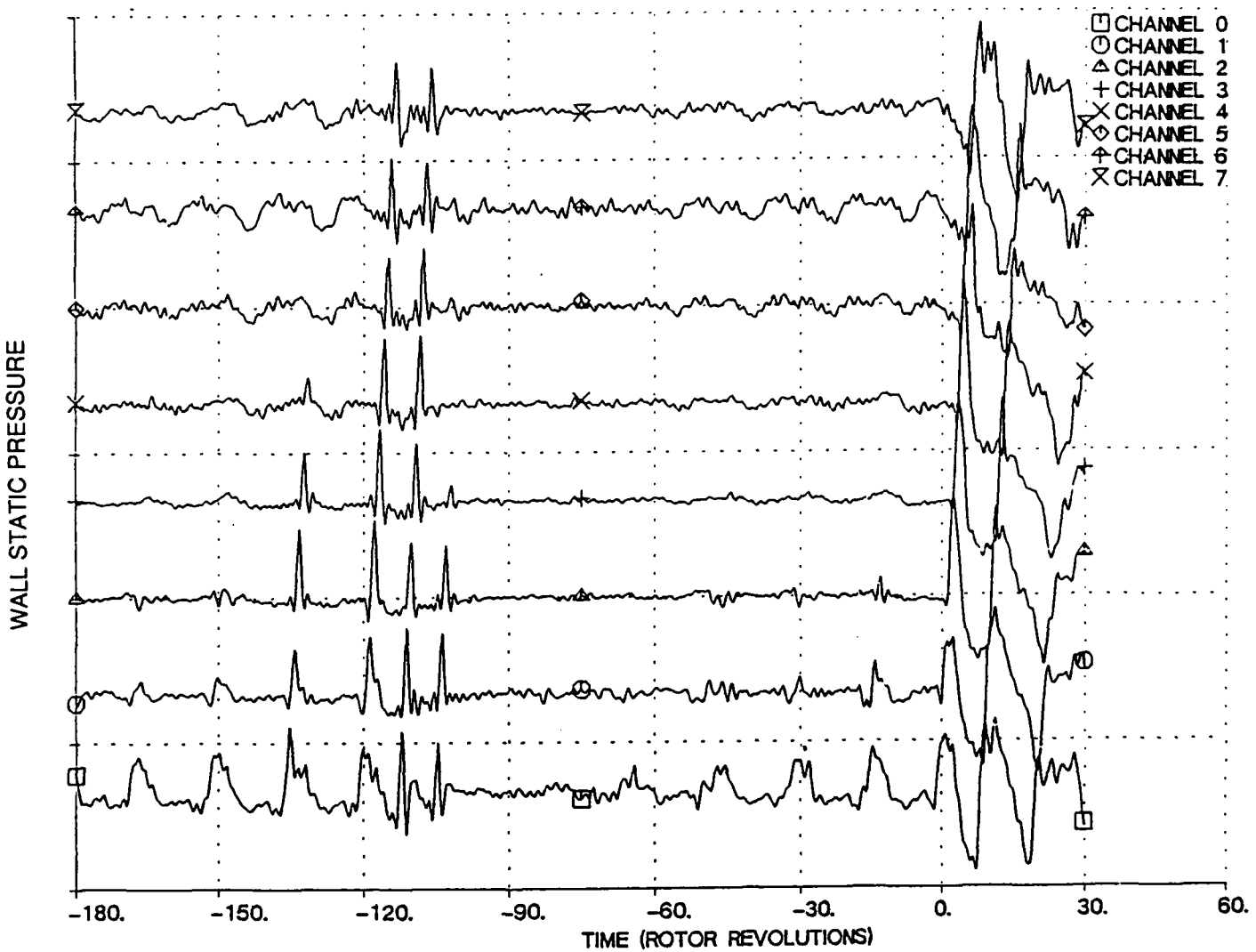

Fig. 18: As Fig. 15, but with inlet distortion.

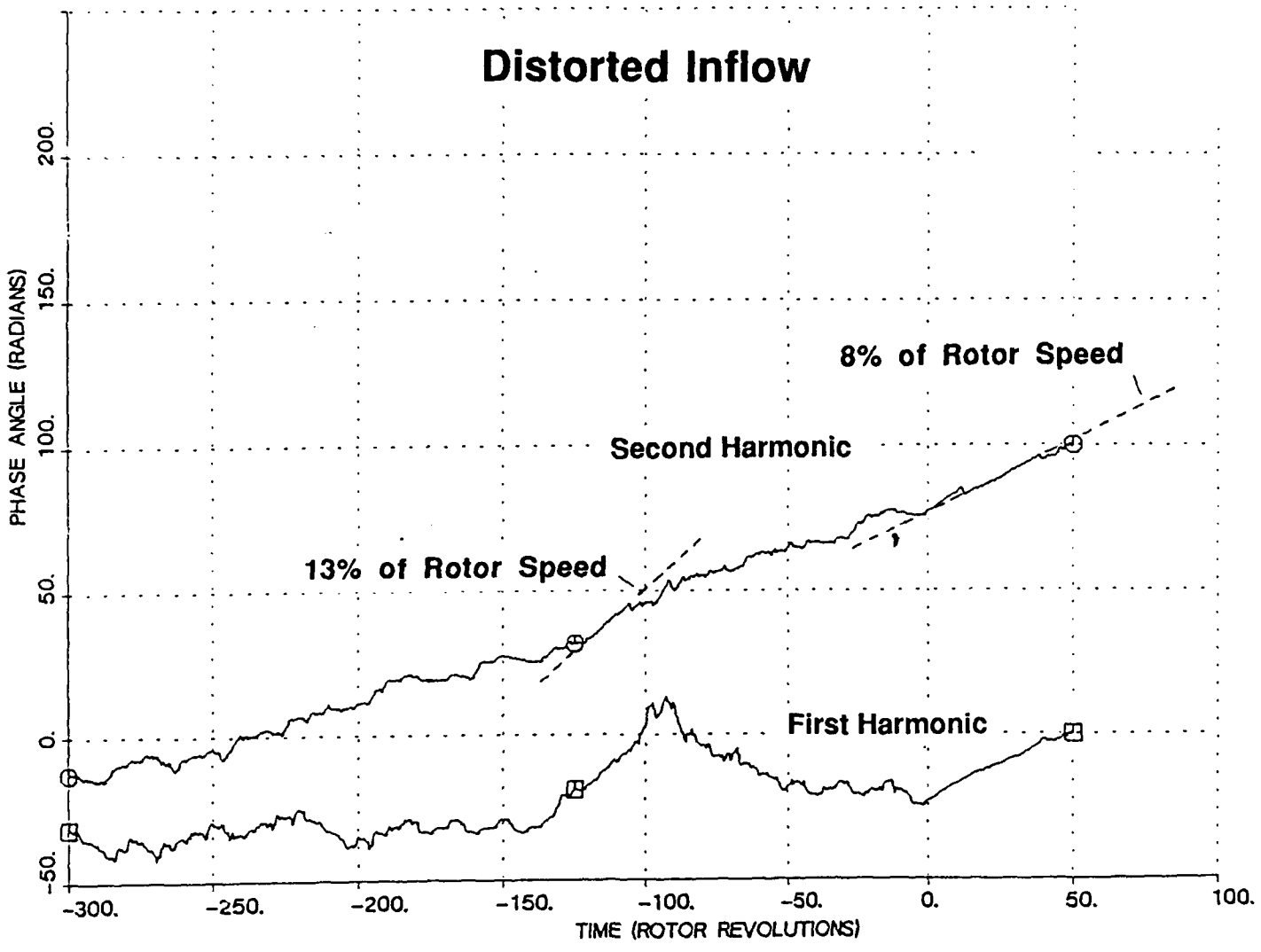

Fig. 19: Phase angle history of the first two spatial harmonics of the high speed compressor with inlet distortion.

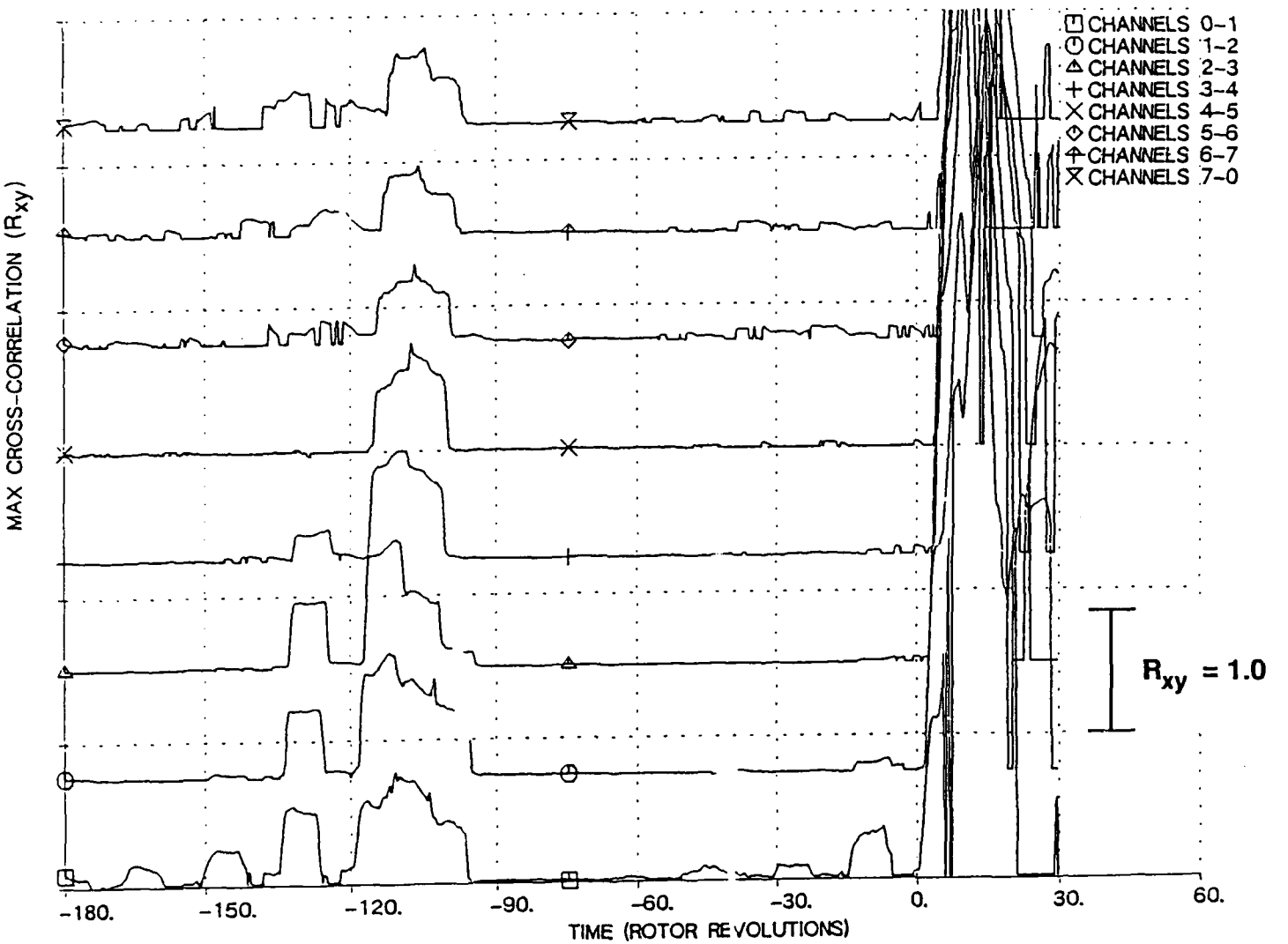

Fig. 20: The maximum value of the cross correlation of the adjacent transducers of Fig. 15 in a high speed, three-stage compressor.

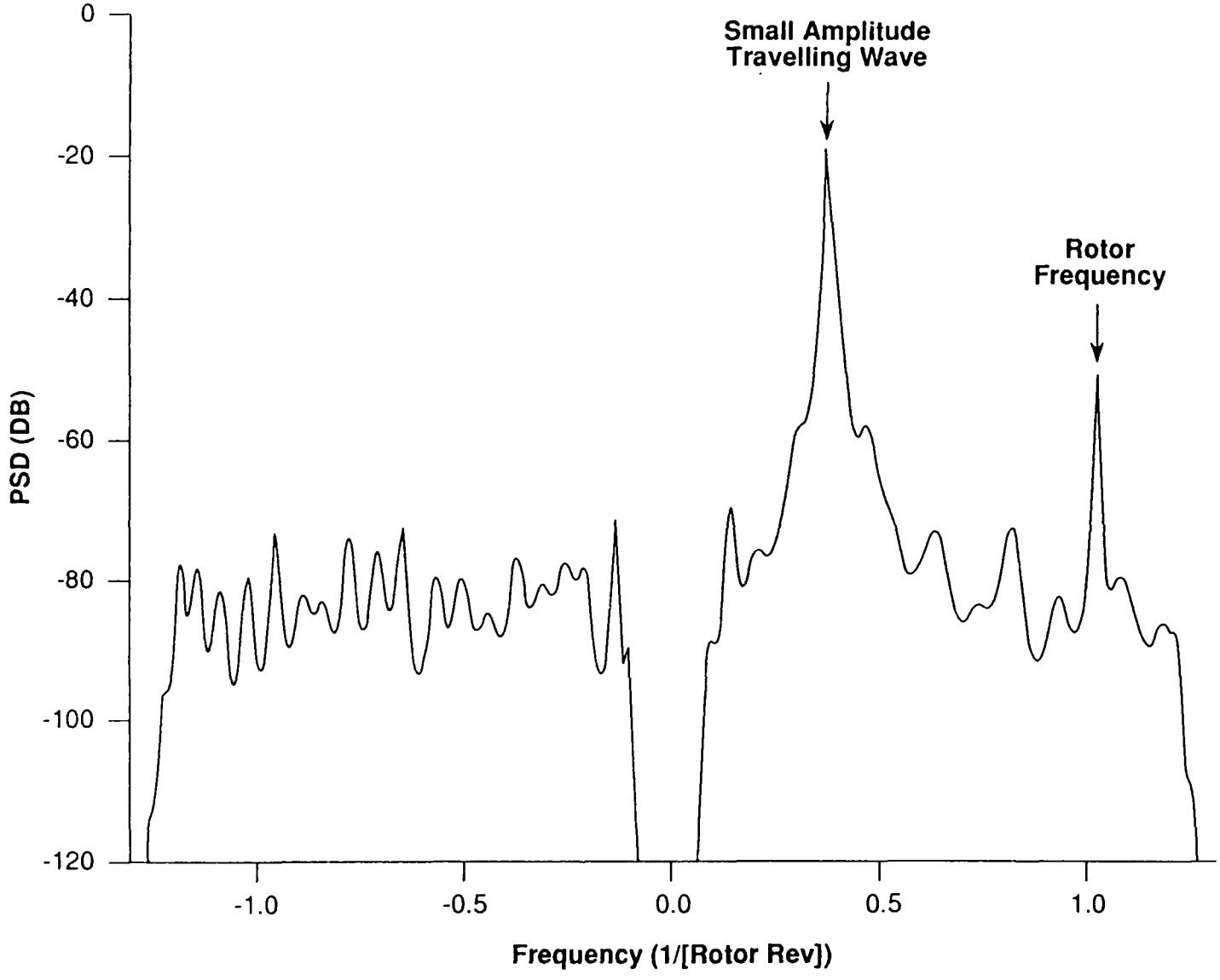

Fig. 21: Power spectral density (PSD) of first spatial harmonic of the axial velocity in the single-stage, low speed compressor before stall.

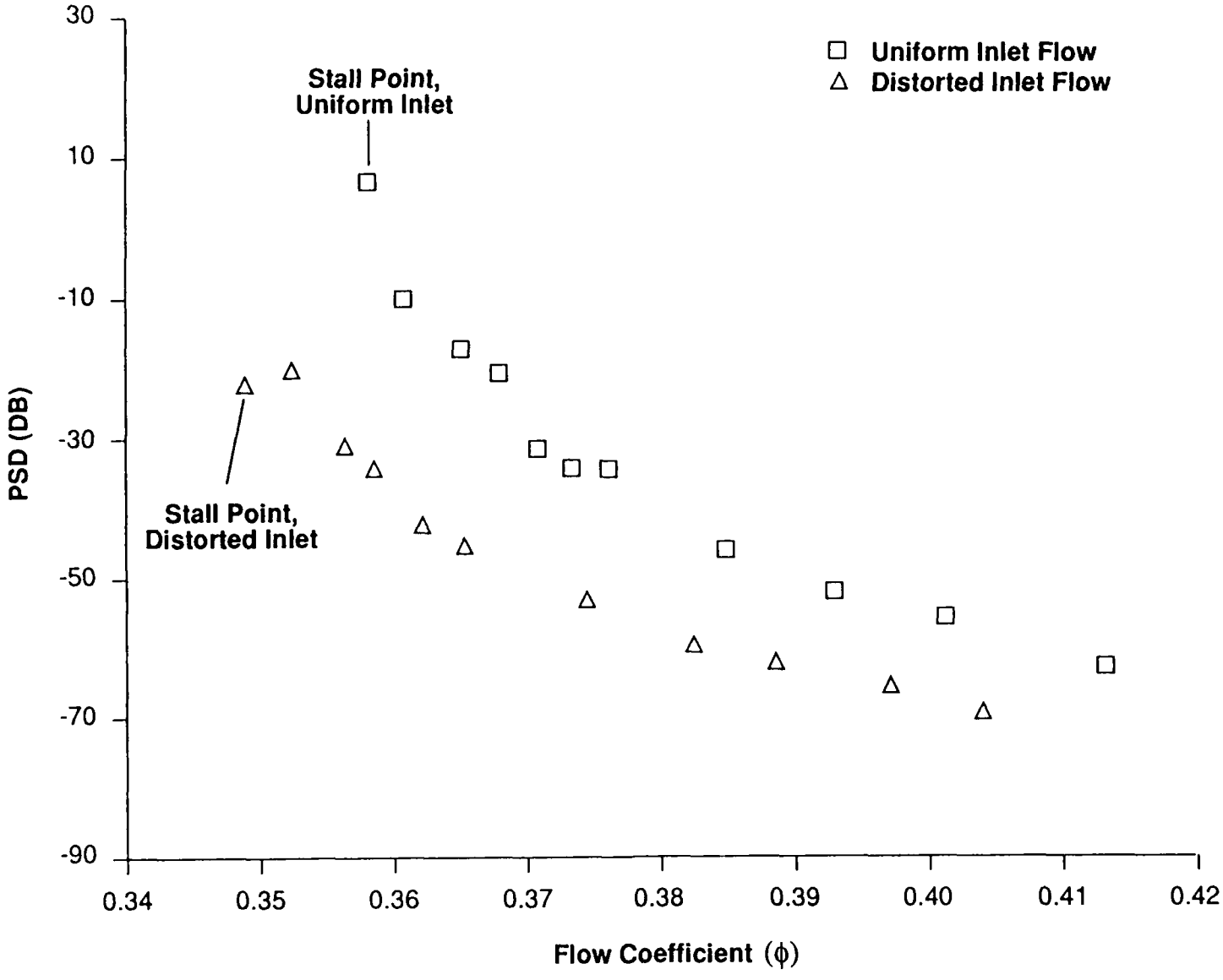

Fig. 22: The peak power of the first spatial harmonic (i.e. the height of the peak in Fig. 21) as a function of flow coefficient (ϕ) on the single-stage, low speed compressor.

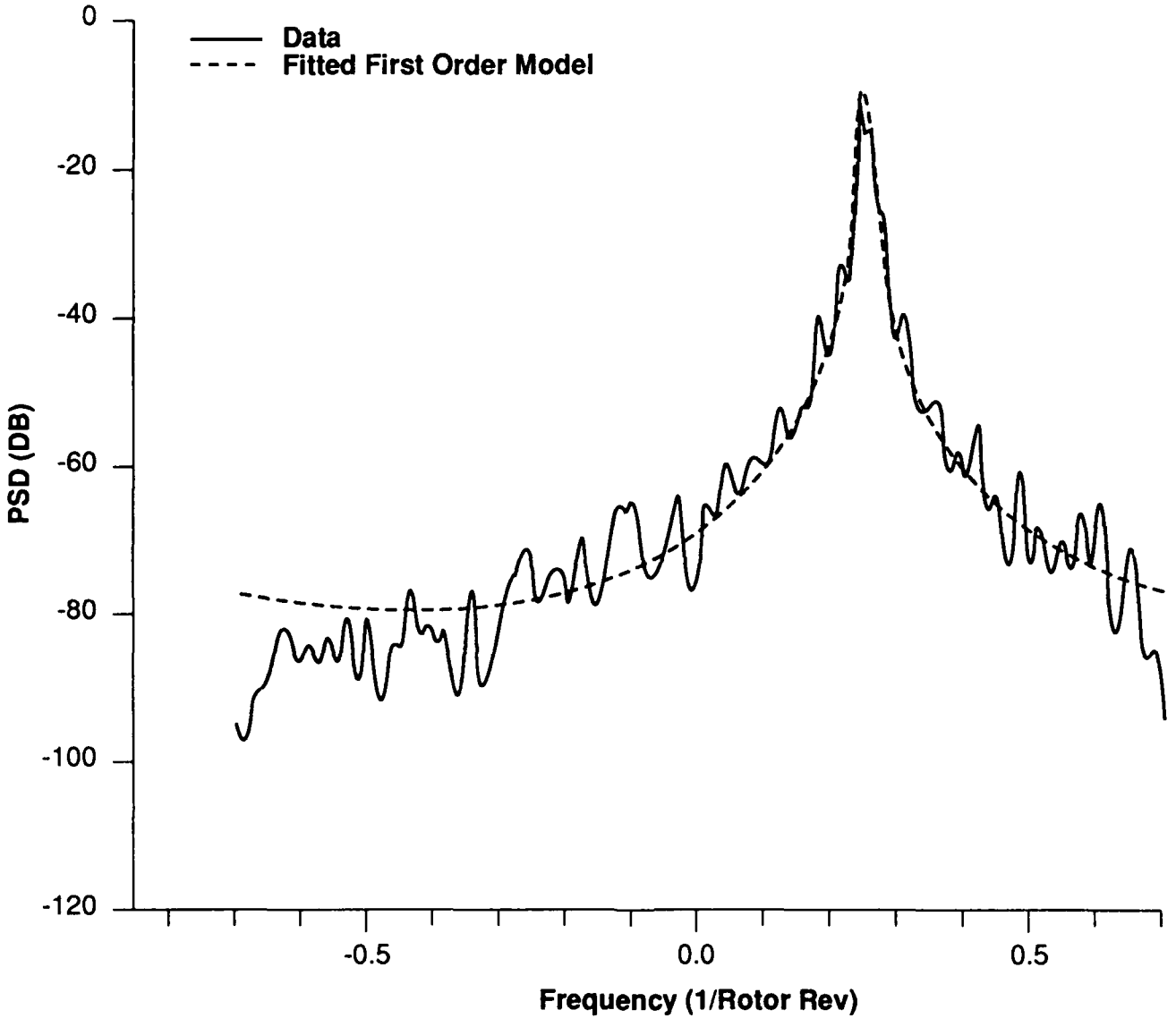

Fig. 23: Comparison of the linear model and measurement of the power spectral density of the first spatial harmonic on the low speed, single-stage compressor.

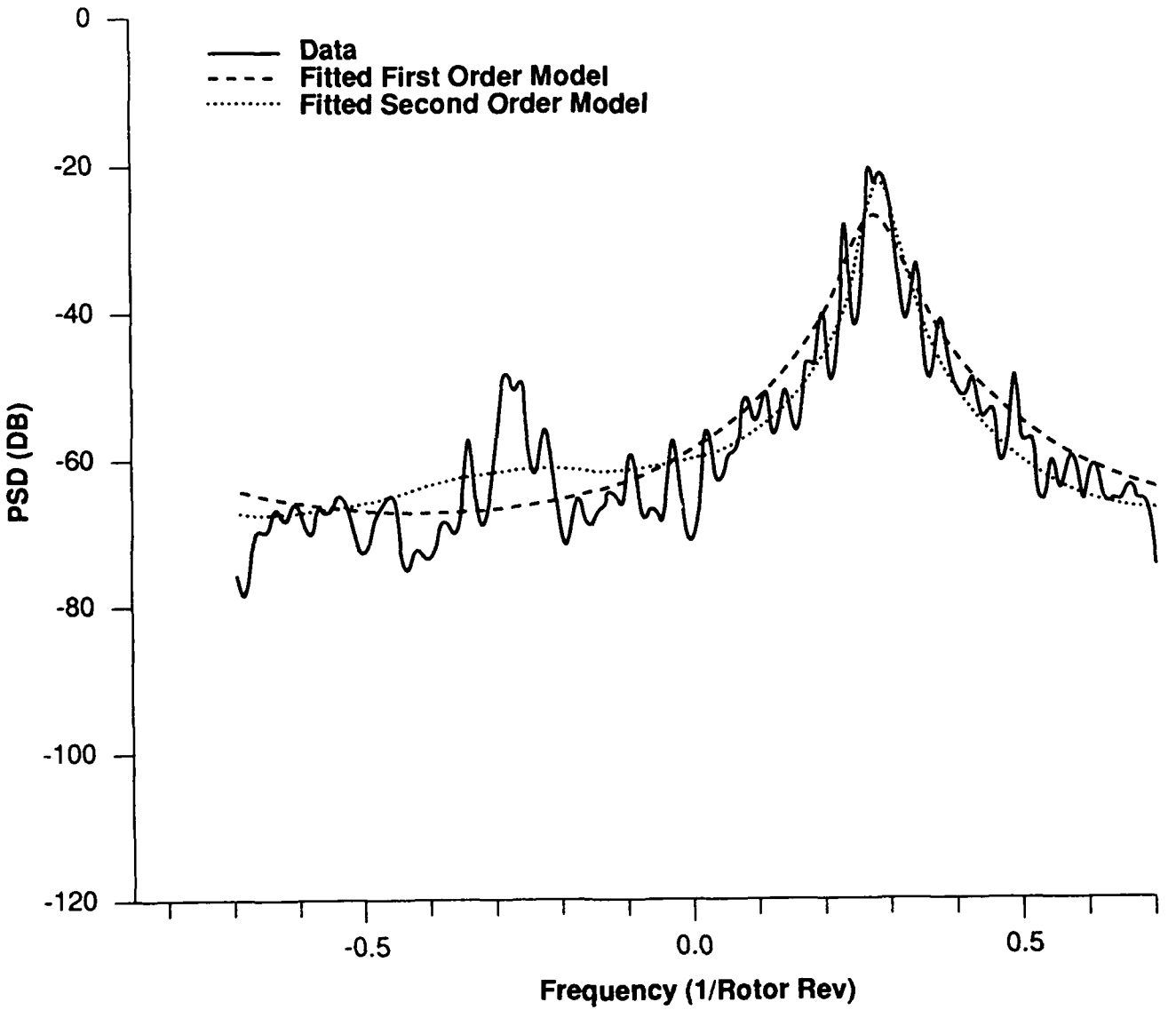

Fig. 24: As Fig. 23, but for second spatial harmonic.

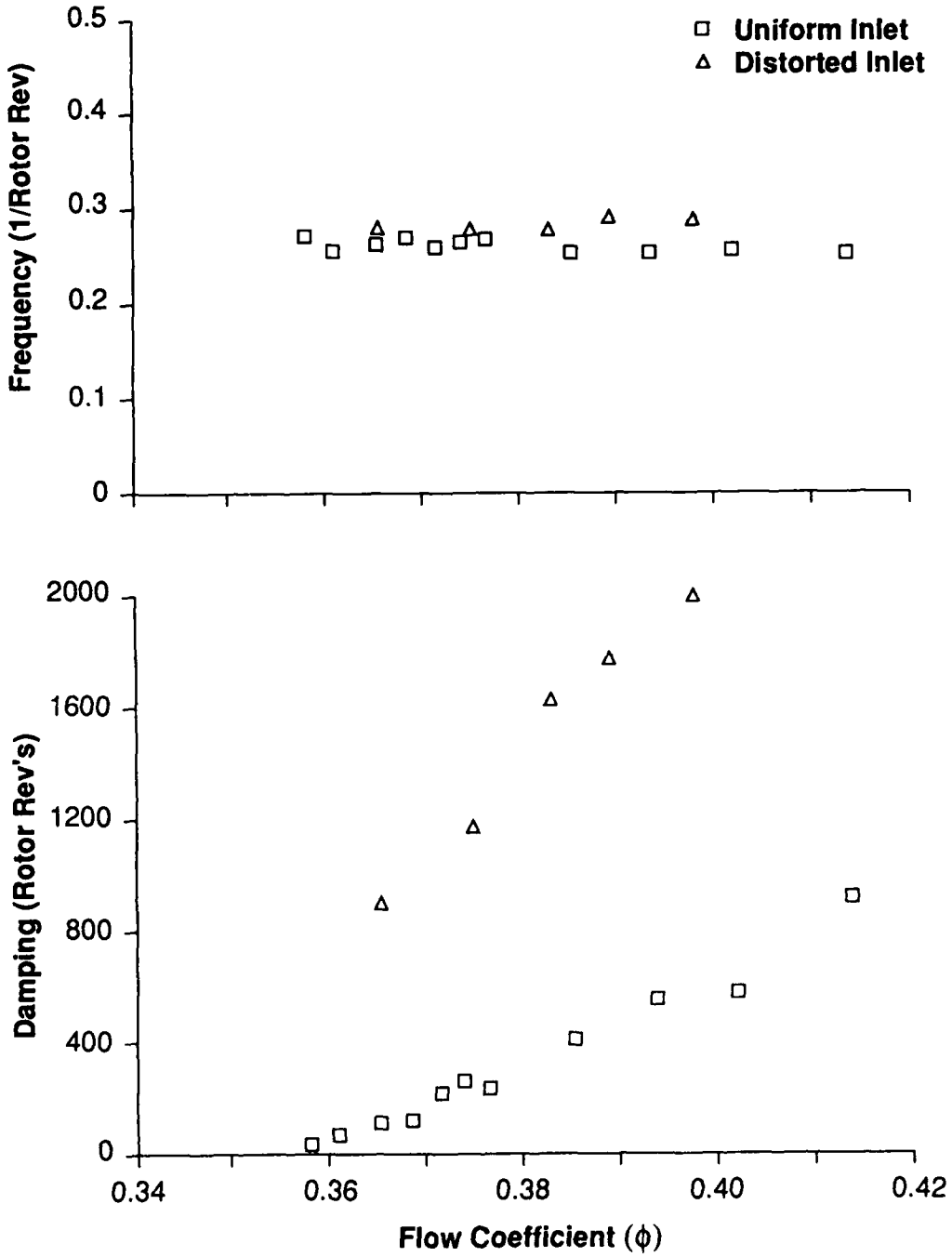

Fig. 25: First spatial harmonic wave damping (σ) and frequency (ω) estimated from the single-stage compressor measurements using parameter identification techniques.

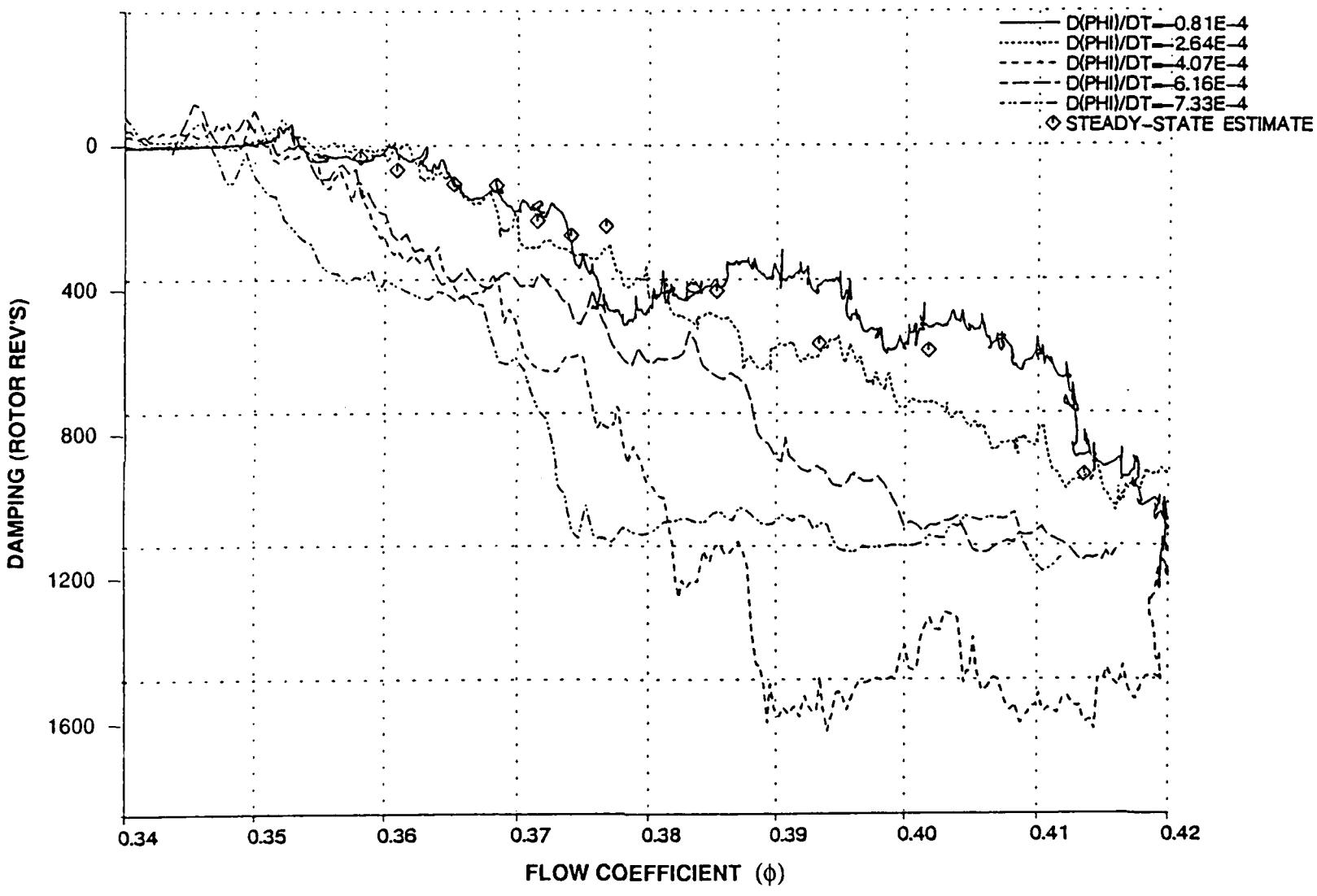

Fig. 26: First spatial harmonic damping, as in Fig. 25, but estimated for various throttle transient rates ($d\phi/dt$).

PART III: DYNAMIC CONTROL OF CENTRIFUGAL COMPRESSOR SURGE USING TAILORED STRUCTURE

ABSTRACT

A new method for dynamic control of centrifugal compressor surge is presented. The approach taken is to suppress surge by modifying the compression system dynamics using structural feedback. More specifically, one wall of a downstream volume, or plenum, is designed to move in response to small perturbations in pressure. This structural motion provides a means for absorbing the unsteady energy perturbations produced by the compressor, thus extending the stable operating range of the compression system.

In the paper, a lumped parameter analysis is carried out to define the coupled aerodynamic and structural system behavior and the potential for stabilization. First-of-a-kind experiments are then carried out to examine the conclusions of the analysis. As predicted by the model and demonstrated with experiment, a moveable plenum wall extended the stable flow range of a centrifugal compression system over 25% for a large range of operating conditions. In addition, because the tailored structure acts to suppress instabilities in their initial stages, this control was achieved with relatively little power being dissipated by the moveable wall system, and with no noticeable decrease in steady state performance. Although designed on the basis of linear system considerations, the structural control is shown to be capable of suppressing existing large amplitude limit cycle surge oscillations.

NOMENCLATURE

a	speed of sound
A_{in}	compressor inlet area
A_p	plenum moveable wall area
B	stability parameter; $B = \frac{U}{2a}\sqrt{V_{plenum}/A_{in}\,L_c} = \frac{U}{2\omega_H L_c}$
C_x	axial velocity
f	Coulomb friction force
F	non-dimensional Coulomb friction force; $F = f/\rho_0 U^2 A_p$
I	rotational inertia of turbospool
L	effective length
m	mass of plenum wall
$\dot{m}$	mass flow
P	pressure
ΔP	pressure difference
ΔP_C	compressor pressure rise
ΔP_T	throttle pressure drop
q	wall displacement
Q	wall frequency parameter
U	impeller exit tip speed
v	non-dimensional wall velocity
V	volume
W	non-dimensional wall aeroelastic coupling parameter
x	wall velocity
ζ	non-dimensional wall damping ratio parameter
η	non-dimensional wall displacement
ρ	density

τ non-dimensional time; $\tau = \omega_H t$

ϕ mass flow coefficient; $\phi = \dfrac{\dot{m}}{\rho_0 U A_{in}}$

ψ plenum pressure coefficient; $\psi = (P_1 - P_0) \Big/ \frac{1}{2} \rho_0 U^2$

ψ_c compressor pressure rise coefficient; $\psi_c = \Delta P_c \Big/ \frac{1}{2} \rho_0 U^2$

ψ_T throttle pressure drop coefficient; $\psi_T = \Delta P_T \Big/ \frac{1}{2} \rho_0 U^2$

ω_H Helmholtz frequency; $\omega_H = a \sqrt{A_{in}/V_p L_c}$

ω_p frequency of wall mass-spring-damper system

$d\psi_c/d\phi$ slope of compressor characteristic

Subscripts

c compressor

in compressor inlet

p plenum

t throttle; tip of impeller exit

0 ambient conditions

1 compressor exit

2 plenum exit

Operators

$\delta( )$ perturbation quantity in analysis

$\bar{( )}$ time averaged

$( )'$ fluctuation

INTRODUCTION

The operating range of turbomachinery compression systems is very often limited by the onset of fluid dynamic instabilities. Surge is a self-excited, essentially one-dimensional instability which is characterized by oscillations in area-averaged mass flow and pressure rise, and is generally the most important instability in centrifugal compression systems. Surge can cause

reduced performance and efficiency of the turbomachine, and even in some cases, failure due to the large unsteady aerodynamic forces on the blades (Stenning, 1980).

To avoid surge, the compression system is generally operated away from the "surge line", the boundary between stable and unstable operation on the pressure rise versus mass flow performance map. Operating the compressor with some margin away from this line, on the negatively sloped part of the compressor speedlines can ensure stable operation. Doing this, however, may result in a performance penalty since peak performance and efficiency often occur near the surge line.(Dean and Young, 1977)

The goal of the research described here is to develop methods to extend the stable operating range by modifying the compression system dynamics to suppress surge. This would allow compressor operation in previously unuseable, or even previously unstable, regions of the compressor map. The experimental phase of the current research is focussed on centrifugal compression systems, although the analysis applies to axial compression systems as well.

DYNAMIC SURGE SUPPRESSION

Surge is the manifestation of a dynamic instability which occurs when the compressor feeds more energy into disturbances than the rest of the system can dissipate. The result is an oscillatory disturbance that grows exponentially until nonlinearities force the oscillation into a limit cycle (surge cycle). The key to dynamic surge suppression, therefore, lies in increasing the system ability to damp (unsteady) disturbance energy (Epstein, Ffowcs Williams, and Greitzer, 1989).

There have been several investigations of surge suppression , all in recent years, using closed loop active control to increase system damping. Ffowcs Williams and Huang (1989) used a movable plenum wall, driven by a signal proportional to the unsteady, plenum pressure, to suppress surge in a centrifugal turbocharger. Pinsley et al. (1989) describe active stabilization using a variable area throttle valve, also driven by a signal proportional to the unsteady plenum pressure. Both of these studies demonstrated that surge can be suppressed in the linear regime, before it grows into a large amplitude disturbance, by modification of system dynamics through

closed loop control.

There has been very little previous work on stabilization using structural feedback. In this approach, the dynamic properties of the system are modified so that the compression system becomes inherently stable, without external input. One limited analytical investigation of such a control scheme was carried out by Chen (1987). He found that a variable area throttle valve, modelled as a mass-spring-damper driven by plenum pressure perturbations, would have a stabilizing effect, but that a flexible plenum wall with no damping would be destabilizing.

SCOPE OF THE PRESENT WORK

The work reported here is directed at surge suppression in centrifugal compression systems using tailored structural feedback. A moveable plenum wall is used as the tailored structure. The moveable wall acts as a mass-spring-damper system driven by unsteady pressure perturbations in the plenum, and its motion is thus coupled to the compression system dynamics. A schematic of the basic compression system and the compression system with the tailored structure is shown in Figs. 1a and 1b.

It will be demonstrated that an appropriately tailored moving plenum wall can significantly extend the stable operating range of a compression system. The aeroelastic coupling between the wall and the basic compression system allows the damper on the moving wall to dissipate mechanical energy associated with flow disturbances, thereby suppressing surge. The degree of suppression depends on matching the structural dynamics to the system fluid dynamics and a set of non-dimensional parameters which govern the interaction between the compression system and the wall are presented and their influence is developed. Experiments are carried out to evaluate the actual performance of the flexible plenum wall system and the analytical model.

SYSTEM MODELLING

The basic lumped parameter model of the compression system has been used by other authors to investigate surge for a rigid plenum configuration, e.g. Emmons, Pearson, and Grant (1955), and Greitzer (1981). In this description, system inertia is represented by the fluid in the

inlet ducting, system compliance is due to the compressibility of the fluid in the plenum, and system damping (positive or negative) is due to the compressor and the throttle.

The differential equations describing the compression system with flexible plenum wall are shown below.

(inlet duct momentum) $$\left(P_0 + \Delta P_c\,(\dot{m}_1) - P_p\right) A_{in} = \frac{d\,(\rho_0\, A_{in}\, L_c\, U)}{dt} \tag{1}$$

(where $\Delta P_c(\dot{m})$ is the compressor pressure rise)

(mass conservation in the plenum) $$\dot{m}_1 - \dot{m}_2 = \frac{d\,(\rho_p\, V_p)}{dt} \tag{2}$$

(throttle pressure drop characteristic) $$P_p - \Delta P_t\,(\dot{m}_2) = P_0 \tag{3}$$

(wall dynamics) $$m\ddot{q} + c\dot{q} + kq = (P_p - P_{\text{auxiliary plenum}})\, A_p \tag{4}$$

Linearizing and non-dimensionalizing the equations of motion as shown in appendix A yields the following non-dimensional equations describing the linear stability of the system.

(inlet duct momentum) $$\frac{d\dot{\delta\phi}_1}{d\tau} = B\left[\left(\frac{d\psi_c}{d\phi}\right)\delta\phi_1 - \delta\psi\right] \tag{5}$$

(mass conservation in the plenum) $$\frac{\dot{d\psi}}{d\tau} = \frac{1}{B}\left[\,\delta\phi_1 - \delta\phi_2\right] - \frac{\rho_p}{\rho_0}\frac{2}{M_t^2}\,\delta v \tag{6}$$

(throttle pressure drop characteristic) $$\delta\psi = \frac{\rho_0}{2\rho_t}\frac{\bar{\phi}^2}{\bar{\psi}}\,\delta\phi_2 \tag{9}$$

(wall dynamics)
$$\frac{d\delta v}{d\tau} = 2WB^2\delta\psi - 2\sqrt{\frac{P_0\rho_p}{P_p\rho_0}}\,\zeta Q\,\delta v - \frac{\rho_p}{\rho_0}Q^2\delta\eta \qquad (7)$$

$$\frac{d\delta\eta}{d\tau} = \delta v \qquad (8)$$

In Eqs. (5) through (9), non-dimensional pressure rise and mass flow coefficients, ψ and ϕ, are defined as:

$$\psi = \frac{\Delta P}{\frac{1}{2}\rho_0 U^2}, \quad \phi = \frac{\dot{m}}{\rho_0 A_{in} U}$$

The non-dimensional wall displacement, η, is given as

$$\eta = \frac{A_p\, q}{V_p}$$

Perturbation quantities are denoted by $\delta(\,)$, whereas steady-state quantities are represented by $\overline{(\,)}$. Non-dimensional time is defined in terms of the Helmholtz frequency, $\tau = \omega_H t$, where the Helmholtz frequency is defined as:

$$\omega_H = a_p\sqrt{\frac{A_{in}}{V_p L_c}}$$

Other definitions can be found in Appendix A.

The parameter $\overline{(d\psi_c/d\phi)}$ is the non-dimensional slope of the compressor pressure rise characteristic and is linked directly to surge. In the regions of the compressor map where this slope is negative, both the throttle and compressor act to damp out flow disturbances. In the positively sloped regions, the compressor adds energy to disturbances while the throttle continues to dissipate unsteady energy. The flow through the system becomes unstable when the compressor adds more energy into disturbances than the throttle can extract.

Non-dimensional Parameters

The behavior of the system described by equations (5) to (9) has a complex parametric dependence involving the following non-dimensional parameters.

The B-parameter has a major influence on the surge dynamics of the compression system

(Greitzer, 1981). It is defined as:

$$B = \frac{U}{2\,\omega_H\,L_c} = \frac{U}{2a_p}\sqrt{\frac{V_p}{A_{in}\,L_c}}$$

For the fixed wall compression system at a given operating point, the magnitude of the positive compressor characteristic slope required for disturbances to grow is set by the B-parameter, which can be viewed as providing a measure of the coupling between mass flow oscillations through the compressor and through the throttle. The larger the B-parameter, the more isolated the throttle is (from the compressor), and the less able to remove energy from flow disturbances. As the B-parameter increases, therefore, surge occurs at a smaller positive compressor slope.

The tip Mach number (based on plenum conditions) is defined as:

$$M = \frac{U}{a_p}$$

The tip Mach number enters the system equations as a measure of the effect of wall motion on the mass balance in the plenum. It thus does not appear explicitly in a fixed wall configuration. The tip Mach number affects the coupling of wall motion to compression system dynamics by determining the degree to which plenum pressure responds to wall motion. The pressure and mass flow fluctuations are functions of tip Mach number (they scale as M^2 for low speeds), but the wall motion is not. The Mach number is thus a measure of this aerodynamic - structural coupling, rather than a representation of the importance of compressibility in the system dynamic model. The larger the Mach number, the smaller the effect a given non-dimensional wall motion has on non-dimensional mass flow and pressure perturbations in the system.

The parameters W, ζ, and Q determine the wall dynamic characteristics relative to the unsteady behavior of the basic (rigid wall) compression system. W is an aeroelastic coupling parameter defined as

$$W = \frac{\rho_0 A_p^2 L_c^2}{m\,V_p}$$

This parameter determines the degree to which wall responds to the pressure fluctuations in the

plenum. Increasing the W-parameter implies a greater wall response to perturbations in plenum pressure.

ζ is the critical damping ratio of the plenum wall mass-spring-damper system, corrected to remain independent of compressor operating conditions. Correction is necessary since the aerodynamic spring constant , and hence, the wall natural frequency, varies with plenum pressure. ζ is defined as

$$\zeta = \frac{c}{2\, m\, \omega_p} \sqrt{\frac{P_p}{P_0}}$$

Q defines the ratio of natural frequencies for the wall mass-spring-damper system and for the fixed wall compression system (the Helmholtz frequency), also corrected so that it is independent of compressor operating point.

$$Q = \frac{\omega_p}{\omega_H} \sqrt{\frac{\rho_0}{\rho_p}}$$

LINEAR STABILITY ANALYSIS

Linearized analysis of the effect of structural control parameters on system stability for a given set of operating conditions leads to the set of equations shown below.

$$\begin{bmatrix} B\left(\frac{d\bar{\psi}_c}{d\bar{\phi}}\right) - s & -2B\frac{\bar{\psi}}{\bar{\phi}} & 0 & 0 \\ \frac{\bar{\phi}}{2B\bar{\psi}} & -\frac{1}{2B}\frac{\bar{\phi}}{\bar{\psi}} - s & 0 & -\frac{\rho_p}{\rho_0}\frac{1}{M^2}\frac{\bar{\phi}}{\bar{\psi}} \\ 0 & 0 & -s & 1 \\ 0 & 2WB^2\frac{\bar{\psi}}{\bar{\phi}} & -\frac{\rho_p}{\rho_0}Q^2 & -2\zeta Q\sqrt{\frac{P_0\rho_p}{P_p\rho_0}} - s \end{bmatrix} \begin{bmatrix} \delta\phi_1 \\ \delta\phi_2 \\ \delta\eta \\ \delta v \end{bmatrix} = \begin{bmatrix} 0 \\ 0 \\ 0 \\ 0 \end{bmatrix} \qquad (10)$$

Equation (10) constitutes an eigenvalue problem for the complex growth rate, s, involving two coupled dynamic systems: the compression system, with variables $\delta\phi_1$ and $\delta\phi_2$, and the moving wall, with variables $\delta\eta$ and δv. The terms associated with the uncoupled fixed wall compression

system and the moving plenum wall dynamics are located on the tri-diagonal of the stability matrix and are shown in the dotted brackets. The two non-zero terms located off the tri-diagonal are the aeroelastic coupling terms.

Solving the eigenvalue problem as a function of B, M, ϕ, W, ζ, and Q and using the experimentally determined compressor characteristics of Pinsley (1988) enables prediction of the instability line for various system and control parameters. The fixed wall behavior is obtained in the limit of either $W = 0$ or $Q = \infty$. Either has the effect of making the wall appear massive and the spring constant stiff,or essentially rigid.

To illustrate the trends obtained by the stability computations, a root locus plot for a fixed wall system with $B = 0.5$ is shown in Fig. 2a. The compressor pressure rise characteristic used is based on a third degree polynomial curve fit of Pinsley's (1988) measured 70K speedline as shown in Fig. 3, the measurements being conducted using a close coupled throttle to avoid surge. The abscissa and ordinate of the root locus plots are non-dimensionalized by the system Helmholtz resonator frequency. The roots are plotted as a function of nondimensional flow coefficient for flow coefficients ranging from 0.175 to 0.070 in increments of 0.005. As the mass flow decreases and the compressor slope increases, the poles are driven from the left half plane (stable) to the right half plane (unstable), with the imaginary axis defining the neutral stability point. The system behaves like a damped (positive or negative) second order oscillator. The neutral stability point for the fixed wall system (at $\phi = 0.116$), as indicated on the compressor characteristic in Fig. 3, occurs near the peak of the characteristic, which is located at $\phi = 0.120$.

The introduction of a moveable plenum wall introduces a second mode of oscillation to the compression system. The root locus plot of the two mode system (with $B = 0.5$, $M = 0.4$) is shown in Fig. 2b, again using the compressor characteristic shown in Fig. 3. One characteristic frequency is somewhat close to the Helmholtz frequency, but there is now another frequency, associated primarily with the wall motion. More importantly, however, is that the neutral stability point occurs well past the peak of the characteristic in the positively sloped region, as also shown in Fig. 3. Away from instability (high mass flow), the moving wall system has one (damped)

oscillatory mode and one non-oscillatory (over-damped) mode. Near instability, the two modes show increased fluid-structure coupling and both become oscillatory.

To optimize the moving wall compression system performance, a parametric study was performed. Since the B-parameter and Mach number are not independent quantities (both scale with wheel speed) , the relation between these two parameters used in this study is based on selecting values for the dimensions of the compression system which were typical of modern compression machines as well as convenient from an experimental view point. The parameter search showed that moveable wall performance is optimized over the range of B-parameters and Mach numbers used with the following control parameters: $W = 0.11$, $\zeta = 1.5$, and $Q = 0.51$. (These parameters were used in developing Fig. 2b.)

The steady state mass flow coefficient (i.e., explicitly rather than through the effect on compressor characteristic slope) is not a very useful indication of stability for the optimized moving wall system. Determining maximum compressor characteristic slope, at which the system was stable, versus B-parameter was found to be much more useful in characterizing the effectiveness of the control strategy. The maximum stable slope versus B-parameter for the fixed wall system and for the (optimized) moving wall system is shown in Fig. 4; as indicated, the moveable wall system is capable of stable operation at much larger positive compressor slopes than the fixed wall system.

We can also plot maximum stable slope versus each of the control parameters about the optimized values to see how rapidly one departs from optimum conditions. Figure 5 thus shows the variations in maximum stable slope versus W, ζ, and Q respectively. The optimized values are indicated by arrows. Although substantial changes in the structural control parameters away from the optimized configuration will degrade performance, the stabilization is insensitive to small ($\pm 25\%$, say) changes in control parameters. The independent effects of B-parameter and tip Mach number, for a system with a fixed set of control parameters, is shown in Fig. 6 where one parameter is held constant and the other varied. As discussed, although the tip Mach number does not directly affect fixed wall system stability, it is an important parameter for the stability of the moving wall system.

ENERGY ANALYSIS

To examine the mechanism associated with stabilization, it is useful to look at the perturbation energy. From this viewpoint, the system is unstable when more energy is fed into any mode of oscillation over a cycle than is removed; neutral stability corresponds to zero net energy input. Because the modes are orthogonal, it is only necessary to consider one mode at a time. If any mode is unstable, the system is unstable.

Figure 7 shows the relative perturbation energy input and dissipation over a cycle at the neutral stability point, as a function of the B-parameter. Energy dissipation due to the wall motion is dominant, being more than ten times that for the throttle over a large range of B-parameters. The stabilization due to the wall is thus direct dissipation through plenum wall motion, rather than modification of the system dynamics to allow the throttle to dissipate more energy, as was the case in the throttle control experiments reported by Pinsley et al. (1989).

TIME-DOMAIN ANALYSIS AND NONLINEAR ASPECTS

The linear analysis yielded a set of optimized, non-dimensional control parameters which gave large increases in the stable flow range. Of interest also is the response beyond the initial instability, i.e. the non-linear system behavior. Non-linear computations were thus performed to assess the effects of finite amplitude disturbances and of non-linearities in the wall dynamics. The equations of motion were integrated using the Newmark time-averaged acceleration method. As in the linear analysis, the compressor characteristic shown in Fig. 3 was used.

As an example of the results, Fig. 8 shows the time response of the optimized system to a small impulse disturbance at the inlet operating near the linearly predicted stability line ($\phi = 0.096$). Wall motion and pressure perturbations exhibit essentially damped harmonic motion. To suppress the disturbance, the maximum non-dimensional wall motion required corresponded to 0.1% of the plenum volume. A more interesting point, to be discussed further in connection with the experiments, is that the non-linear computations showed that introducing wall motion into a fixed wall system undergoing deep surge cycles could suppress the surge. In other words, even though

the the control scheme was designed based on linear analysis, it was useful for oscillations that were strongly non-linear.

An important use of the non-linear analysis was to examine effect of Coulomb friction in the wall dynamics. The presence of Coulomb friction, in a strict sense, invalidates the linearity assumption. However, the degree to which the accuracy of the linear model is affected is a function of the ratio of the Coulomb friction forces compared to the other, essentially linear, forces in the system (Halfman, 1962). To assess this, a constant magnitude friction force was imposed on the wall, in the direction opposite to its motion, to model the sliding friction present in an actual design.

One important result of the Columb friction is that it prevents the wall from responding to disturbances below a certain threshold. Disturbances must grow to a critical amplitude before the wall can respond. Therefore, in a strict sense, operating points to the left of the natural surge line remain linearly unstable for the actual (non-ideal) tailored structure system. The linear instability that results from the presence of Coulomb friction, grows into a limit cycle, whose amplitude (for a given compression system and set of control parameters) is a function of the non-dimensionalized friction force, F, defined as

$$F = \frac{f}{\rho_0 U^2 A_p}$$

and the slope of the compressor characteristic.

The effect of Coulomb friction on surge suppression is demonstrated in Fig. 9 where the root mean square of the calculated limit cycle pressure fluctuations divided by the steady state pressure rise is plotted versus the local compressor characteristic slope, for various non-dimensional friction levels. (The vertical dashed line denotes the value of slope corresponding to the results in Fig. 10, discussed below.) The maximum value of the slope prior to deep surge (large amplitude oscillation) decreases with increasing friction levels. The deep surge boundary for the non-linear system with Coulomb friction agrees well with the linear stability boundary in the limit of zero friction. With increasing Coulomb friction levels, however, the performance of

the moveable plenum wall system approaches that of the fixed wall system. Analysis showed that the moveable plenum wall became unable to suppress surge past the rigid wall surge line for non-dimensional friction levels greater than F = 0.02.

As examples of the predicted limit cycle due to different levels of Coulomb friction, the time response of systems with various levels of Coulomb friction to a small impluse (0.001 $\overline{\Psi}$) is shown in Fig. 10. Parameters are given in the figure caption. The amplitude of each limit cycle is indicated in Fig. 9.

The disturbance decays in the system without Coulomb friction, but grows into a limit cycle in the systems with Coulomb friction. For the system with a small amount of Coulomb friction (F = 0.006) the limit cycle is small and approximately sinusoidal (mild surge) with frequency near the predicted Helmholtz frequency. However, for the system with larger Coulomb friction (F = 0.030), the limit cycle is no longer sinusoidal and contains regions of reversed flow (deep surge).

EXPERIMENT DESIGN

The basic prediction is that a properly designed moving plenum wall can substantially increase the stable flow range of a centrifugal compression system. To investigate this experimentally, a design study was undertaken to match the non-dimensional control parameters while minimizing the effects of non-linearities, in a physically realistic device.

The conceptual design was based on use of an existing centrifugal compressor facility, constructed to investigate active throttle control of surge. The facility is described in detail by Pinsley (1988); however, the major components will be outlined here. The centrifugal compressor was a Holset model H1D turbocharger. The impeller has an inlet area of 0.00125 m^2 with a hub to tip radius ratio of 0.37. The impeller exit tip diameter is 0.055 m. The compressor has no inlet guide vanes, 6 blades, 6 splitter blades, and a vaneless diffuser. A schematic of the basic compression system facility is shown in Fig. 11.

DESIGN OF MOVEABLE PLENUM WALL

Several different ways to mechanically implement the control scheme were reviewed. A

major constraint was that the wall had to be capable of withstanding large steady state and transient pressure loading, yet still respond to small amplitude perturbations in plenum pressure. A rigid plenum wall and an aerodynamic spring were determined to be practical solutions to these constraints.

To serve as the moveable wall, the rigid piston was mounted on a shaft, guided by linear bearings, and allowed to float between the main plenum and an auxilliary plenum. The seal between the two plenums was made with a low friction, convoluted diaphragm. A small diameter tube connected the two plenums so they were isolated for high frequency pressure disturbances (i.e. surge oscillations), but steady state pressures were equalized so that no steady state load existed on the piston. A mechanical spring was used to maintain a constant equilibrium position for the piston over various operating conditions since at steady state, the plenum wall had no preferred position. The mechanical spring also allowed the steady state position of the wall to be adjustable.

Because the presence of the steady state equalization tube could affect the behavior of the aerodynamic spring, computations were carried out to quantify the effect of leakage between the two plenums. with the leakage modelled as flow through an orifice plate. The results are shown in Fig. 12, where the decrease in maximum slope prior to surge is plotted versus non-dimensional orifice area for the optimized system at typical operating conditions. Leakage caused small amplitude limit cycles similar to those predicted to occur as a result of Coulomb friction, and it is important that leakage be kept to a minimum.

A viscous dashpot was used for the damping. To minimize Coulomb friction, a low friction, pnuematic, double acting actuator was modified to serve as a damper. The actuator was filled with 5W-30 oil and the ports on either end were connected through a variable area valve. Testing of various dashpots developed from the same basic design, showed that the force-velocity relation for the dashpot was closely linear over the expected range of wall velocities, as well as easily adjustable.

The final rig specifications are given below and a detailed drawing of the moveable plenum wall apparatus is shown in Fig. 13.

Design Specifications for the Flexible Plenum Wall Experimental Facility

B Parameter	1.3 to 2.0
Helmholtz Frequency	18.5 Hz to 19.9 Hz
W Parameter	0.11
Q Parameter	0.51
ζ Parameter	1.5 to 3.0
Area of Wall	0.0669 m^2
Mass of Wall	6.2 kg
Volume of Plenum	0.0108 m^3
Inlet Duct Length	1.16 m
Inlet Area	0.00125 m^2
Auxiliary Plenum Volume	0.0388 m^3
Aerodynamic Spring Constant	24,000 n/m to 35000 n/m
Mechanical Spring Constant	2100 n/m
Damping Ratio	1000 n s/m to 2000 n s/m
Maximum Wall Motion	+/-1.25 cm
Coulomb Friction	10 n

EXPERIMENTAL DATA AND ANALYSIS

The compression system was investigated with fixed and flexible wall for three different sets of structural control parameters, at B parameters ranging from 1.3 to 2.0. Steady state measurements were used to map the compression system performance and to define the surge line for both fixed and flexible wall systems. Time-resolved measurements were used to evaluate the model assumptions and to determine the performance characteristics of components in the compression system and in the flexible wall.

Steady State Behavior

The experimental compression system could be operated in a fixed wall configuration by

shutting the steady state pressure equalization line and bleeding the auxiliary plenum to atmospheric pressure. Pressure in the main plenum then forced the wall against its upper stops, yielding a fixed wall configuration. Forcing the plenum wall against the upper stop resulted in increasing the plenum volume approximately 5%, and, hence, the B-parameter 2.5%, which had a slightly destabilizing effect on the fixed wall compression system. Any movement of the surge line to the left due to wall motion will thus slightly underestimate the actual increase in stable flow range, although this difference is small compared to the difference seen between the fixed and flexible wall systems.

The compressor was operated at corrected speeds (referenced to 288°K) ranging from 60,000 rpm to 100,000 rpm, corresponding to a range of B-parameters of 0.65 to 1.0. The steady state performance is reported in terms of inlet total to plenum static pressure ratio and the mass flow is given in standard cubic feet per minute (SCFM). Mass flow is also given in some of the figures in terms of non-dimensional flow coefficient.

Because it was of interest to operate with the moveable plenum wall in the optimized as well as in the non-optimized configurations, speedlines for the moveable wall system were recorded with various levels of wall damping. The wall was operated at the theoretically optimized configuration ($W = 0.11$, $Q = 0.51$, $\zeta = 1.5$) as well as at values of $\zeta = 2.25$ and 3.0.

The steady state compressor performance map for the three moveable wall configurations and the fixed wall system, is shown in Fig. 14. The steady state pressure rise is unaffected by the presence of the moving wall in the stable flow range of the fixed wall system, but the surge line is moved to the left substantially. Also, the degree of surge suppression achieved is dependent on the moveable wall control parameters, as predicted. The optimized configuration performed the best, with the performance of the other two configurations decreasing as one moved farther from optimum. A surge line recorded for the moveable plenum wall system with a lower than optimum damping ratio ($\zeta = 0.75$) confirmed that movement in either direction in parameter space away from the optimal damping ratio was destabilizing.

Figure 15 shows the root-mean-square value of the fluctuations in plenum pressure versus

mass flow coefficient for the fixed wall system and the optimized moveable plenum wall system at B = 0.91 (90K speedline). On the negative sloped region of the speedline (above $\phi = 0.155$), the rms of the pressure fluctuations for the fixed and moveable wall system are the same. However, small amplitude limit cycles exist in the stabilized region. These can be attributed to Coulomb friction in the wall motion and the pressure equilization leakage. Small amplitude limit cycles also occur over a limited range of mass flow in the fixed wall system prior to deep surge, but these appear to be a result of non-linearities in the compressor and throttle characteristics.

Figure 16 shows the predicted and the experimentally determined surge lines for the rigid wall and for the optimized system. The predicted surge line is based on the linear instability point as determined by the eigenvalue stability analysis described previously. The compressor characteristics used are from a simple third degree polynomial curve fit of the speedlines measured by Pinsley (1988). The results are also plotted in Fig. 17 as predicted versus measured mass flow coefficient at surge, for fixed wall and optimized systems.

The experimental results can be compared to the non-linear calculations by examining the amplitudes of pressure fluctuations in the plenum as a function of mass flow. As inputs to the calculation, the friction force present during wall motion was measured to be approximately 10 newtons and the leakage was estimated to be equivalent to a 0.003 meter diameter orifice plate. The results of the calculation and experiment for the optimized system operating at B = 0.91 are shown in Fig. 18, where the amplitude of the small plenum pressure limit cycles before the onset of deep surge are shown versus mass flow coefficient. The linear stability boundary is also shown in Fig. 18 for comparison. The linear analysis does not predict the small amplitude limit cycles in the stabilized region, but it is able to accurately portray the onset point for deep surge. The reason is that the oscillations are the result of non-linear effects, described above. If the non-linear effects are small, which is inherent in the experimental design, the linearly predicted stability limit corresponds to the onset of deep surge. The non-linear analysis shows limit cycles in the stabilized region, although the detailed relationship between mass flow and limit cycle amplitude is not captured.

TRANSIENT SYSTEM BEHAVIOR

Time resolved measurements were recorded for the fixed wall compression system and for the moving wall system at three control parameter configurations. The measuremehts were made on the 70K and 90K speedlines, corresponding to B-parameters of 0.73 and 0.91. The data shown is from the former, at the points marked on Fig. 19.

As noted previously, the flow through the compression system becomes progressively more unsteady as the system approaches the surge line. To demonstrate this, the time resolved non-dimensional mass flow coefficient and the non-dimensional pressure rise for the fixed wall system are shown in Fig. 20 for 3 operating points (marked A-C in Fig. 19). The transient mass flow measurements are based on a linearized hot wire calibration and therefore, the large oscillations in mass flow are presented for qualitative information only. The data shown correspond to points in both the stable and un. ›le operating regions.

For flows near point A, on the negative slope region of the compressor characteristic, stable operation with only slight unsteadiness is exhibited.

Point B is slightly to the left of the peak of the compressor characteristic. Small amplitude limit cycles (mild surge) are seen. The frequency of the mild surge cycle is approximately 14.5 Hz, compared to the predicted Helmholtz frequency of 17.5 Hz.

Points C and below, on the positive slope region of the speedline, are in deep surge. The time averaged pressure rise and mass flow are decreased and the frequency of the deep surge oscillations has been changed to approximately 10 Hz. The hotwire does not distinguish reversed flow, and the reversed flow regions are shown with a dashed line. The decrease in frequency is due to non-linearities associated with plenum blow-down and re-pressurization as described by Fink (1988).

With the moving wall system small amplitude limit cycles existed over the stabilized region. Figure 21 shows the non-dimensional mass flow, pressure rise, and corresponding non-dimensional wall motion for the medium damping configuration operating at the 70K speedline for

4 operating points, D, E, F, and G, shown on the compressor characteristic in Fig. 19.

Point D is in smooth operation on the negatively sloped region of the map. The steady-state and unsteady behavior is similar to point A for the fixed wall configuration. The position of the wall is shown to be stationary, indicating that the disturbances in the stable system are not large enough to overcome the wall friction.

Points E and F are located on the positively sloped, stabilized region of the characteristic and exhibit small amplitude limit cycles. The maximum wall motion required to stabilize the system is approximately 0.1% of the plenum volume and the power dissipated is approximately 0.05% of the steady power of the compression system.

At point G, in deep surge, the pressure and mass flow traces are similar in amplitude to those with the fixed wall although the fluctuations have a much lower natural frequency (4-5 Hz). Also, in deep surge, the wall is shown to be hitting the displacement limiters, indicated by the flat spots on the time trace of the wall motion.

The moveable plenum wall also demonstrated the ability to suppress deep surge if the wall were freed (by equalizing the pressures in the aerodynamic spring and in the main plenum) during a fixed wall surge cycle. This is demonstrated by the time history shown in Fig. 22, where fixed wall surge is suppressed by equalizing the auxiliary plenum pressure, thus freeing the wall from the displacement limiters. The time traces in Figure 22 show the wall bouncing on the stops as the auxiliary plenum pressure equalizes. When the wall clears the stops, the deep surge cycle is suppressed. Although not shown, the wall continues to move towards its steady state equilibrium position as the pressures in the auxiliary and main plenums equalize.

Two other points should be made about the time history. First, the time scale over which the surge suppression occurs is considerably longer than any time scale associated with the system oscillations because it is set by the filling time (through the small equalization tube) of the auxiliary plenum. Second, as seen in previous figures, the deep surge regime is one in which the oscillations are strongly non-linear, with mass flow oscillations 100% of the time averaged value. This indicates that the use of tailored structure can suppress surge even when the oscillations have

large amplitude. In this connection it should be noted that similar behavior has been found by Pinsley et al. (1988) and Ffowcs Williams and Huang (1989) using different active control schemes. Such behavior, which is captured by the numerical calculations, emphasizes that successful use of dynamic control is not restricted to the small amplitude regime.

DYNAMIC RESPONSE OF SYSTEM COMPONENTS

Compressor Behavior

One of the major assumptions used in modelling the compression system is that the compressor remains on its steady state characteristic during transient operation, at least for frequencies on the order of the Helmholtz frequency. To check this, the unsteady pressure rise versus mass flow relation (i.e. the transfer function) can be calculated directly from the unsteady data and compared to the quasi-steady slopes. The unsteady data was taken from operating points exhibiting small amplitude limit cycles. The instantaneous pressure rise versus mass flow slope was determined from measurements of inlet mass flow and plenum pressure correcting for the inertia of the fluid in the inlet duct. Only self-excited oscillations were examined, so that measurements were obtained only at or near the system resonant frequency where there was an acceptable signal to noise ratio.

The compressor slope, as measured, yielded a real and imaginary part. The real part of represents the instantaneous slope of the compressor characteristic. The imaginary part can be viewed as a lag term, similar to the lag term discussed by Fink (1988), which accounts in a rudimentary fashion for the unsteady aerodynamics within the compressor. The real part of the transfer function is plotted versus steady state mass flow coefficient for the 70K and 90K speedlines in Fig. 23. The slope of the compressor characteristic plotted in Fig. 23 contains data from both fixed and moveable wall systems, indicating that, as would be expected, the presence of the wall has no noticeable effect on the instantaneous characteristic slope. Also plotted in the figure are the slopes resulting from two methods of fitting the steady-state data. One method was the derivative of a third order polynomial curvefit, the other is a third order polynomial fit of the

derivative of a cubic spline fit of the steady state compressor data. As shown, the compressor characteristic slopes determined from the steady state data and those determined from unsteady data are in reasonably good agreement. In particular,the unsteady data falls within the variance between the two steady state slopes calculated by curve fits. The assumption of quasi-steady behavior thus appears to be an adequate representation of the instantaneous compressor slope over the range of flow coefficients investigated.

The time lag for both the 70K and 90K speedlines was approximately 5-10 milliseconds, corresponding to 0.065-0.13 Helmholtz resonator periods. The compressor through flow time can be estimated at approximately 3.0 milliseconds. The lag term is thus on the order of the through time of the compressor and it seems reasonable to attribute the lag to unsteady aerodynamic effects within the compressor passages. This is in agreement with the conclusions of Fink (1988), who determined that a lag term on the order of compressor through flow time was needed for agreement between the predicted and experimental behavior of a compression system in deep surge. Fink also found that a lag term of this order should have a negligible effect on system stability over the range of B-parameters investigated. It thus appears that the quasi-steady compressor slope is adequate for predicting the onset of surge.

Another assumption used in the present treatment is that the wheel speed remains constant for perturbations in mass flow and pressure rise. This is not strictly correct since pressure and mass flow perturbations vary the power requirements of the compressor causing the wheel speed to also vary. Fink (1988) assessed the constant wheel speed assumption and showed that variable wheel speed had a stabilizing effect on the compression system. The degree of stabilization was shown to be a function of a non-dimensional parameter, defined as

$$\text{Wheel inertia parameter} = \frac{2\,\rho_o\,L_c\,A_{in}\,R_T^2}{I}$$

where I is the moment of inertia of the wheel. Using Fink's results, variations in wheel speed were found to have negligible effect on the stability of the compression system used in the present experiments.

An alternative way to address this point is to note that if the wheel speed and pressure

fluctuations were strongly coupled, the non-dimensional pressure rise and wheel speed variations during mild surge would be roughly the same order. However, for a typical (say 2.5% rms) pressure fluctuation, the measured wheel speed fluctuations are only 0.2%, an order of magnitude less. The assumption of constant wheel speed is thus adequate for modelling the small perturbation response, and hence linear stability, of the compression system.

Behavior of Tailored Structure

The time-resolved data was also used to characterize the performance of the moving wall. Analysis of the Fourier content of the wall displacement and force in the damper signals showed that the dashpot had a constant damping constant over the range of frequencies with a signi.. .t Fourier component. The aerodynamic spring was also shown to behave linearly, as modelled. Details of the measurements are given by Gysling (1989).

CONCLUSIONS

Dynamic control using tailored structure has been shown to be effective in suppressing centrifugal compressor surge. The use of a moveable plenum wall shifted the surge line to the left appproximately 25 to 30% in flow over a significant portion of the corrected speed range examined. The effectiveness of surge suppression is a function of a set of non-dimensional parameters which govern the aeroelastic coupling of the wall to the compression system dynamics.

The present scheme was found to be quite robust, suppressing surge over a wide range of operating conditions with no adjustment to the parameters. The moveable wall was also demonstrated to be capable of suppressing an existing, (highly non-linear), surge cycle. In the stabilized region of the compressor map, the moveable wall supressed surge with no time average performance penalty.

The amount of control action (wall motion) required is a function of the non-linearities in the wall dynamics, such as Coulomb friction and leakage. For the optimized configuration investigated in this research, the nominal limit cycle wall motion in the stablized region was

roughly 0.1% of plenum volume, with frequencies near the Helmholtz frequency. Pressure fluctuations in the stabilized region were on the order of 0.5% of the mean pressure rise of the compressor.

Time-resolved data was used to verify some of the major assumptions in the modelling of the compression system. Compressor transfer function measurements showed that a quasi-steady compressor characteristic gave a reasonable representation of the instantaneous compressor characteristic slope. These measurement also indicated that the improvement in surge margin is due to modification of the system dynamics, rather than a result of modifying the compressor characteristic by altering the local flow in the compressor. The smallness of the measured wheel speed variations supported the predictions that wheel speed variation would not significantly affect system stability.

In general, all aspects of the experimental investigations confirmed that the lumped parameter model of the compression system provided a useful description of the system dynamics, both with and without the moveable plenum wall.

The physical mechanism responsible for the surge suppression with the flexible wall is unsteady energy dissipation due to the wall motion.

The maximum stable compressor characteristic slope is a better measure of the effectiveness of this control scheme rather than the minimum stable mass flow coefficient. The steady state mass flow coefficient has little effect, in an explicit way, on the stability of the compression system with the moveable wall, and the dominant influence of mass flow is only through the relation between mass flow and compressor slope, implied by the characteristic.

Non-linear solution of the system equations showed the existence of small amplitude limit cycles in the stabilized region in agreement with measurement. These limit cycles were found to result primarily from Coulomb friction and leakage.

ACKNOWLEDGEMENTS

The project was conducted at the Gas Turbine Lab under a grant from the Air Force Office of Scientific Research, Dr. J. M. McMicheal and Capt. H. Helin, program managers. This support is gratefully acknowledged. Financial support for D.L. Gysling was provided by the Air Force Research in Aero Propulsion Technology (AFRAPT) program, AFSOR-85-0288. The authors also wish to express their appreciation to Dr. G.R. Guenette for his extremely useful technical advice and assistance throughout this research.

REFERENCES

Chen, G.T., "Active Contol of Turbomachinery Instabilities -- Initial Calculations and Results", M.S. Thesis, Department of Aeronautics and Astronautics, MIT, August 1987.

Dean, R.C., Jr. and Young, L.R.,"The Time Domain of Centrifugal Compressor and Pump Stability and Surge", ASME *Journal of Fluids Engineering*, March 1977, pp.53-63.

Emmons, H.W., Pearson, C.E., and Grant, H.P., "Compressor Surge and Stall Propagation", *ASME Transactions*, Vol.77, April 1955, pp. 455-469.

Epstein, A.H., Ffowcs Williams, J.E., and Greitzer, E.M., "Active Suppression of Compressor Instabilities", *J. Propulsion and Power*, Vol. 5, March 1989, pp. 204-211.

Ffowcs Williams, F.E., and Huang, X., "Active Stabilization of Compressor Surge", *J. Fluid Mech.*, Vol. 204, August 1989, pp. 245-262.

Fink, D.A., "Surge Dynamics and Unsteady Flow Phenomena in Centrifugal Compressors", Ph.D Thesis, Department of Aeronautics and Astronautics, MIT, May 1988.

Gysling, D.L., "Dynamic Control of Centrifugal Compressor Surge Using Tailored Structure," M.S. Thesis, Department of Aeronautics and Astronautics, MIT, August 1989.

Greitzer, E.M., "The Stability of Pumping Systems -- The 1980 Freeman Scholar Lecture", *Journal of Fluids Engineering*, Vol. 103, June 1981, pp.193-242.

Halfman, R.L., Dynamics, Addison-Wesley Publishing Company, Inc., Reading, MA, 1962, p. 335.

Pinsley, J.E., "Active Control of Centrifugal Compressor Surge", M.S. Thesis, Department of Aeronautics and Astronautics, MIT, October 1988.

Pinsley, J.E., Guenette, G.R., Epstein, A.H., and Greitzer, E.M., "Active Stabilization of Centrifugal Compressor Surge," submitted to 1990 ASME Gas Turbine Conference.

Stenning, A.H., "Rotating Stall and Surge", ASME *Journal of Fluids Engineering*, Vol. 102, March 1980, pp.14-20.

APPENDIX A
DERIVATION OF THE EQUATIONS OF MOTION FOR THE MOVEABLE PLENUM WALL SYSTEM

Consider the compression system shown in Fig. 1b. The following assumptions are used: the flow in the inlet ducting is 1-D, incompressible, inviscid, and unsteady; the plenum pressure is spatially uniform and plenum processes are isentropic; the fluid inertia in the throttle is negligible; the compressor follows a quasi-steady characteristic; and the throttle pressure drop mass flow relation is parabolic.

The momentum equation applied to the compressor duct yields

$$P_0 + \Delta P_c(\dot{m}_1) - P_p = \frac{L_c}{A_{in}} \frac{d\dot{m}_1}{dt} \tag{A.1}$$

where L_c is the equivalent length of the compressor duct. Mass conservation in the plenum yields

$$\dot{m}_1 - \dot{m}_2 = \frac{d(\rho_p V_p)}{dt} \tag{A.2}$$

The pressure drop across the throttle can be written in terms of the throttle mass flow as

$$\Delta P_T(\dot{m}_2) = \frac{1}{2} \frac{\dot{m}_2^2}{\rho_T A_T^2} \tag{A.3}$$

Finally, the motion of the wall is given by

$$m\ddot{q} + c\dot{q} + kq = (P_o - P_{aux\ plenum})\, A_p \tag{A.4}$$

where q is defined as the position of the wall away from the equilibrium position of the wall.

Writing the fluid dynamic variables as mean $(\bar{(\ )})$ plus small perturbations $(\delta(\ ))$ and linearizing the compressor and throttle characteristics about a time-mean operating point yields equations for the perturbation quantities:

$$\left(\frac{d\Delta P_c}{d\dot{m}}\right) \delta\dot{m}_1 - \delta P_p = \frac{L_c}{A_{in}} \frac{d(\delta\dot{m}_1)}{dt} \tag{A.5}$$

$$\delta\dot{m}_1 - \delta\dot{m}_2 = \frac{V_p}{a_p^2} + \rho_p \frac{dV_p}{dt} \tag{A.6}$$

In Eq. (A.6), the isentropic assumption has been used.

We introduce the following non-dimensional quantities

$$\phi = \frac{\dot{m}}{\rho_0 A_{in} U} \qquad \tau = \omega_H t$$

$$\psi_c = \frac{\Delta P_c}{\frac{1}{2}\rho U^2} \qquad B = \frac{U}{2\omega_H L_c}$$

$$\psi_T = \frac{\Delta P_T}{\frac{1}{2}\rho U^2} \qquad \eta = \frac{A_p Q}{\overline{V}_p}$$

$$\psi = \frac{P_p - P_0}{\frac{1}{2}\rho U^2} \qquad M = \frac{U}{A_p}$$

Using these equations, Eqs. (A.5) and (A.6) can be written as

$$\left(\frac{\overline{d\psi_c}}{d\phi}\right)\delta\phi_1 - \delta\psi = \frac{1}{B}\frac{d\delta\phi_1}{d\tau} \tag{A.7}$$

and

$$\delta\phi_1 - \delta\phi_1 = B\frac{d\psi}{d\tau} + \frac{\rho_p}{\rho_0}\frac{B}{M^2}\frac{d\eta}{d\tau} \tag{A.8}$$

The throttle pressure drop equation can be written as

$$\delta\psi = \frac{\rho_0}{\rho_T}\left(\frac{d\psi_T}{d\phi}\right)\delta\phi_2$$

or (A.9)

$$\delta\psi = \frac{\rho_0}{\rho_T}\left(\frac{\overline{\phi}^2}{2\overline{\psi}}\right)\delta\phi_2$$

For the wall motion, we define the following non-dimensional control parameters:

$$W = \frac{\rho_0 A_p^2 L_c^2}{mV_p}$$

$$\zeta' = \frac{c}{2m\omega_p}$$

$$Q' = \frac{\omega_p}{\omega_H}$$

The wall dynamics can then be written in non-dimensional form as:

$$\frac{d^2\delta\eta}{d\tau^2} + 2\zeta' Q' \frac{d\delta\eta}{d\tau} + Q'^2\,\delta\eta = WB^2\delta\psi \tag{A.10}$$

Using the algebraic relation between $\delta\psi$ and $\delta\phi_2$, the throttle characteristic can be used to eliminate $\delta\psi$ from the set of non-dimensional equations. In addition, we can define

$$v = \frac{d\eta}{d\tau}$$

as a non-dimensional wall velocity to convert Eq. (A.10) into two first order equations. Rearranging these equations, and making use of Eq. (A.9), yields the following stability matrix:

$$\begin{bmatrix} B\left(\frac{d\bar{\psi}_c}{d\bar{\phi}}\right) - s & \frac{2B\bar{\psi}}{\bar{\phi}} & 0 & 0 \\ \frac{1}{B}\frac{\bar{\phi}}{2\bar{\psi}} & -\frac{1}{B}\frac{\bar{\phi}}{2\bar{\psi}} - s & 0 & -\frac{\rho_p}{\rho_0}\frac{1}{M^2}\frac{\bar{\phi}}{2\bar{\psi}} \\ 0 & 0 & -s & 1 \\ 0 & WB^2\frac{2\bar{\psi}}{\bar{\phi}} & -Q^2 & -2\zeta Q - s \end{bmatrix} \begin{bmatrix} \delta\phi_1 \\ \delta\phi_2 \\ \delta\eta \\ \delta v \end{bmatrix} = \begin{bmatrix} 0 \\ 0 \\ 0 \\ 0 \end{bmatrix} \tag{A.11}$$

The control parameters Q' and ζ' are referenced to the Helmholtz frequency of the compression system, which varies slightly with operating conditions. They can be modified so that they remain independent of operating conditions. Thus, substitution of the following corrected control parameters yields the stability matrix given as Eq. (10).

$$Q = Q'\sqrt{\frac{\rho_0}{\rho_p}} \qquad \text{and} \qquad \zeta = \zeta'\sqrt{\frac{P_p}{P_0}\frac{\rho_0}{\rho_p}}$$

We also note, for reference, that expanding the determinant for the 2x2 system governing the fixed wall compression system dynamics leads to the characteristic equation shown below:

$$s^2 + \left[\frac{1}{\frac{2\bar{\psi}}{\bar{\phi}} B} - B\left(\frac{\overline{d\psi_c}}{d\phi}\right) \right] s + \left[1 - \left(\frac{\overline{d\psi_c}}{d\phi}\right) \frac{\bar{\phi}}{2\bar{\psi}} \right] = 0$$

Dynamic instability occurs when the first term in brackets becomes negative. The condition for this is

$$\frac{d\psi_c}{d\phi} > \frac{1}{2B^2 \frac{2\bar{\psi}}{\bar{\phi}}}$$

which is the fixed wall stability limit.

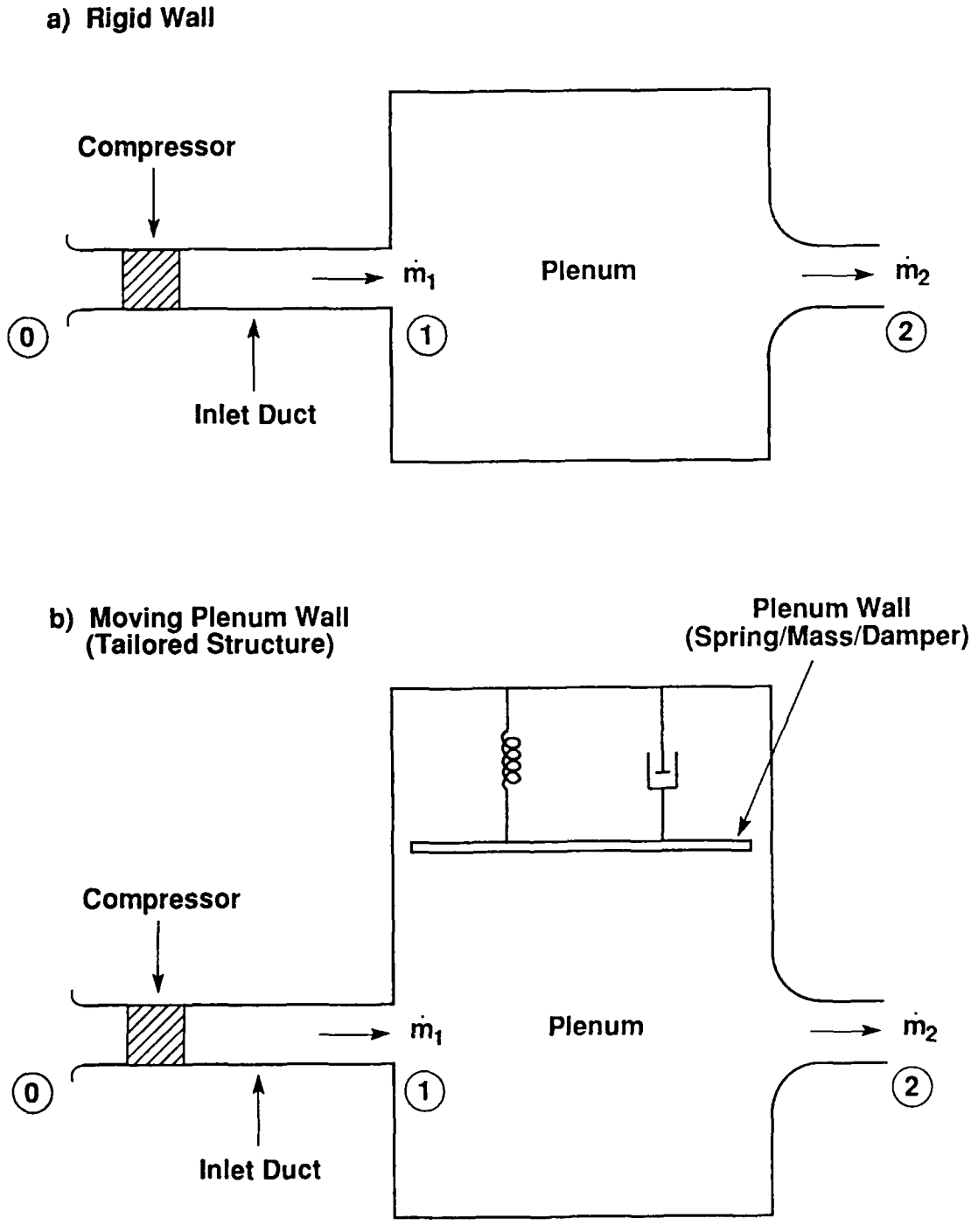

Fig. 1: Schematic of rigid (fixed) wall (a) and moveable plenum wall (b) compression systems

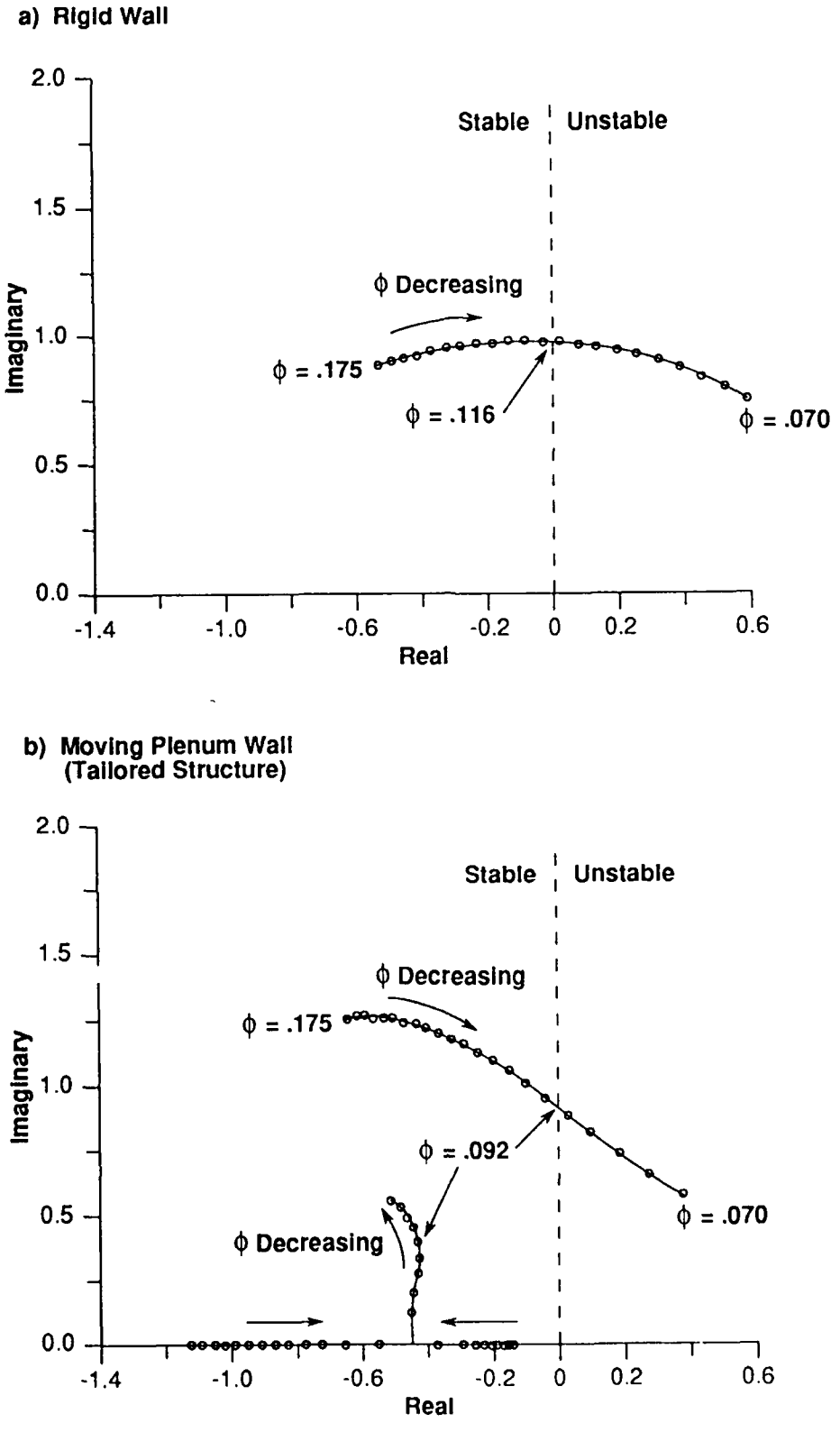

Fig. 2: Root locus plots for rigid wall (a) and moveable plenum wall (b) compression system: B = 0.5, M = 0.4, W = 0.11, ζ = 1.5, Q = 0.51 for moveable wall system

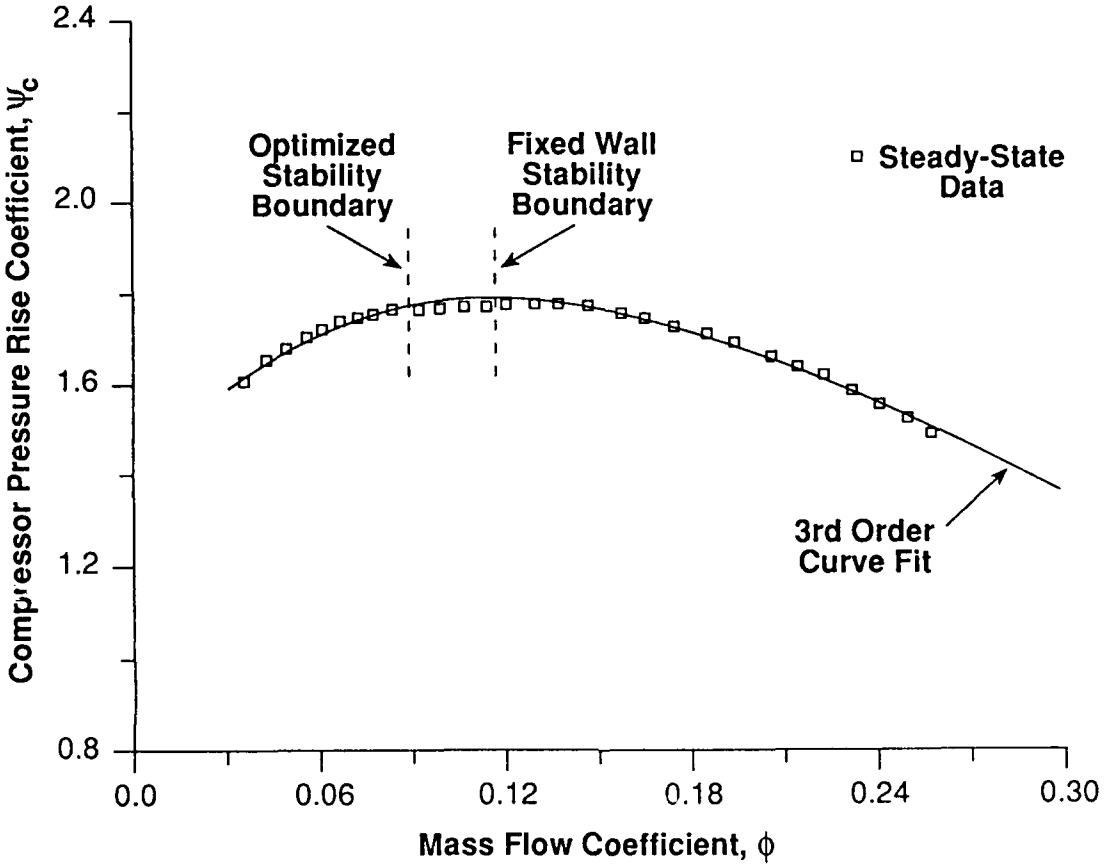

Fig. 3: Compressor pressure rise characteristic used in analysis; data of Pinsley (1988)

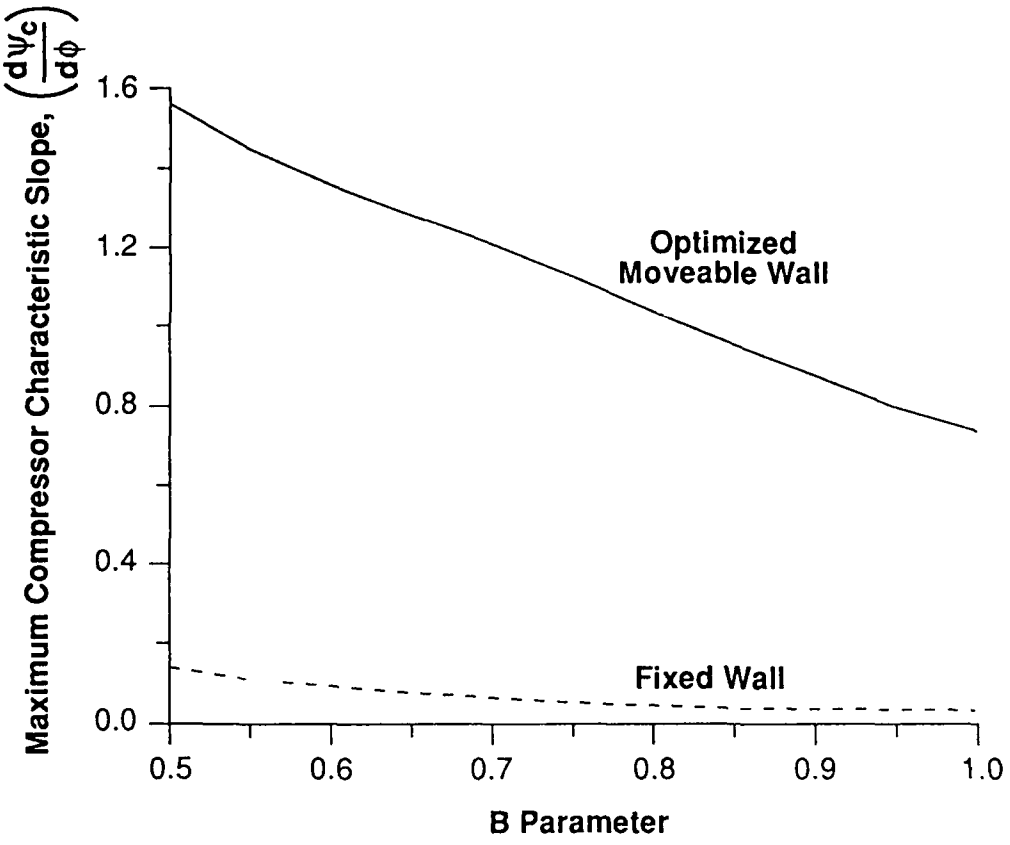

Fig. 4: Maximum achievable compressor characteristic slope with stable operation versus B-parameter

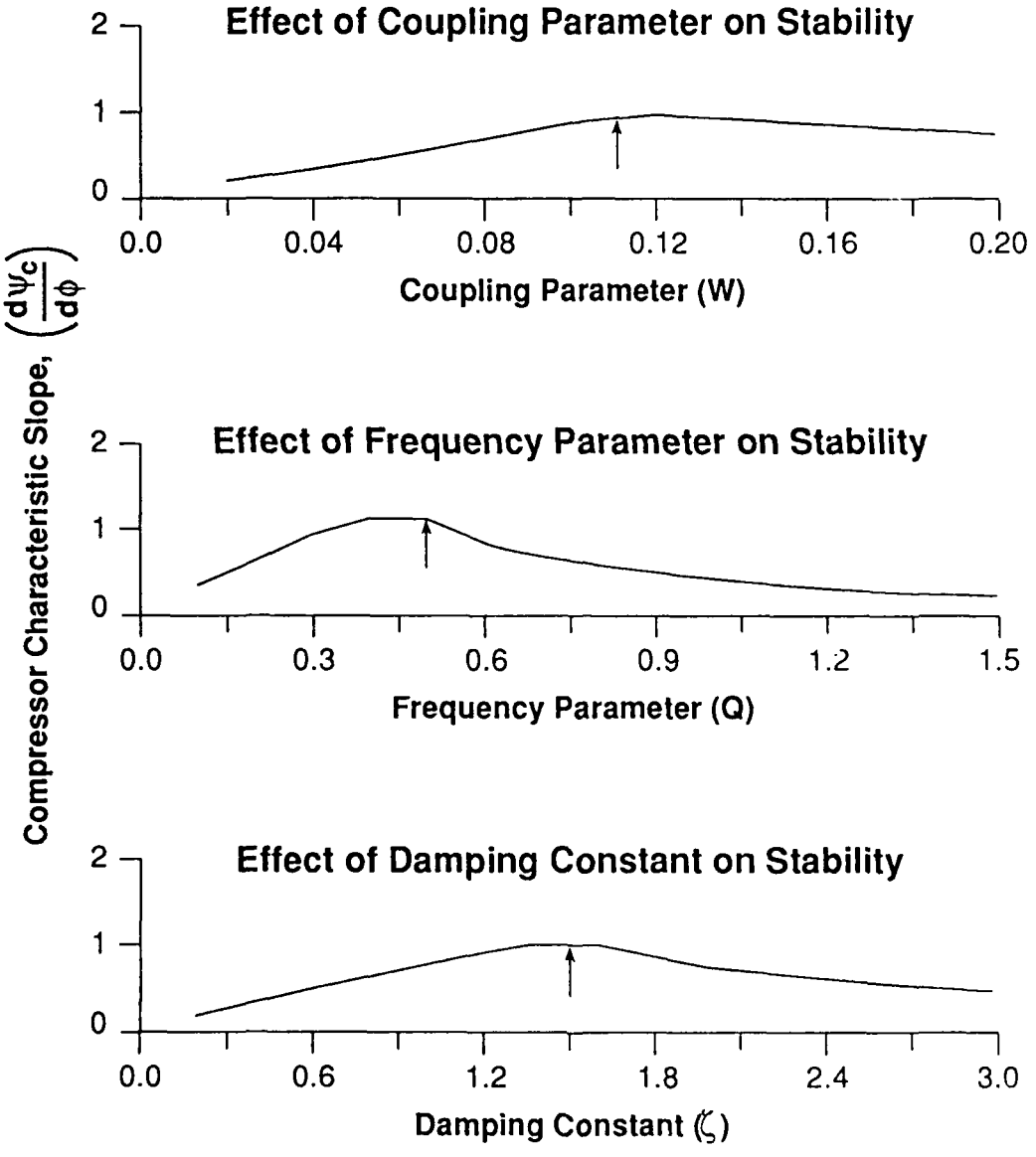

Fig. 5: Effect of tailored structure control parameters on maximum achievable compressor characteristic slope for stable operation

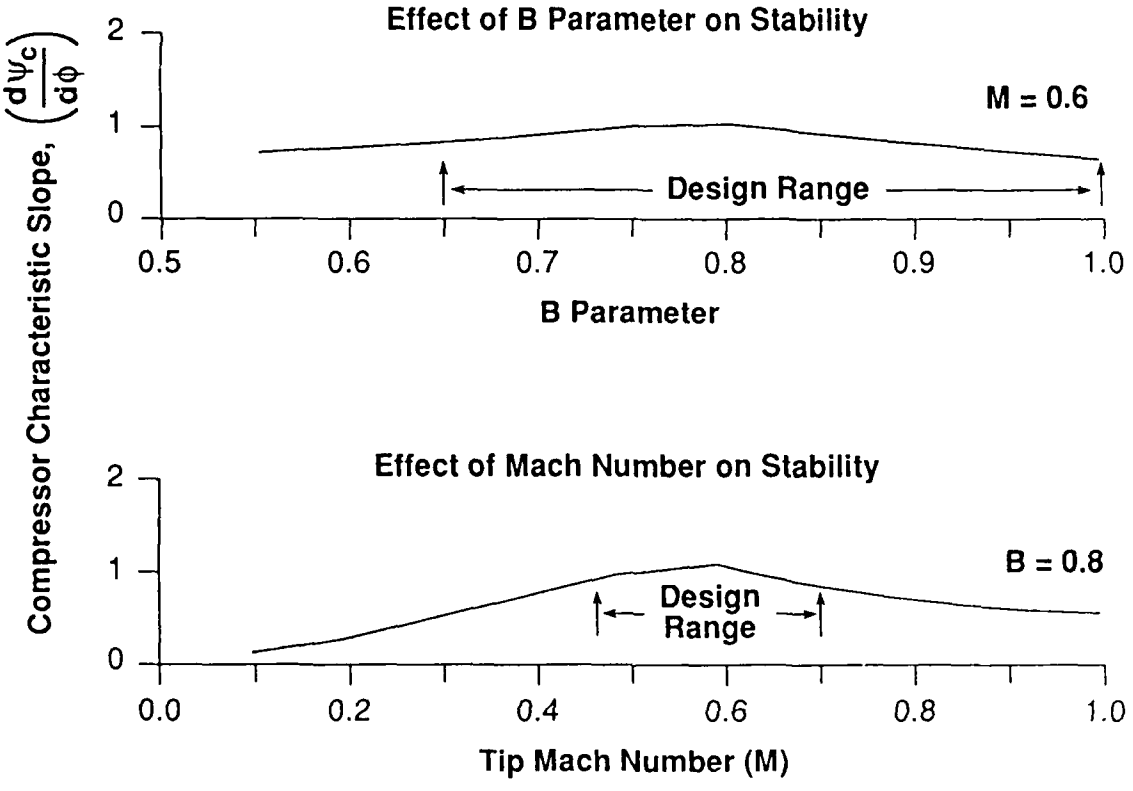

Fig. 6: Independent effects of B-parameter and tip Mach number on maximum achievable compressor characteristic slope for stable operation

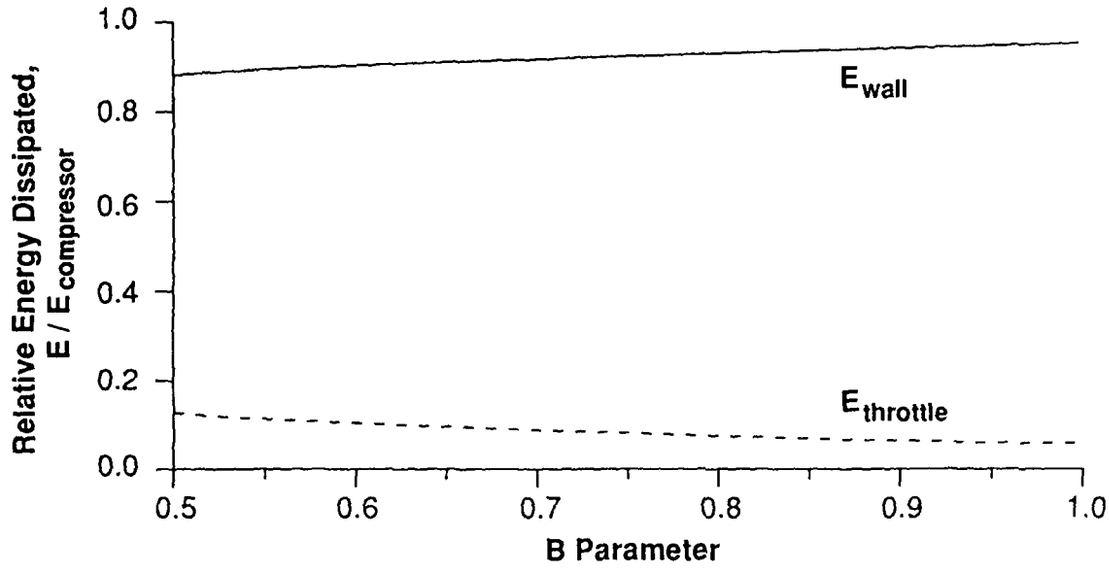

Fig. 7: Comparison of perturbation energy dissipation in throttle and in moving wall system; relative units

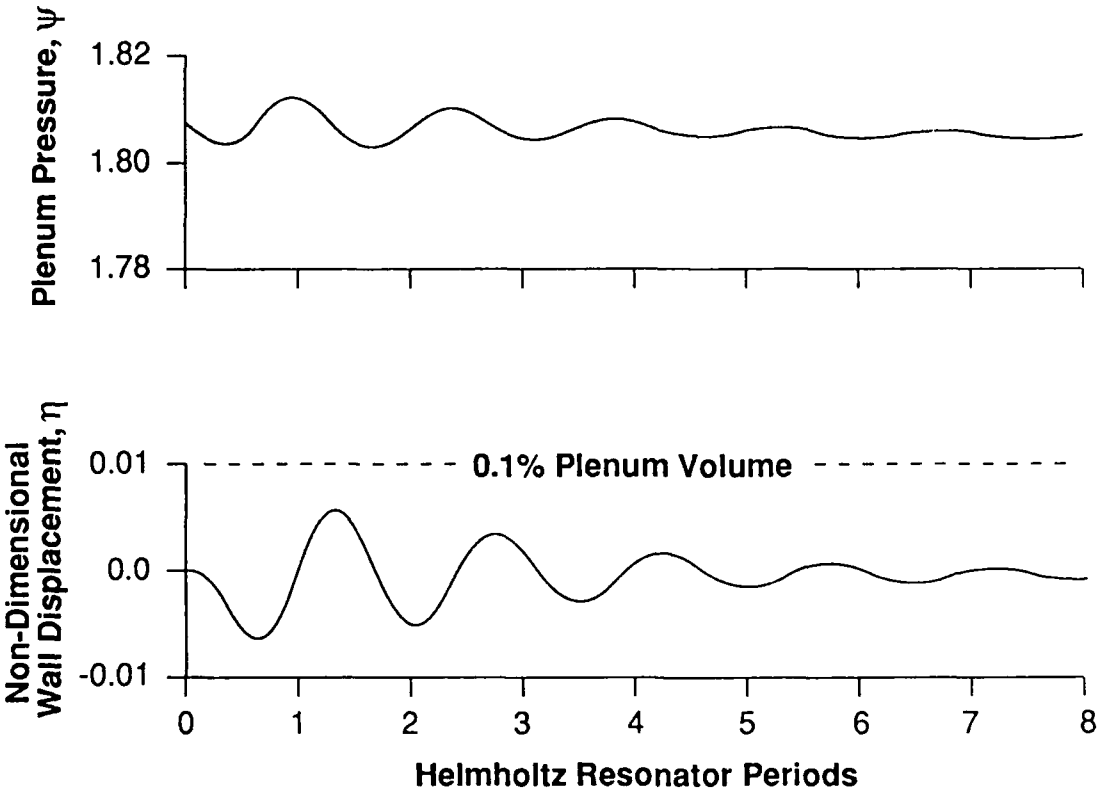

Fig. 8: Wall motion and plenum pressure response to impulse of $10^{-2}\bar{\psi}$; optimized system parameters

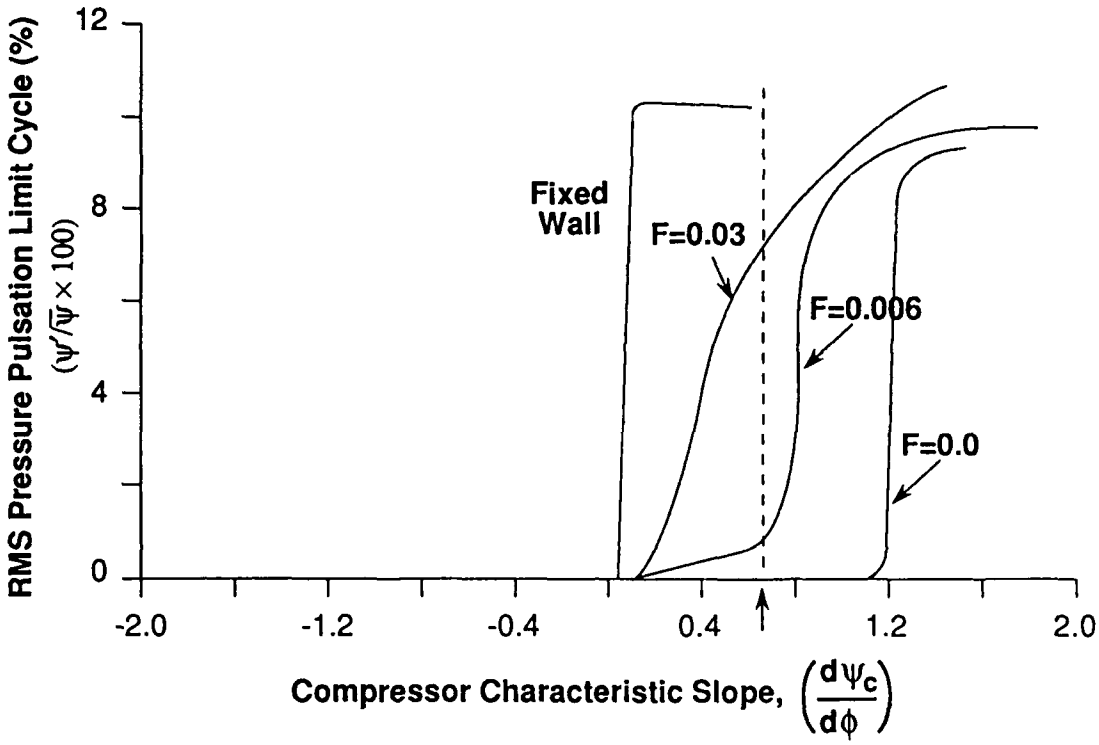

Fig. 9: Effect of Columb friction on limit cycle amplitude; optimized system parameters

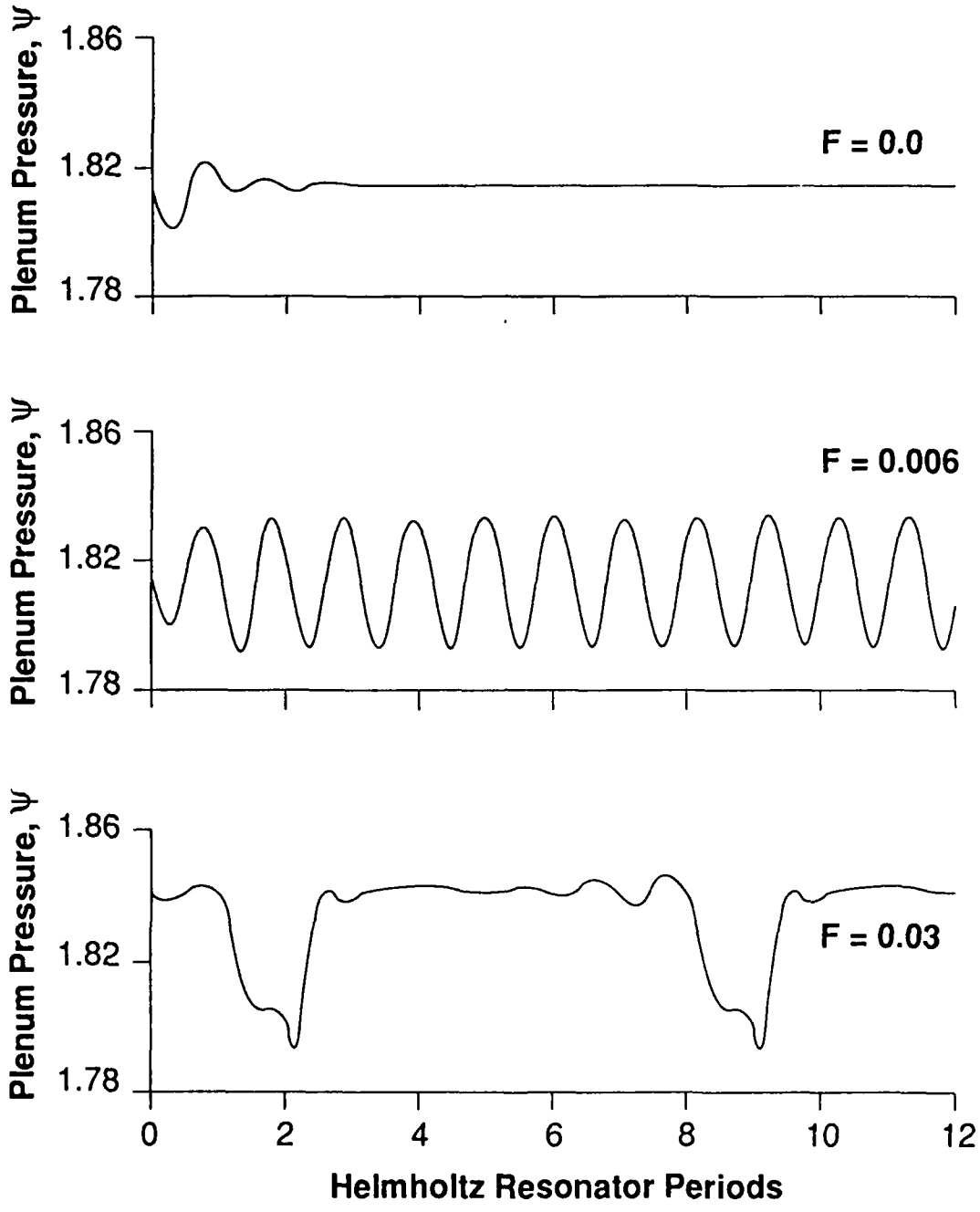

Fig. 10: Effect of Columb friction on transient system response, at a compressor characteristic slope $\left(d\psi_c/d\phi\right) = 0.66$ (dashed line on Fig. 9)

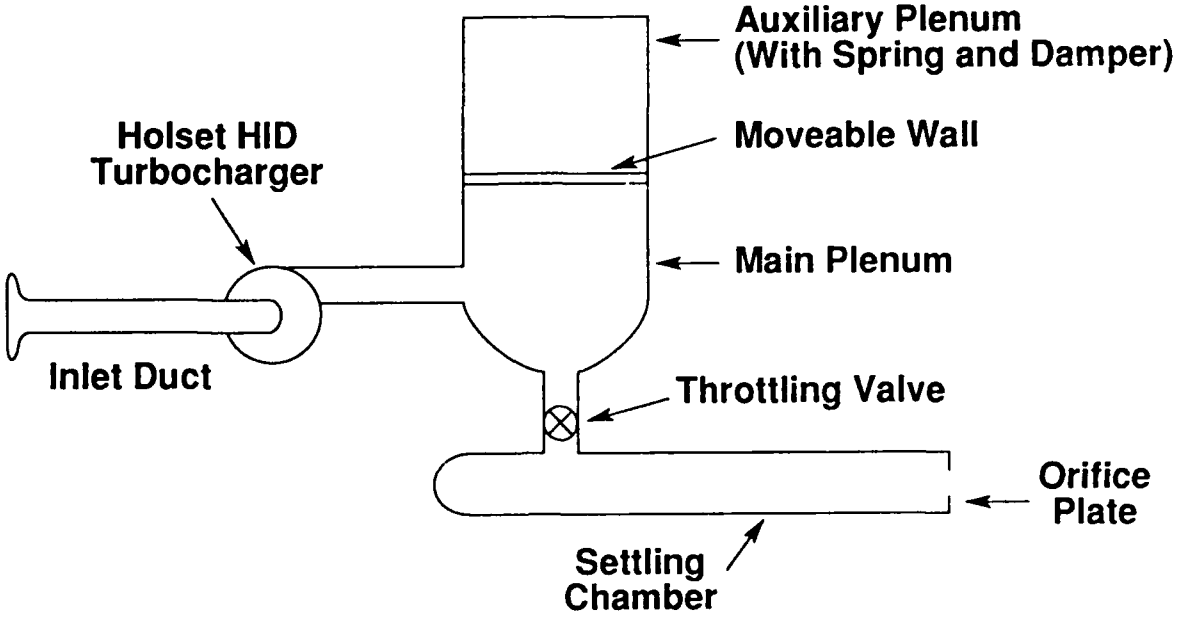

Fig. 11: Schematic of experimental facility

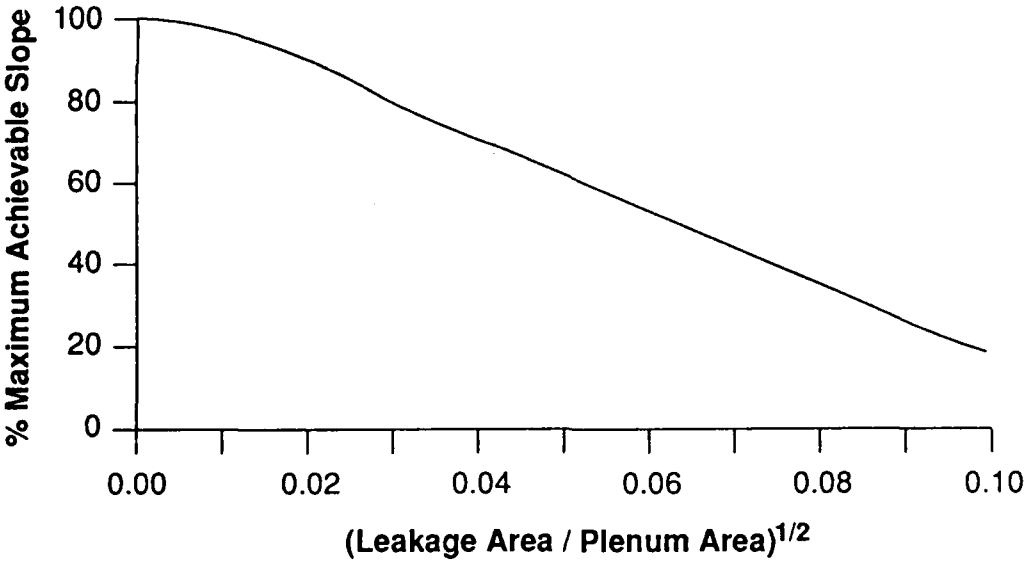

Fig. 12: Effect of leakage on maximum achievable compressor characteristic slope for stable operation with optimized system

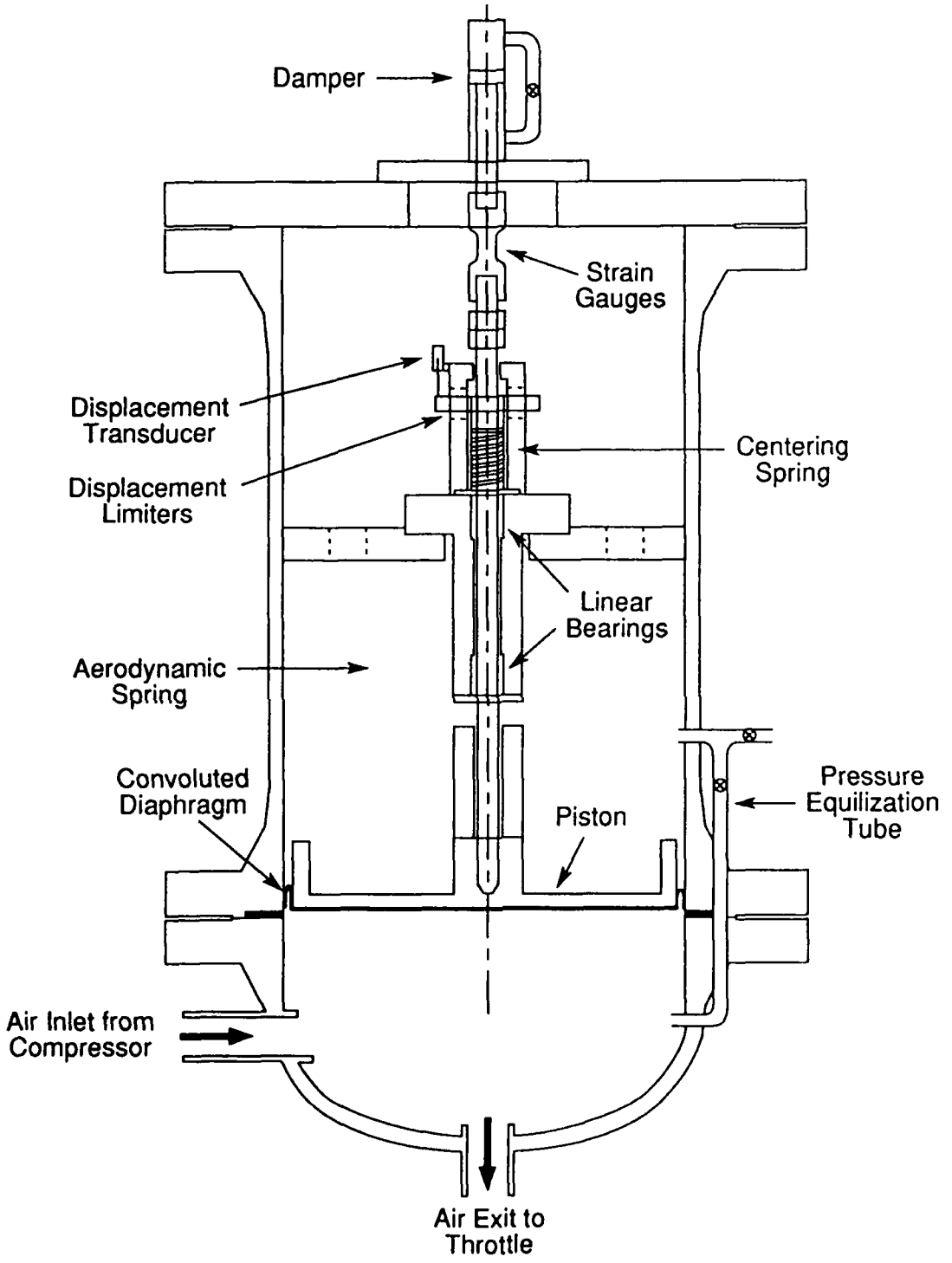

Fig. 13: Moveable plenum wall (tailored structure) showing mass-spring-damper system

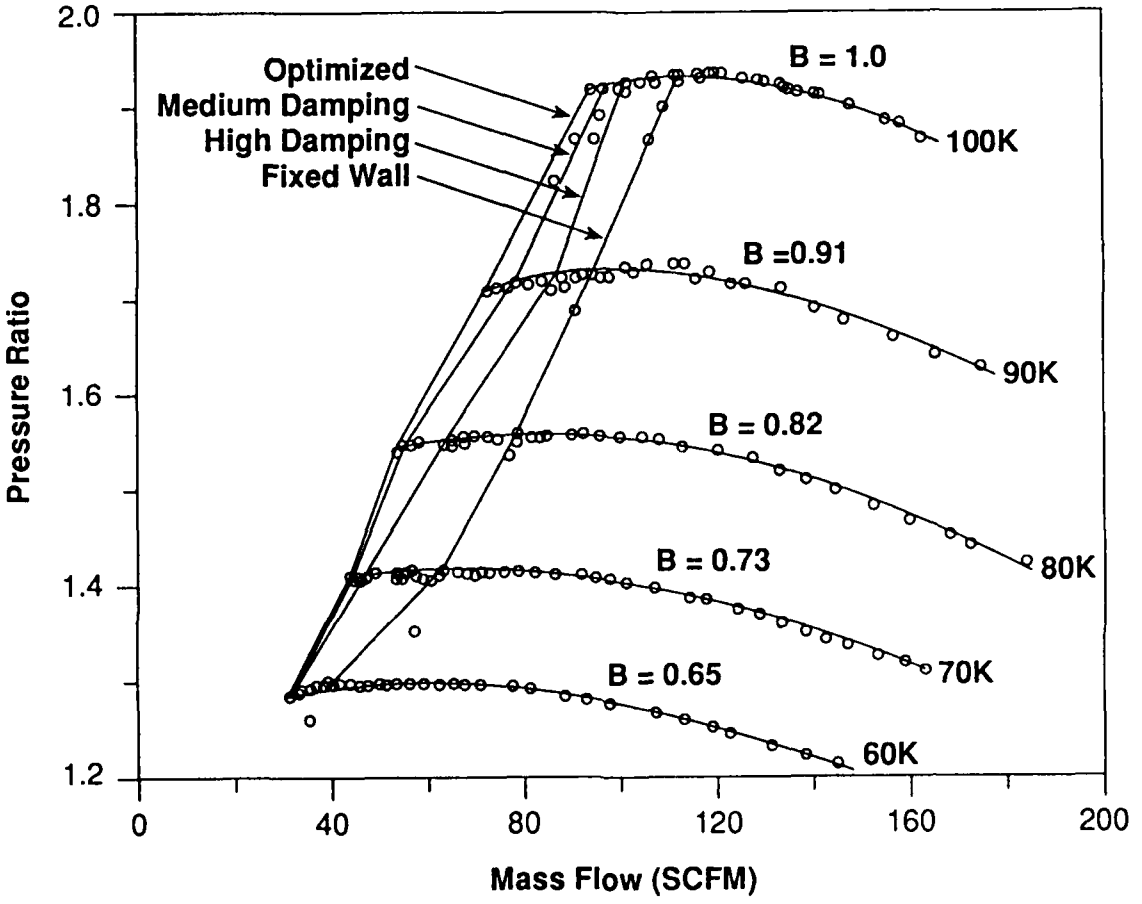

Fig. 14: Compressor map showing increase in stable flow region due to tailored structure for three values of damping; damping values ζ = 1.5, 2.25, 3.0, other parameters at optimized values

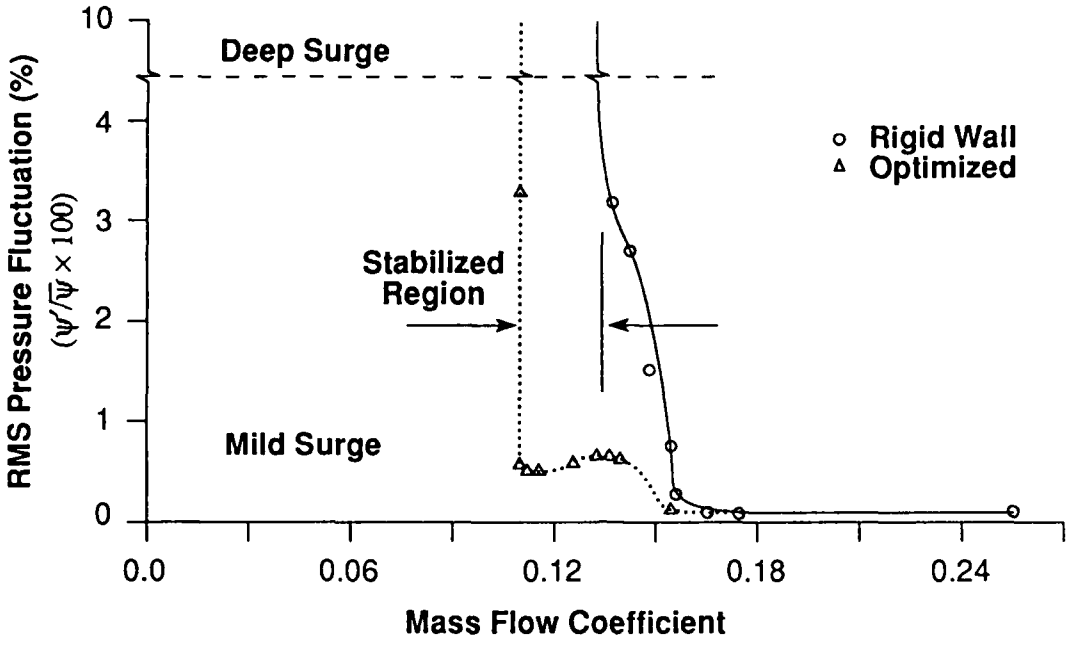

Fig. 15: Limit cycle pressure pulsation amplitude versus mass flow coefficient; 90K speedline, optimized moveable wall system

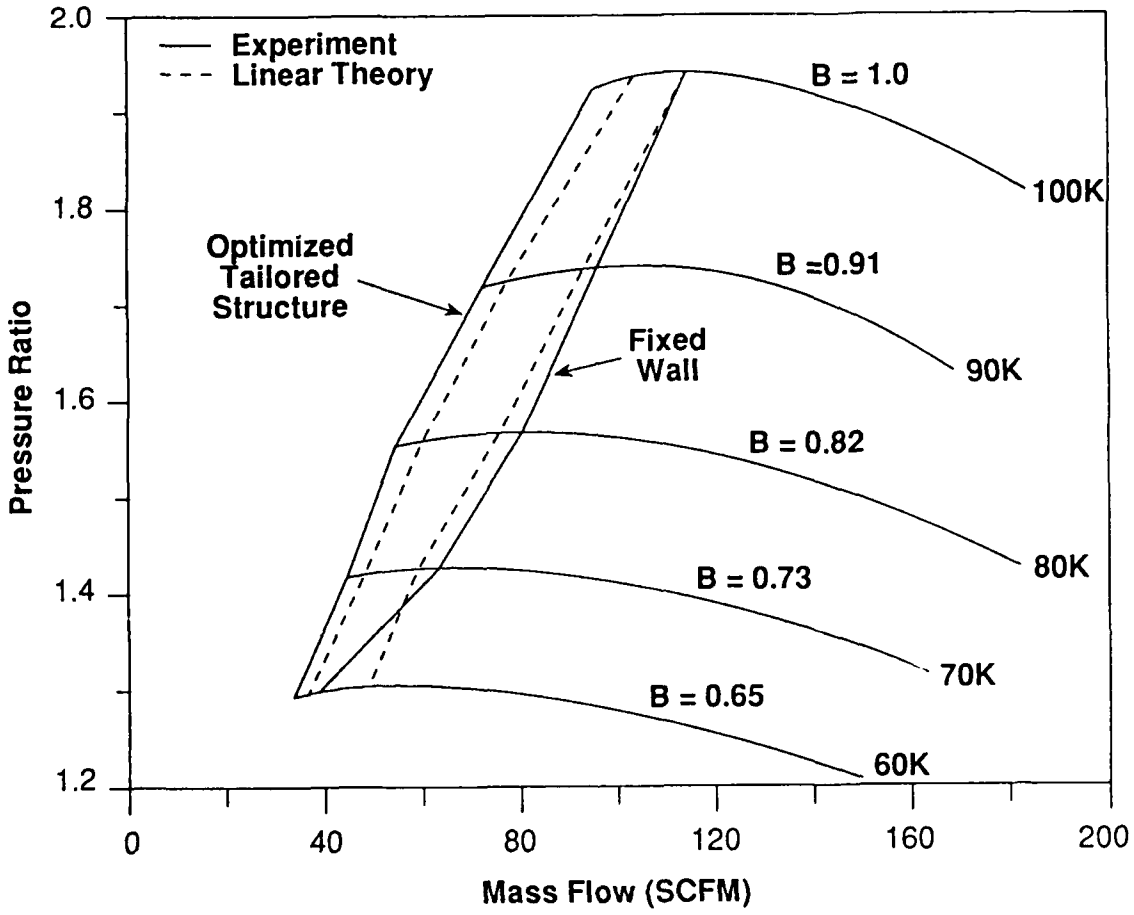

Fig. 16: Predicted and measured stability limits; compressor characteristics approximated by third order fit

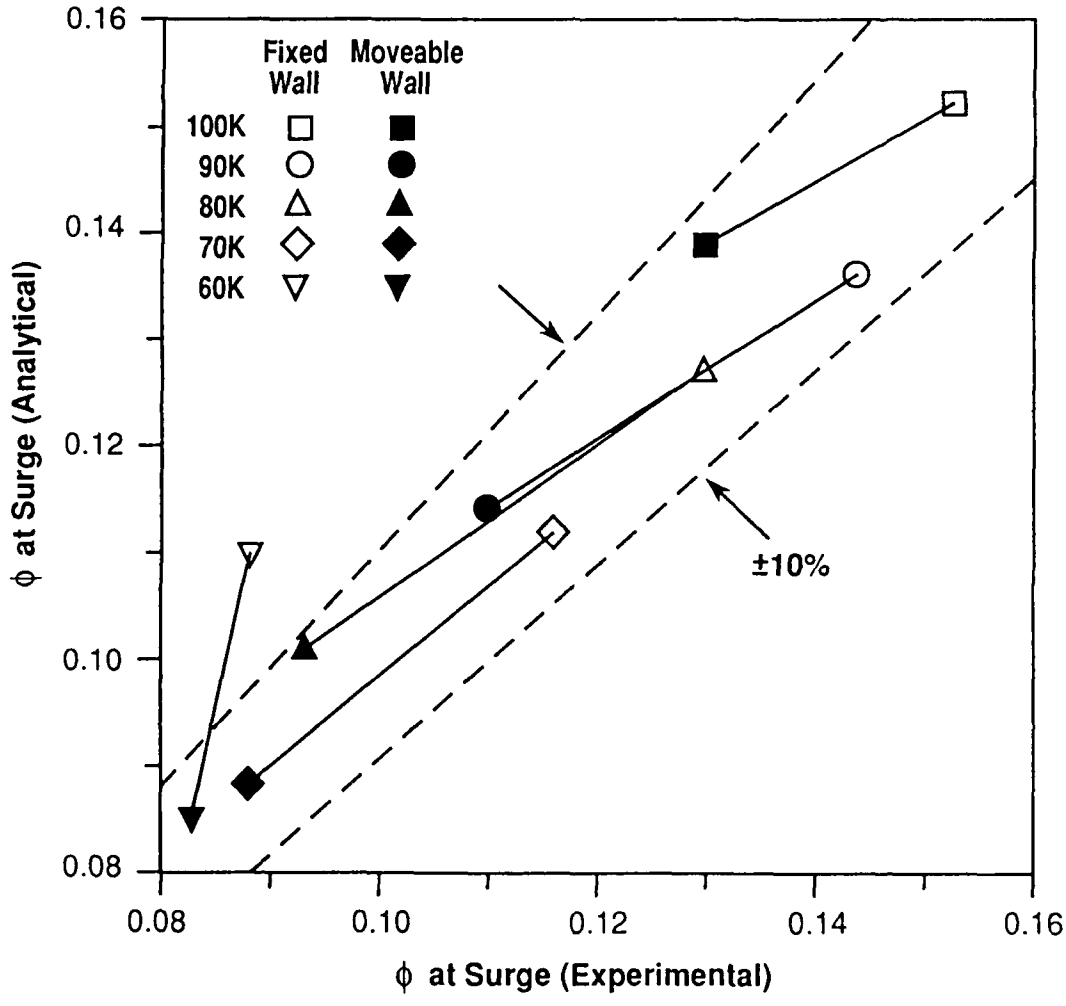

Fig. 17: Predicted and measured mass flow coefficients at deep surge inception; moveable wall optimized system

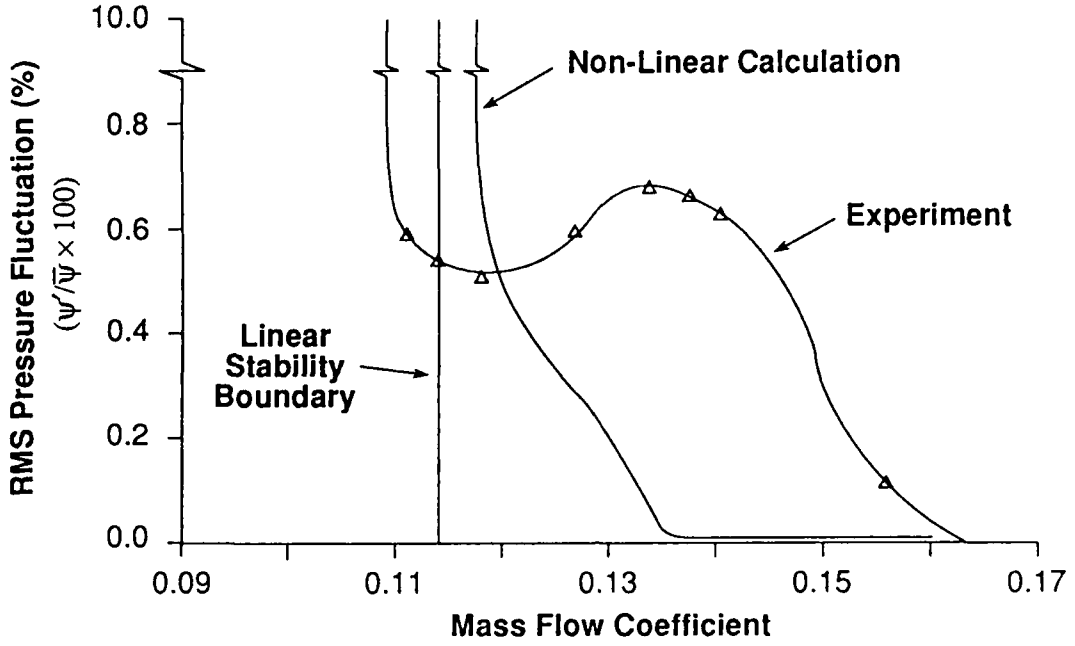

Fig. 18: Amplitude of pressure fluctuations versus mass flow; optimized system

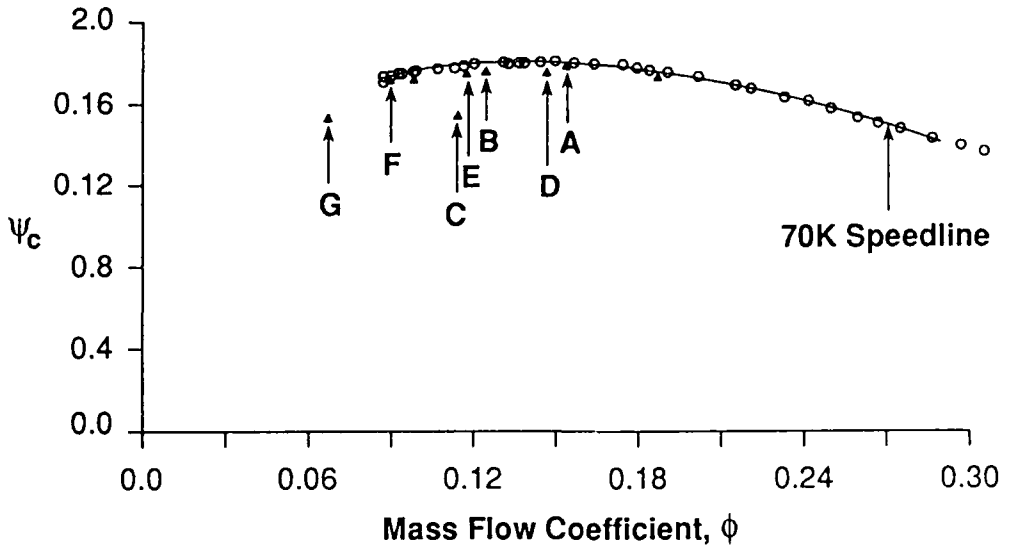

Fig. 19: Compressor characteristic with points at which time-resolved data is shown

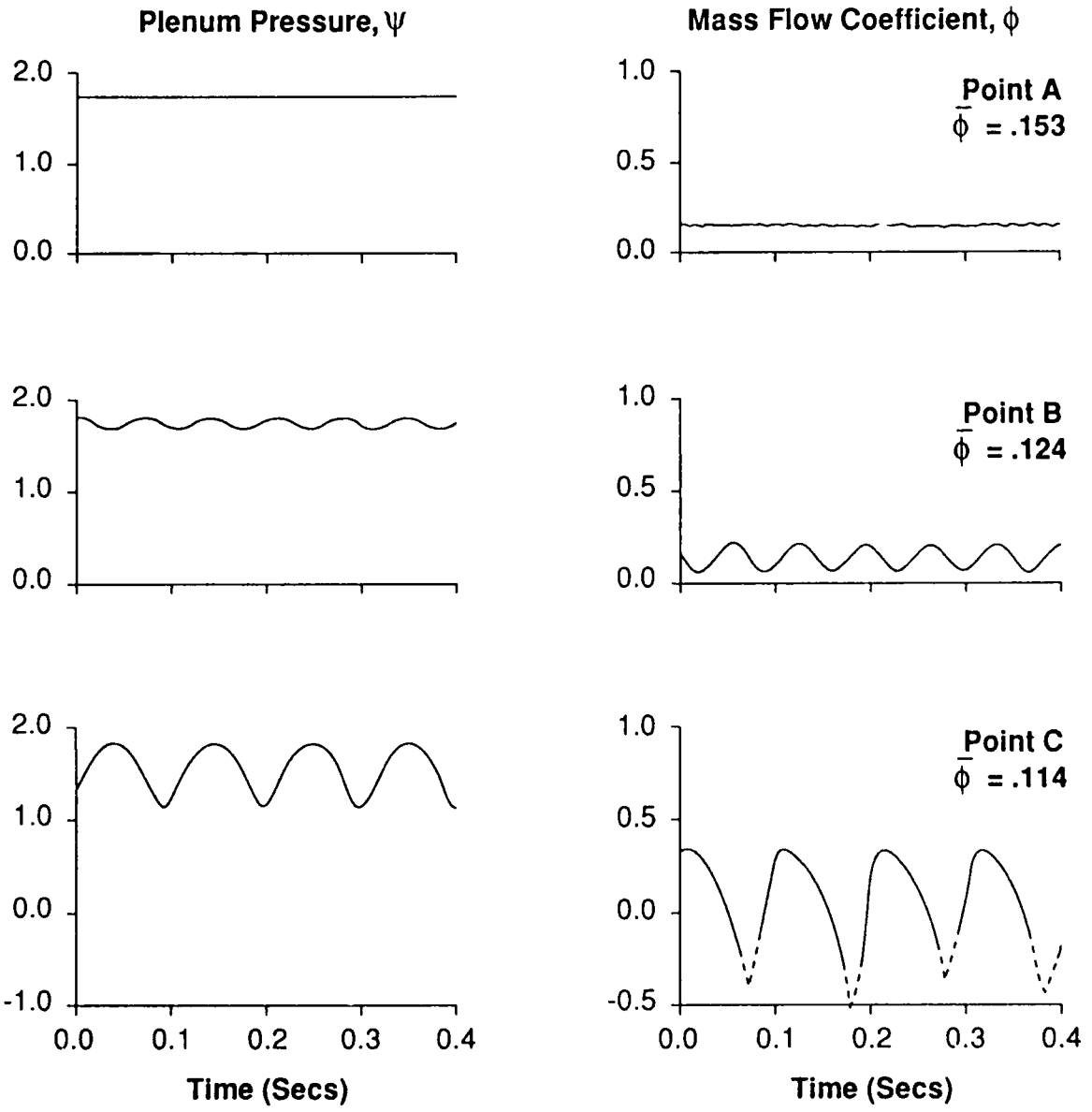

Fig. 20: Time-resolved plenum pressure and mass flow in fixed wall system, 70K speed, B = 0.73

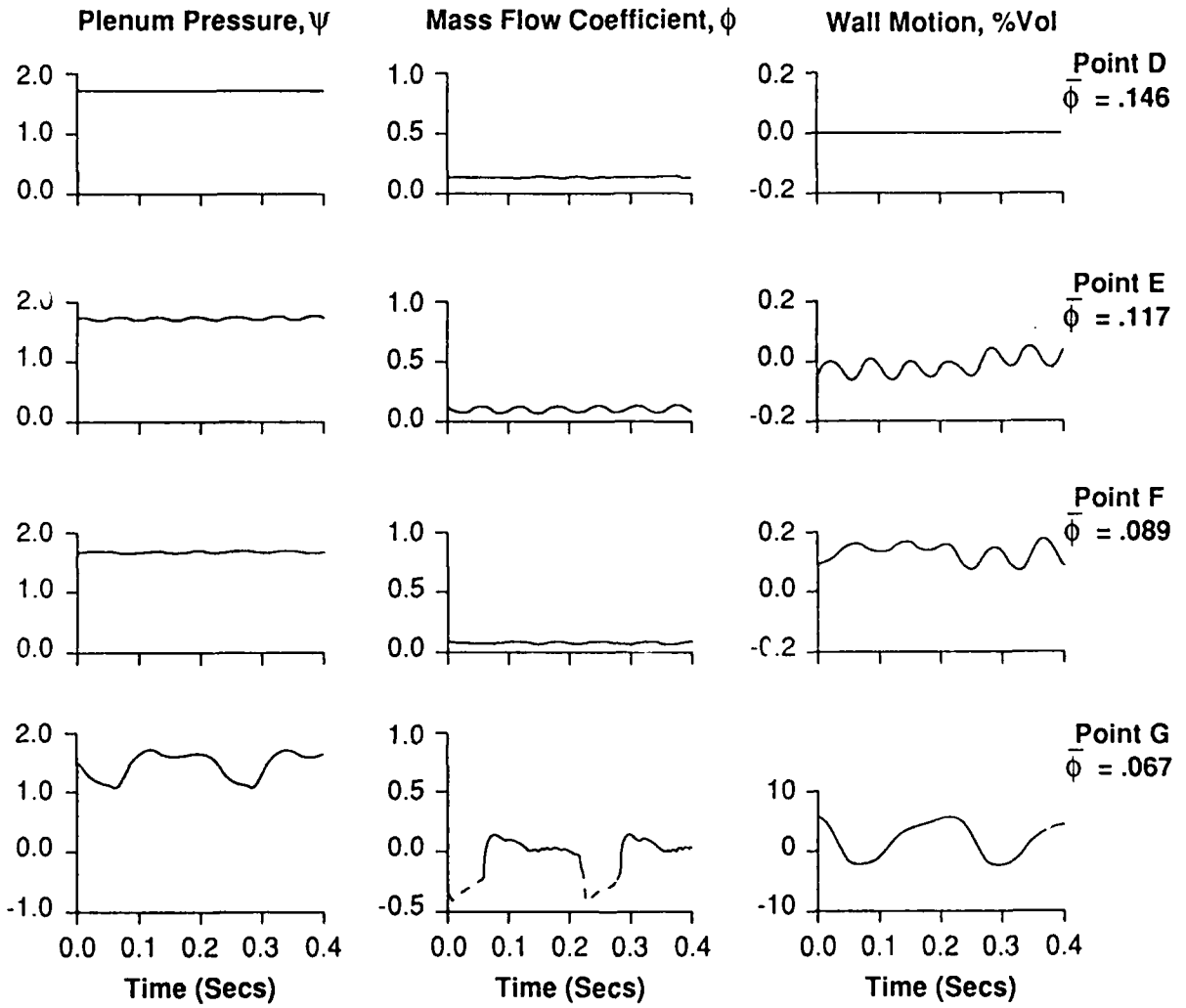

Fig. 21: Time-resolved plenum pressure, mass flow, and wall motion in optimized moveable wall system, 70K speed, B = 0.73

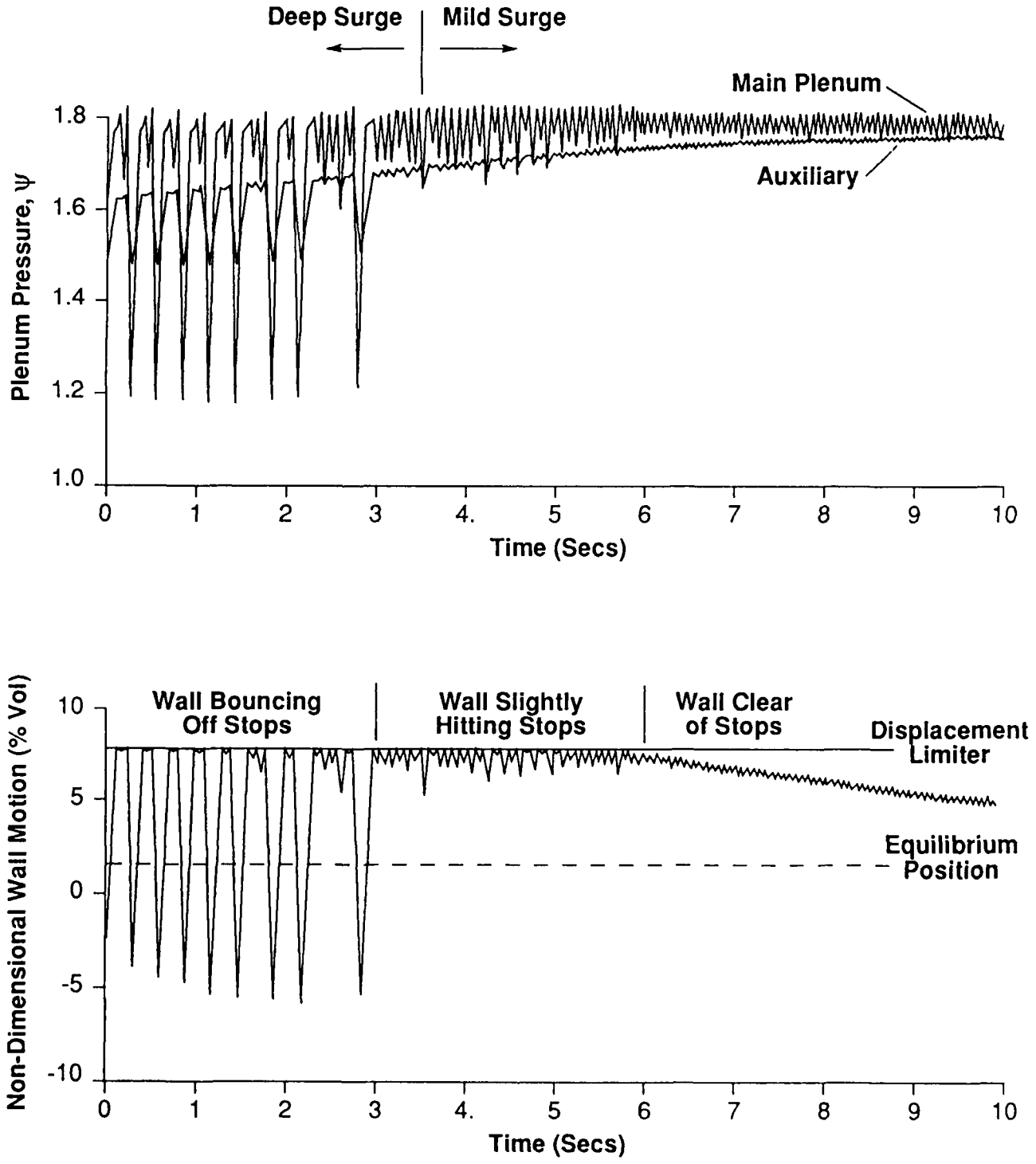

Fig. 22: Suppression of fixed wall system deep surge when wall is released, optimized system, B = 0.91

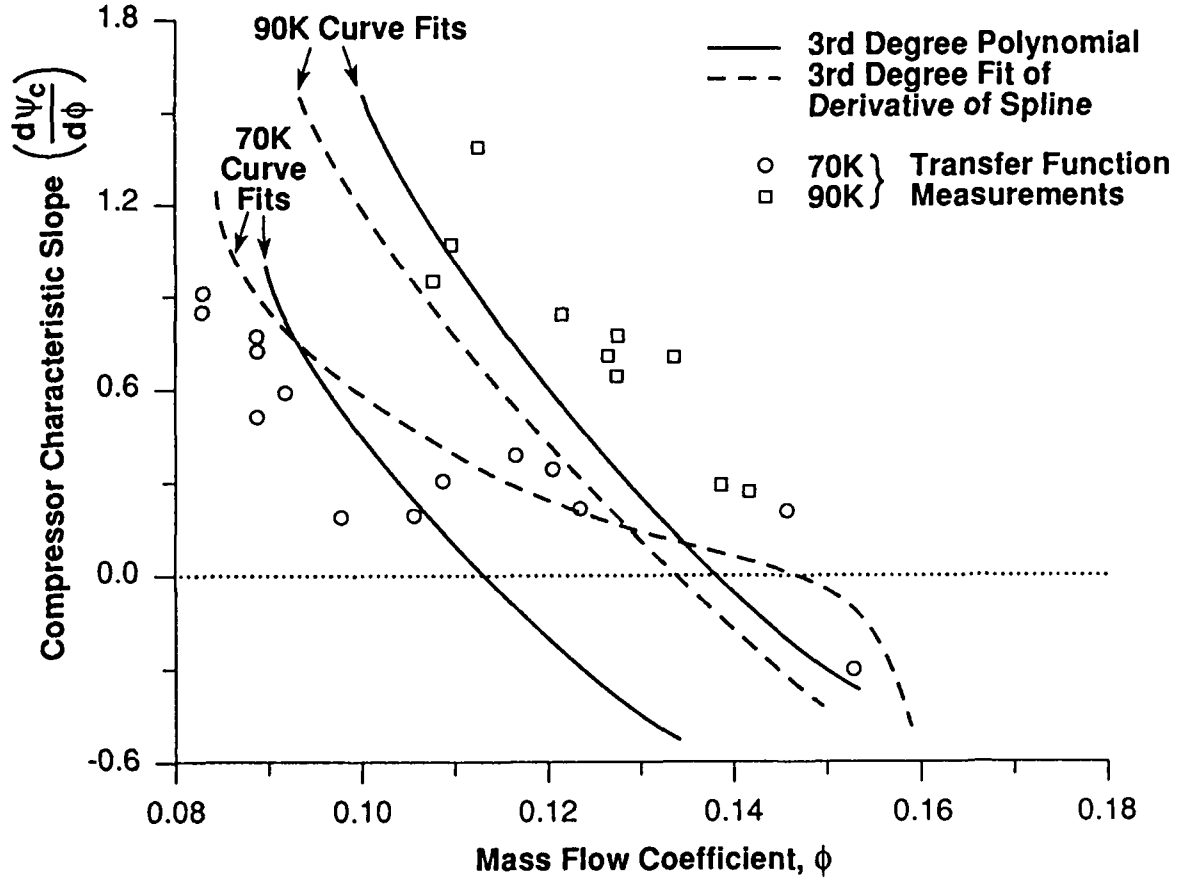

Fig. 23: Measured instantaneous and steady-state compressor characteristic slopes and values obtained from curve fits